الجمهورية الجزائرية الديمقراطية الشعبية
People's Democratic Republic of Algeria
وزارة التعليم العالي والبحث العلمي
Ministry of Higher Education and Scientific Research

جامعة زيان عاشور بالجلفة
Ziane Achour University of Djelfa

كلية العلوم والتكنولوجيا
Faculty of Science and Technology

Department: Electrical Engineering

Order N°: 002 / 2021

Defense authorization N° 055/2021

DOCTORAL THESIS

3rd Cycle Doctoral (D-LMD)

Presented by

Anissa Khiter

With a view to obtaining the doctoral diploma in 3rd Cycle Doctoral (D-LMD)

Branch: Electronics

Specialty: Signal Image and Systems

Topic

Filtering of Electrocardiogram (ECG) signals

Supported, on 20 /02 / 2021, before the jury composed of:

Last and first name	Grade	Institution of affiliation	Designation
Mr Omar MANSOUR	Professor	University of Djelfa	President
Mrs Amel Baha Houda ADAMOU-MITICHE	Professor	Universiy of Djelfa	Supervisor
Mr Lahcen MITICHE	Professor	University of Djelfa	Examiner
Mr Noureddine BOUGUECHAL	Professor	University of Batna	Examiner
Mr Ali CHEKNANE	Professor	University of Laghouat	Examiner

Djelfa University, FST - 2021

الجمهورية الجزائرية الديمقراطية الشعبية
République Algérienne Démocratique et Populaire
وزارة التعليم العالي والبحث العلمي
Ministère de l'Enseignement Supérieur et de la Recherche Scientifique

جامعة زيان عاشور بالجلفة
Université Ziane Achour de Djelfa

كلية العلوم والتكنولوجيا
Faculté des Sciences et de la Technologie

Département : Génie Electrique

N° d'Ordre : 002/ 2021

Autorisation de Soutenance N° 055/2021

THESE DE DOCTORAT

Doctorat 3ème Cycle (D-LMD)

Présentée par

Anissa Khiter

En vue de l'obtention du diplôme de Docteur en 3ème Cycle D-LMD

Filière : Electronique

Spécialité : Signal Image et systèmes

Thème

Filtrage des signaux Electrocardiogramme (ECG)

Soutenue publiquement, le 20 /02 /2021, devant le jury composé de :

Nom et Prénom	Grade	Etablissement de rattachement	Désignation
Mr Omar MANSOUR	Professeur	Université de Djelfa	Président
Mrs Amel Baha Houda ADAMOU-MITICHE	Professeur	Université de Djelfa	Directeur de thèse
Mr Lahcen MITICHE	Professeur	Université de Djelfa	Examinateur
Mr Noureddine BOUGUECHAL	Professeur	Université de Batna	Examinateur
Mr Ali CHEKNANE	Professeur	Université de Laghouat	Examinateur

Université de Djelfa, FST, 2021

Dedication

I dedicate this humble work to all those I love, and to those who love me. Especially to my dear parents, my dear husband and my children: Jawed, Baraa, Anas and Rahaf

Acknowledgment

First of all, I would like to thank Almighty God for giving me so much courage and patience to do this work.

I would like to express my sincere gratitude to the director of my thesis, Mrs**. Amel B.H. Adamou Mitiche**; professor at the faculty of technology, Zian Ashour University of Djelfa (UD), for supervising me during these years, for their valuable advices pertinent observations, and patience, as well as extensive follow-up throughout the work period of this thesis.

Also, I would like to express my sincere gratitude to Pr. Omar Mansour for agreeing to chair the jury of my thesis, as well as Pr. Lahcene Mitiche, Pr. Noureddine Boughechal and Pr. Ali Cheknane for accepting to be the examiners of this thesis.

ملخص

مخطط كهربية القلب (ECG) هو إشارة غير ثابتة وذات تردد منخفض تعكس النشاط الكهربائي الكلي لعضلة القلب. إنه حساس للغاية لأنواع مختلفة من الضوضاء أثناء عملية التسجيل مثل ضوضاء العضلات (MA) وضوضاء التجوال الأساسي (BW) وضوضاء الحركة الكهربائية (EM) حيث تتداخل أطيافها مع طيف إشارة مخطط كهربية القلب بأشكال وكميات مختلفة، والتي يؤدي إلى مسح الإشارة الأصلية. في هذا العمل، نظرًا لأن المرشحات التقليدية لم تنجح في إزالة الضوضاء دون تشويه إشارة ECG، يُقترح مرشح متكيف جديد لضوضاء MA وBW وEM من إشارة ECG التالفة؛ يعتمد المرشح على خوارزمية SC-LNLMS ذات حجم خطوة متنوع ومعامل تسرب متنوع. تم إجراء الاختبار باستخدام إشارات ECG الخالية من الضوضاء من قاعدة بيانات عدم انتظام ضربات القلب MIT-BIH والضوضاء من قاعدة بيانات اختبار إجهاد الضوضاء (nstdb). من أجل مقارنة قيمة، تم اقتراح طريقة أخرى لتقليل الضوضاء وهي مزيج من طريقتين موجودتين مسبقًا؛ التحويل المويجي الثابت (SWT) ووظيفة خوارزمية المربع المتوسط المعياري (NLMS) تظهر النتائج التجريبية أن مرشح تقليل الضوضاء المقترح الأول (SC-LNLMS) يحقق نسبة إشارة إلى ضوضاء خرج أفضل (SNR)، تحسن SNR، أقل متوسط الخطأ المربع (MSE)، واحتفظ بالإشارة الأصلية
خالية من التشوهات عند السعة المنخفضة عند مقارنتها بالطريقة القائمة على SWT وNLMS والتقنيات الأخرى الموجودة في الأدبيات.

الكلمات المفتاحية:
إشارة ECG، الضوضاء، إلغاء الضوضاء، معامل التسرب، أقل مربع تطبيع، مرشح التصحيح الذاتي، التحويل المويجي الثابت

Abstract

The Electrocardiogram (ECG) is a non-stationary, low-frequency signal that reflects the total electrical activity of the heart muscle. It is very sensitive to different types of noise during the recording process such as Muscle noise (MA), Baseline Wander noise (BW), and Electro Motion noise (EM) artifact as its spectra overlap the spectrum of the ECG signal with different shapes and quantities, which leads to blanking out the original signal. In this work, since the conventional filters did not succeed in removing noise without distorting the ECG signal, a new adaptive filter for MA, BW, and EM noise removing from corrupted ECG signal is proposed; the filter is based on Self-Correcting Leaky Normalized Least Mean Square algorithm SC-LNLMS with varied step size and varied leakage coefficient. Testing was performed using noise-free ECG signals from the MIT-BIH Arrhythmia Database and the noise from Noise Stress Test Database (nstdb). For a valuable comparison, another method of the noise reduction has been suggested which is a combination of two existing methods; the Stationary Wavelet Transform (SWT) and a variant of a Normalized Least Mean Square algorithm (NLMS). The experimental results show that the first proposed denoising filter (SC-LNLMS) achieves better output signal-to-noise ratio (SNR), improvement SNR , lower Mean Square Error (MSE) and keep the original signal free from distortions at low amplitude when compared to the SWT and NLMS based method and other existing techniques in the literature.

Keywords:
ECG signal, noises, noise canceller, the leakage coefficient, normalized least mean square, self-correcting filter, stationary wavelet transform.

Résumé

L’électrocardiogramme (ECG) est un signal de basse fréquence non stationnaire qui reflète l'activité électrique totale du muscle cardiaque. Il est très sensible à différents types de bruit pendant le processus d'enregistrement tels que le bruit Musculaire (MA), le mouvement de la Ligne de Base (BW), et le bruit d'Electro-Mouvement (EM) car ses spectres chevauchent le spectre du signal ECG dans différentes formes et quantités, conduit à masquer le signal d'origine. Dans ce travail, étant donné que les filtres conventionnels n'ont pas réussi à supprimer le bruit sans déformer le signal ECG, un nouveau filtre adaptatif pour la suppression du bruit MA, BW, et EM du signal ECG corrompu est proposé; le filtre est basé sur l'algorithme des Moindres Carrés Normalisés à fuite automatique SC-LNLMS avec un pas et un coefficient de fuite variés. Les tests ont été réalisés en utilisant les signaux ECG sans bruit de la base de données MIT-BIH Arhythmia et le bruit de la base de données Noise Stress Test (nstdb). Pour une comparaison valable, une autre méthode de réduction du bruit a été suggérée qui est une combinaison de deux méthodes existantes; la transformée en ondelettes stationnaire (TOS) et une variante de l'algorithme des Moindres carrés Normalisés (NLMS). Les résultats expérimentaux montrent que le premier filtre de débruitage proposé (SC-LNLMS) permet d'obtenir un meilleur rapport signal / bruit de sortie (SNR), un SNR amélioré, une erreur quadratique moyenne (MSE) plus faible, et maintenir le signal original exempt de distorsions à faible amplitude par rapport à la méthode basée sur TOS et NLMS et avec d'autres techniques existantes dans la littérature.

Mots clés:
Signal ECG, bruits, suppresseur de bruit, coefficient de fuite, moindres carrés normalisés, filtre auto-correcteur, transformée en ondelettes stationnaire.

Table of contents

List of figures

List of tables

List of abbreviations

AV	Atrio-Ventricular
aVF	augmented Vector Foot
aVL	augmented Vector Left
aVR,	augmented Vector Right
BW	Baseline Wander
CWT	Continuous Wavelet Transform
DENLMS	Delayed Error Normalized LMS
DWT	Discret Wavelet Transform
ECG	Electrocardiogram
EM	Electro Motion
EMD	Empirical Mode Decomposition
EMG	Electromyogram
EWT	Empirical Wavelet Transform
GID	Grey Incidence Degree
IMF	Intrinsic Mode Functions
ISWT	Inverse Stationary Wavelet Transform
LLMS	Leaky Least Mean Square
LMS	Least Mean Square
LNLMS	Leaky Normalized Least Mean Square
LSMU	Log Scale Modified Unified
MA	Muscle noise
MMF	Mathematical Morphological Filtering
MSE	Mean Square Error
NLM	Non Local Mean
NLMS	Normalized Least Mean Square
NSTDB	Noise Stress Test Database
PLI	Power Line Interference
PNS	Parasympathetic Nervous System
PRD	Percent Root Mean Square Difference
RMS	Root Mean Square
SA	Sinoatrial node
SC -LNLMS	Self-Correcting Leaky Normalized Least Mean Square
SNR	Signal to Noise Ratio
SNS	Sympathetic Nervous System
SWT	Stationary Wavelet Transform

General introduction

General introduction

The heart is the most important organ in the vital cardiovascular system, which performs many physiological processes related to certain types of different biomedical signals that reflect their nature and activities [1]. Bio-electrical signals such as the electrocardiogram (ECG) are signals that reflect the electrical activity of the human heart in real-time. And given their importance in detecting some heart diseases that may lead to death, scientists have paid great attention to this signal, whether in how it is generated, recorded, or in how it is filtered from all types of noise that may interfere with some of their characteristics and thus prevent a correct interpretation of human heart health.

The heart is a muscle located behind the rib cage between the lungs. It consists of three walls, four chambers, and four valves that make it an organic pump divided into right and left sides, the. The right side receives the blood and pumps it to the lungs to complete the pulmonary circulation. And from the lungs, the left side receives the blood and pumps it to all parts of the body, thus completing the systemic circulation [2]. The heart's pumping process goes through two primary phases called systole and diastole. The sequence of these two phases forms the cardiac cycle and is the basis of the normal anatomy and physiology of the heart. The cardiac cycle begins immediately after the heart receives electrical stimulation based on a natural electrical pacemaker called SA node [3] [4], where this electrical stimulation follows an electrical path through the entire heart muscle, forcing it to depolarize and repolarize in a successive manner. The heart muscle has the ability to generate electrical impulses at a constant rate (from 60 to 100 beats per minute at rest) [5]. During depolarization and repolarization of cardiac cells, changes occur in membrane potentials from resting potentials to action potentials i.e. an electrical signal is generated, where it can be collected and measured by an electrocardiogram (ECG) [6].

An electrocardiogram (ECG) is a graphical representation recording that reflects the electrical activities of millions of cardiac muscle cells. The ECG underwent gradual discovery developments from 1887, where Augustus DE Waller recorded the first "electrocardiogram" (ECG) of a healthy human heart using a capillary electrometer [7] [8], to 1924 where the first 12-channel electrocardiogram was created [9] [10]. The ECG signal is recorded through electrodes placed over the skin and then displayed graphically. It includes 10 electrical electrodes attached to the body, which provide 12 different viewpoints of the heart’s electrical activity [11]. These views are known as leads, this why it is called the 12-lead standard ECG. The 12-lead standard ECG consists of 12 leads, six distributed on the frontal plane (I, II, III,

aVR, aVF, aVL), and six distributed on the horizontal plane (V1-V6) [12]. A normal one cardiac cycle of ECG signal consists of three waves, which have been by convention named; P, QRS complex, and T wave, also consists of segments and intervals. The P wave is a positive deflection that reflects sequential depolarization of the atria, QRS complex reflects the ventricular depolarization, T wave is a rounded positive deflection that represents ventricular repolarization, PR interval extends from the onset of the P wave to the onset of Q wave, where PQ segment extends from the offset of the P wave to onset of Q wave, ST-segment extends from the ends of the QRS complex to the onset of the T wave, The QT interval is the time extended from the onset of Q wave to the offset of T wave [13].

There are mainly two types of noises encountered in ECG signals: a physiological type incorporating muscle (EMG) noise, while the second type is of a technical nature incorporating baseline wander (BW), electrode motion artifacts, and power line interference. In some cases, the lower amplitude wave may interfere as the P wave, in others; The QRS complex may be completely interfered with EMG noise, and likewise, very large baseline wander variance can prevent the distinction of an anomaly of the plus or minus type in the S-T segment [14]. These examples and other interferences between the noises and the ECG signal have become misleading to an accurate diagnosis of cardiac activity, and thus filtering the signal from such noises has become necessary.

A filter is a physical hardware or software that is applied to a noisy signal with the aim of minimizing the effect of the noise at the filter output according to some criterion such as mean square error (MSE) [22]. Minimizing the mean square value of the error obtained by the difference between the desired signal and the filter output is a helpful manner to such filter optimization. For stationary inputs, the obtained solution is known as the Wiener filter. The minimum point of the error performance surface, which is obtained by plotting the value of the MSE versus the adjustable filter coefficients, represents the optimum Wiener solution. However, this solution is insufficient when dealing with non-stationary signals like noisy ECG signals [23], thus, the practical solution to Wiener filter like adaptive filtering was required.

An adaptive filter is a self-designing filter that is able to adjust its coefficients automatically to adapt the input signal through a recursive adaptive algorithm; it does not need prior knowledge about input data characteristics, where after successive iteration the adaptive can track time variation in the statistics of non-stationary input [22]. Adaptive noise canceller is one configuration of the adaptive filter consists of two components, a filtering process and an

adaptive process [23]. A filtering process includes calculating the output linear filter and then creates an estimation error between the desired signal and filter output. The linear filter itself can take different structures, that are vastly manipulated in filtering non-stationary signals [25] [26] [27], the Finite Impulse Response (FIR) filter based on the transversal structure is the most popular used due to its inherent stability, it is first described by Kallmann [28] as a continuous time device, and then it has been implemented in digital circuitry. The output of the FIR filter is an expression that is called a finite convolution sum which convolves the filter input with a finite duration impulse response of the filter [23, 29]. Once the filter output is obtained, then generating an estimation error between the desired signal and this output is the second step. The estimation error is used to establish the objective function (cost function) like mean square error (MSE). In the adaptive process, according to the obtained cost function during the filtration process, the filter coefficients are automatically adjusted using a performing mechanism. The mixture of these two components operating with each other forms a feedback loop around this mechanism that called an adaptive algorithm. The least mean square algorithm (LMS) is the commonly known adaptive algorithm and the most used in many applications of the adaptive filter, this algorithm is obtained by applying the method of steepest descent that uses the gradient vector on the optimum Wiener solution [29, 30]. The resulted LMS algorithm is described in words as the updated value of the coefficient vector equals the old coefficient vector plus the product of a positive constant (step size parameter) times the input vector and the error signal. The step size parameter has to satisfy certain condition to ascertain the stability and rate of convergence [22]. Although the LMS algorithm is easy to implement and robust, it is sensitive to the round off error that is resulted from the quantization process [31], and suffer from slow rate convergence due to selecting the small value of step size, while selecting a large value results in a lower error estimation performance [32]. The Normalized least mean squares algorithm (NLMS) which is a variant of the LMS algorithm was proposed to overcome the limitation of slow convergence by normalizing the power of the input, and thus the step size parameter becomes a time-varying version. While the limitation of the sensitivity of the round off error was solved by introducing a leakage coefficient into the LMS algorithm [33], the resulted new algorithm is called leaky least mean square (LLMS) algorithm [34], where the leakage coefficient also should satisfy some condition in order to ascertain the stability during the digital implementation of the LMS algorithm [35], and reduce the misalignment in noise cancellers [30].

Several works have been carried out in the context of baseline wander noise removal [38-44], muscle noise removal [45-53], and electro motion artifact removal from ECG signal [54-59]. In this work, based on the general structure and working principle of the noise canceller adaptive filter, we proposed an adaptive filter named self-correcting leaky normalized least mean square adaptive noise canceller with varied step size and varied leakage coefficient (SC-LNLMS), our aim is to remove the muscle noise, the base wander noise and electro motion artifact which may corrupt the ECG signal with taking care to preserve the standard shape of that signal, our proposed adaptive filter is a multistage noise canceller. In the first stage, the noisy ECG signal passes through digital FIR filter, the resulted output is then subtracted from the desired signal to get the error. According to this error, the FIR filter coefficients are updated via leaky normalized least mean square algorithm. All following stages have the same structure and algorithm as the first stage, but the noisy input (corrupted ECG signal) to each stage is the FIR filter output from the previous stage and so on, also the step size and leakage coefficient are varied from stage to stage. the MSE and noise to signal ratio are two criteria that have been used to evaluate the performance of the proposed adaptive filter in addition to a comparative study with other existing techniques was made to show the effectiveness of the proposed method. The clean ECG signals and the noises were taken from the MIT-BIH database available on physionet [60-61].

The domain of stationary wavelet transformation (SWT) plus a variant of NLMS algorithm also is proposed to denoising ECG signal form noises, this method is presented and experimented into this thesis. As for the rest of the existing techniques, we were taking the results from their original articles [47] [49] [50-52]. The stationary wavelet transform SWT is an offshoot of the conventional discrete Wavelet transform (DWT), but it differs in its shifted invariant main characteristic. SWT localizes signal features in the time–frequency domain which made it widely used in the domain of filtering, when using SWT is never sub-sampled, and the filters are up-sampled, i.e. the obtained coefficients have the same length as the original signal, its main application is denoising contaminated signals and images. SWT denoising consists of three steps. In the first step, the signal is decomposed by using an appropriate level and an appropriate wavelet function (Daubechies, Coiflets, Symlets, discrete Meyer, Biorthogonal, and Reverse Biorthogonal) to obtain two sab-band coefficients named approximate and detail coefficients. In the second step, an appropriately selected threshold and selected thresholding rule (soft, hard, hyperbolic, nonnegative garrote and firm thresholding) [74] [75] are applied on details coefficients to obtain thresholded coefficients. In the last step,

the approximation coefficient obtained at the last decomposition level, and the thresholded coefficients are used by the inverse stationary wavelet transform to obtain the denoised signal. We propose to add a variant of NLMS algorithm as the second stage of denoising to smooth out the signal and get the best results for comparison.

The contribution of this thesis is divided into four chapters:

The first chapter briefly presents the heart anatomy and physiology and the basics of electrocardiography. Anatomy includes: the study of the shape, structure of the heart and blood vessels, and define the path of blood flow .while physiology includes the study of the mechanical function of the heart in pumping blood and sending it to all parts of the body, then studying the electrical component that stimulates this mechanical component**.** The electrocardiography presents the generation, recording the ECG signal, and the unwanted noises that may corrupt it.

The second chapter presents a theoretical reminder on adaptive filtering with its basic properties, main configurations, and the operation mechanism between the filtering process component and the adaptive process component in the noise canceller adaptive filter configuration that is used in the proposed algorithm.

The third chapter introduces some related work in ECG signal filtering presented in the literature, followed by a detailed description of different steps of the proposed adaptive filter which is based on adaptive noise canceller configuration and leaky normalized least mean square algorithm with varied step size and leakage coefficient, as well as an overview on stationary wavelet transform method and a description of the proposed second method based on SWT and NLMS algorithm for noise removal from corrupted ECG signal for the purpose of comparison with the first proposed method.

The fourth and last chapter explains the results achieved from the filtration of ECG signals from three types of unwanted noises by the implementation of the proposed approach. These are discussed and compared with results obtained when using stationary wavelet transform with the NLMS algorithm method, and those of other researchers in the literature.

Chapter 1

Heart and electrocardiogram basics

1.1. Introduction:

An electrocardiogram (ECG) reflects a series of electrical activity in the heart, it is a non-invasive, painless test performed by people of all ages to screen for common heart conditions such as myocardial infarction and monitor their condition as an arrhythmia, this test is performed either at rest or while exercising in sports. It is used in the doctor's office, hospital room, operating room, and ambulance [2]. Prior knowledge of the heart basics is necessary to understand the basics of the ECG signal, so the first chapter presents the anatomy and the physiology of the heart within the first part, while the second part presents the basics of electrocardiography.

1.2 Heart Anatomy:

The heart is an essential and important organ of the cardiovascular, it is approximately the size of a person’s fist, its main function is to pump and propel oxygen-rich blood and nutrients to all the cells and tissues of the body, the heart is classified as a strong conical muscle (upside-down triangle) located in the rib cage (ribs and vertebrae), between the lungs, slightly tilted to the left, and settles on the diaphragm.

1.2.1 Heart’s wall

From superficial to deep; the heart wall consists of three basic layers of tissue, epicardium, myocardium, and endocardium.

a) Epicardium

The heart wall is surrounded by a thin protective membrane known as the pericardial membrane or sac (Pericardium), this sac consists of two different sub-layers: external fibrous pericardium and serous inner pericardium, where this latter consists of two sub-layers: parietal pericardium, which merges with the fibrous pericardium, and internal visceral pericardium, or epicardium, which is the inner layer of the heart. The parietal pericardium and visceral pericardium are separated by a space called the pericardial cavity, filled with lubricating serous fluid [15].

b) Myocardium

Also called the cardiac muscle, it is the middle and thickest heart's wall. The cardiac muscle is covered by a collection of blood vessels that supply it, and the nervous fibers that help to regulate it. Heart muscle fibers consist of 3 billion heart cells (of one or more nuclei) [16] encapsulated by the surface plasma membrane, the cells are linked together by an intercalated disc that helps support simultaneous contraction of the muscle, and it also consists of large numbers of gap junctions (channels) that can open or close to allow or prevent the passage of ions, and help synchronize the contraction. This muscle tissue contracts with each heartbeat, and composed of two types of cardiac muscle cell**s,** myocardial contractile cells, and myocardial conducting cells [2].

- Myocardial contractile cells constitute the largest part of the cells in the atria and ventricles, they conduct impulses and are responsible for contractions that pump blood through the body.
- Myocardial conducting cells (Nodal cells) are specialized cells able to generate and diffuse the electrical impulses that rapidly spread throughout the heart, and thus activate the contractions phenomena. These cells have four main characteristics; contractility (the extent to which a cell contracts after receiving a stimulus), automaticity (It is the cell's ability to automatically initiate an impulse), conductivity (the ability of a cell to spread an electrical impulse from a cardiac cell to another), and excitability (results from the ions exchange through the cell membrane and denotes how well a cell reacts to an electrical stimulus) [15].

c) Endocardium

The innermost layer of the heart wall, this layer provides protection to the valves and heart chambers. It consists of squamous epithelium tissue called endothelium with small blood vessels and bundles of smooth muscle. It is also the inner lining of the heart's chambers, where blood circulates [6].

1.2.2 Heart's chambers

The heart consists of four basic chambers distributed on two sides, the left side and the right side, each side contains the upper atria and the lower ventricle. The two sides are separated by a vertical muscular wall called a "septum". The two upper atria receive blood from the veins, and the two lower ventricles pump blood to the arteries, the right atrium receives blood via

superior and lower vena cava (the largest veins in the body), while the left atrium receives oxygenated blood via four pulmonary veins, the right ventricle pumps venous blood to the pulmonary artery, and the left ventricle pumps oxygenated blood to the aorta (see figure 1.1). The ventricles and atria cells are made up of 99 percent of myocardial contractile cells [6].

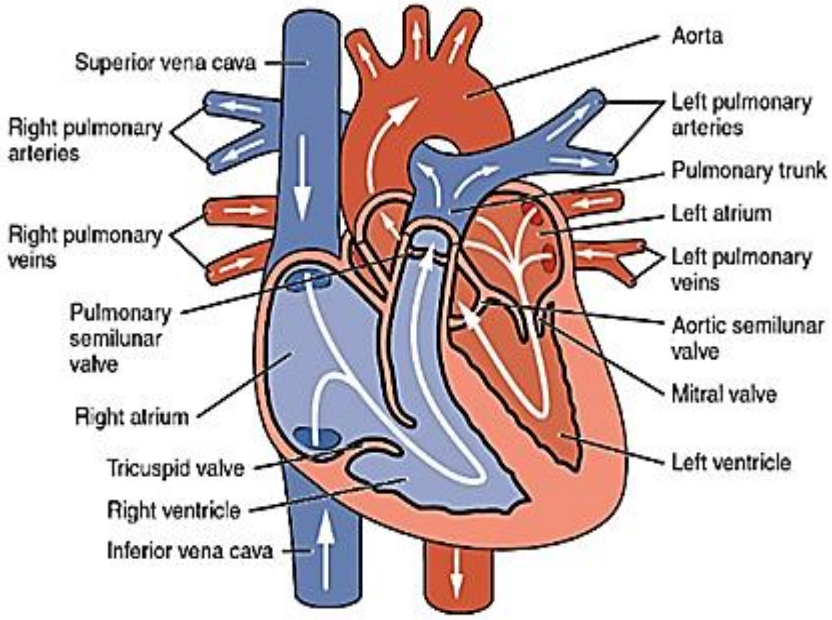

Figure 1.1 Heart anatomy [15].

1.2.3 Heart's valves

The heart has four valves, whose importance is that they allowing the blood to flow in one direction and preventing its reflux.

- **Two atrioventricular (AV) valves,** called tricuspid and mitral valve, the tricuspid valve is located between the right atrium and the right ventricle. Its function is to allow blood to flow from the right atrium to the right ventricle. It opens and closes when the right atrium relaxes and when it contracts consecutively. When relaxing, this valve allows oxygenated blood to flow from the right atrium to the right ventricle. As for contraction, this valve closes to prevent the blood from refluxing and thus the blood goes its way to the pulmonary artery via the pulmonary valve [5]. The mitral valve (bicuspid) is located at the opening between the left atrium and left ventricle, its function is to allow blood to flow from the left atrium to the left ventricle. It opens and closes when the left atrium relaxes and when it contracts consecutively. When relaxing, this valve allows

oxygenated blood to flow from the left atrium to the left ventricle. As for contraction, this valve closes to prevent the blood from refluxing and thus the blood goes its way to the aorta via the aortic valve. Both valves consist of leaflets. The tricuspid valve has three, while the mitral valve consists of two leaflets. The leaflets in each valve are attached by chordae tendineae to the papillary muscles that emanate from the ventricular wall and which control the opening and closing of the valves [2] (see figure 1.1).

- **Two semilunar valves** called pulmonic and aortic valve, the pulmonary or pulmonic valve is located between the right ventricle and the pulmonary artery. Once the right ventricle contracts; the blood pressure increases causing this valve to open and push the deoxygenated blood out of the heart into the artery. When the ventricle relaxes, the pressure inside the heart decreases, so this valve closes, preventing blood from returning to the heart. The aortic valve is located at the base of the aorta; it opens and closes when the left ventricle relaxes and when it contracts consecutively. When contracting, this valve opens to allow oxygenated blood to flow into the aorta. As for relaxation, this valve closes to prevent the blood from returning and causing it to rush into the aorta. These valves are called semilunar valves because they consist of three cusps of endothelium strengthed with connective tissue similar to three half-moons (see figure 1.1) [14].

1.2.4 The mechanism of blood flow:

The mechanism of blood flow to and from the heart requires a group of veins and arteries, the veins carry blood to the heart, and the arteries carry it from the heart.

The Oxygen-free blood (with blue color as shown in figure 1.2) returns to right atrium from the upper extremities, head, neck and chest, via the superior vena cava, and from the lower extremities via inferior vena cava. From there, the blood is forced to flow through tricuspid valve into the right ventricle from where it is pumped through the pulmonic valve into the pulmonary arteries and then into the lungs where gases are exchanged and the blood supply with nutrients, then the oxygenated blood (with red color as shown in figure 1.2) returns to the left atrium through the four pulmonary veins, which achieves the pulmonary circulation (small circulation). Then, the left atrium contracts and forced oxygenated blood to move through the mitral valve into the left ventricle. The mitral valve closes, so the left ventricle contracts and pumps blood through the pulmonary valve into the aorta and from there to the rest of the body organs and tissues (exception the lungs) [2]. The aorta branches into smaller and smaller arteries

that connect to every tissue in the body. Around every tissue in the body there is a network of capillaries connecting arteries and veins. All the veins in the body drain into the upper and lower vena cava, where they carry blood back to the right atrium, completing a circuit called the systemic circulation.

The heart itself, like any organ or tissue in the body, needs its own blood supply to obtain the oxygen and nutrition that are needed for the continuous contraction process, and this nutrition takes place through the very short coronary circulation through two arteries originating from the aorta immediately after it exits the left ventricle and passes on both sides of the heart, as representing the shape of the crown, and therefore called the two coronary arteries, each of which feeds half of the heart [12].

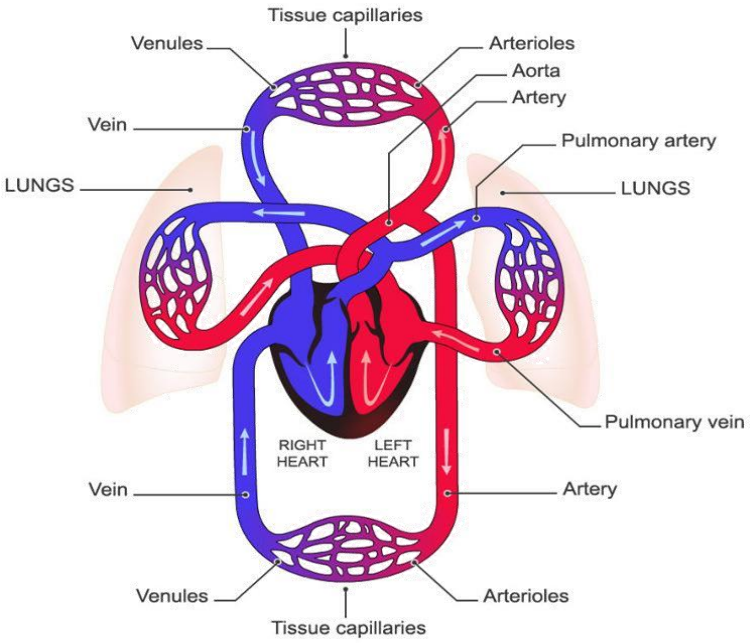

Figure 1.2 The blood circulation system [12].

1.3 Heart physiology

Cardiac physiology is the study of the healthy and vital function of the heart, this study includes: the cardiac cycle, cardiac muscle innervating process, and cardiac conduction system.

1.3.1 Cardiac cycle

The cardiac cycle or the mechanical component of the heart rhythm can be defined as the sequence of contraction and relaxation of the cardiac muscle in order to pump blood throughout the body in less than a second. Each cardiac cycle begins at the beginning of a heartbeat and

ends with the beginning of another, and is divided into two main stages called systole and diastole [2, 3]. The diastolic phase is the phase of relaxation of the ventricles and the heart filling with blood brought in by the veins and is characterized by the opening of the two atrioventricular (AV) valves and the closing of two semilunar valves as shown by figure (1.3), diastole phase occupies ⅔ of the cardiac cycle duration under resting conditions. In the phase of systole, the ventricles contract, and blood is pumped from the heart to the arteries and is characterized by the closure of the two atrioventricular (AV) valves which gives a "lub" sound, and the opening of the two semilunar valves as shown by figure (1.3), systole phase occupies ⅓ of the cardiac cycle duration under resting conditions. The cardiac cycle is completed when the chambers of the heart fill with blood and blood is pumped out of the heart, implying a succession of ventricular contraction and ventricular diastole [6].

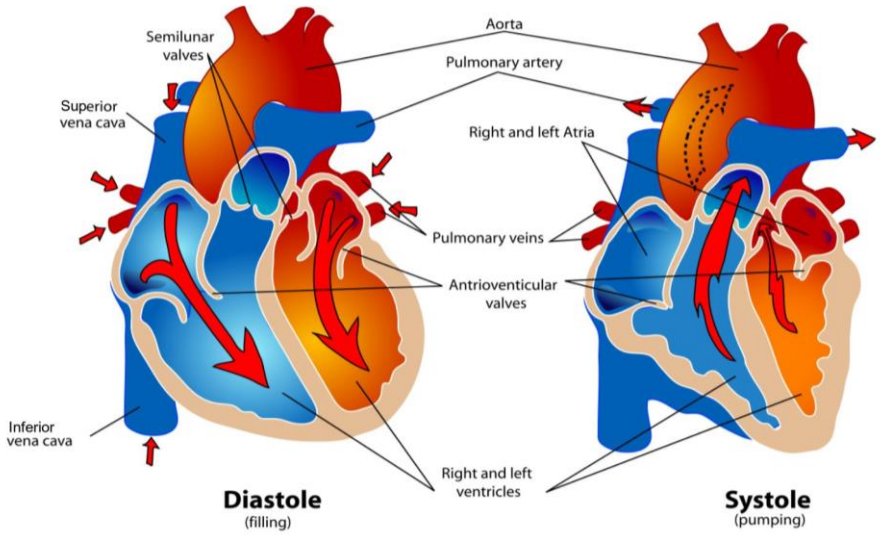

Figure 1.3. Cardiac cycle [15].

When the heart beats, a single cardiac cycle consists of five sequenced events, isovolumic ventricular contraction, ventricular ejection, isovolumic relaxation, ventricular filling, and atrial contraction.

- **Ventricular filling**; the atrial pressure exceeds the ventricular pressure, which causes the two atrioventricular (AV) valves to open and blood flows from the atria to the ventricles (during this stage, about 70% of the ventricular filling occurs); this stage ends when the two atrioventricular (AV) valves close and the ventricular relaxation begins [17].
- **Atrial contraction**: The atria contract and the two atrioventricular (AV) valves open, the atria supply the ventricles with 30% of the blood for each heartbeat, this phase is completed

before the ventricular contraction begins. The ventricular filling phase and atrial contraction are called the ventricular filling phase (mid to late diastole) [2].

- **Isovolumic ventricular contraction**; begins with an increase in pressure within the ventricles due to ventricular depolarization, which causes the closure of the two atrioventricular (AV) valves while the two semilunar valves remain closed during the entire stage [17].
- **Ventricular ejection**; begins when the ventricular pressure exceeds the aortic and pulmonary arterial pressure, causing the two semilunar valves to open and the ventricles to drain blood. The isovolumic ventricular contraction phase and the ventricular ejection phase are called the ventricular systole phase (atria in systole) [12].
- **Isovolumic relaxation**; in this stage, the ventricular pressure decreases (but the volume remains constant), which leads to the closure of the aortic valve and the pulmonary valve, and the pressure in the aorta and pulmonary artery increases. Atrial relaxation occurs when the atria fill with blood (during this stage all valves are closed). This phase is also called early diastole.

Each heart muscle contraction controls blood flow in the form of a heart rate measured in beats per minute. The duration of the cardiac cycle increases with the decrease in the heart rate and decreases with the increase in the heart rate because the duration of the cardiac cycle is inversely proportional to the heart rate. The normal resting heart rate ranges from 60 to 100 beats per minute [3].

1.3.2 Cardiac muscle's innervating

There are two branches of the autonomic (involuntary) nervous system that supply the heart and control the heart rate; the sympathetic (adrenergic) nervous system (SNS) and the parasympathetic (cholinergic) nervous system (PNS). The sympathetic nervous system (SNS) liberates the hormones (catecholamines - epinephrine and norepinephrine) to precipitate the heart rate, automaticity, atrioventricular (AV) conduction, and contractility. While the parasympathetic nervous system (PNS) (and specifically the vagus nerve that carrying the impulses) liberates the hormone acetylcholine to decelerate the heart rate and the conduction of impulses through the AV node and ventricles [15]. There are other factors that temporarily speed up the heart rate such as stress, caffeine, excitement, and medications such as nitrates, while factors that help slow the heart rate such slow and deep breathing, medications such as beta-blockers, vomiting [6].

1.3.3 Electrical activity of cardiac muscle

The cardiac cycle occurs after the emergence of the electrical component that is directly responsible for it. The electrical component is the generation and transmission of electrical impulses (action potential). Due to automaticity and the ability properties (mentioned in section 1.2) of a cluster of sub-specialized cardiac muscle cells called sinoatrial (SA) node; an electrical impulses are generated, and then, due to the conductivity property of cardiac muscle cells; these impulses are rapidly transmitted throughout the myocardium from the SA node through the electrical conduction system. During the impulses transmission process, the cardiac cells follow depolarization and repolarization cycles with each heartbeat. Depolarization (in electrical term) causes the contraction phase, and repolarization causes the relaxation phase [6].

1.3.3.1 Action potential of cardiac cells

In a basal and rest conditions, normal myocardial cells maintain their polarization (relaxation) with a membrane potential difference called resting potential which reaches about -70 mV [19]. The membrane potential difference is caused by the difference in ion concentration on both sides of the membrane cellular, where different ions are involved: the sodium Na^{+}, potassium K^{+}, and calcium Ca^{++} [16]. At rest, the cell membrane is nearly 100 times more permeable to potassium than sodium [15]. Therefore, potassium diffuses out of the cell more than the sodium diffuses into it, which results in more negative charges inside the cell due to the open potassium channels, and the positive and negative charges remain uniformly distributed at each of the two mediums inside and outside the cell. After the electrical stimulation occurs, the sodium channels in the cell membrane open to allow sodium ions to pass through to the inside of the cell, and quickly the inner part of the cell becomes positive compared to the surface of the membrane, which leads to the depolarization of the cell (i.e. shrinks) and the emergence of a new potential contrary to the underlying resting membrane and capable to spread, called action potentials, followed by the process of cellular repolarization (when the cell returns to its resting state) [2, 12].

During ion exchange, two types of current can be distinguished: "inward" currents are those in which a positive charge enters the cell and that makes the membrane potentials more positive, which we call "depolarization", "outward" currents are those in which a positive charge leaves the cell and that makes the membrane potential more negative. This is what we call "repolarization".

The electrical changes in the myocardium cell during the depolarization - repolarization cycle is illustrated by the ventricular action potential curve represented in figure (1.4), where this curve is consist of five different phases; phase 4, phase 0, phase 1, phase 2, and phase 3.

- **Phase 4** is the baseline that membrane potential starts and completes at it. Potassium channels are open, and ion potassium diffuses out of the cell, where potassium currents are essential determinant of resting membrane potentials (- 90mV) [4].
- **In phase 0 (Fast Depolarisation)**; the voltage sodium channels open, and the sodium ions rapidly flow into the cell, resulting in a rapid and steep depolarization. While the calcium moves slowly in the cell (intracellular space) causes a positive resting membrane potential. Sodium channels become almost inactive after opening as long as the cell is devoid of polarization and cannot create an additional working voltage in that cell (the membrane potential elevates to about +30 mV) [11].
- **In phase 1(Notch);** the potassium channels rapidly repolarize the cell before the plateau stage due to the influx of potassium ions out of the cell. Higher potassium currents during the notch phase allow more repolarization so that the plateau appears at lower voltages; while lower potassium currents allow less repolarization and a plateau phase appears at higher voltages (notch phase takes about 3–5 ms) [13].
- **In phase 2 (the plateau),** the calcium continues to flow inward and binds to ryanodine receptors on the SR, while maintaining the membrane potential, the membrane potential decreases towards the resting state, the calcium channels gradually become negative, and the potassium channels gradually open up, so the potassium continues to flow out of the cell (plateau phase takes about 175 ms) [15].
- **In phase 3 (Repolarisation);** after the calcium channels are closed, the cell quickly restores the potassium ions, and the potassium currents succeed in repolarizing the cell, while the sodium is restored to the outside after the sodium channels start to activate, and thus the membrane potential becomes more negative. The potassium channels open completely and the cell becomes polarized again and this allows the cycle to restart (The repolarization takes about 75 ms).

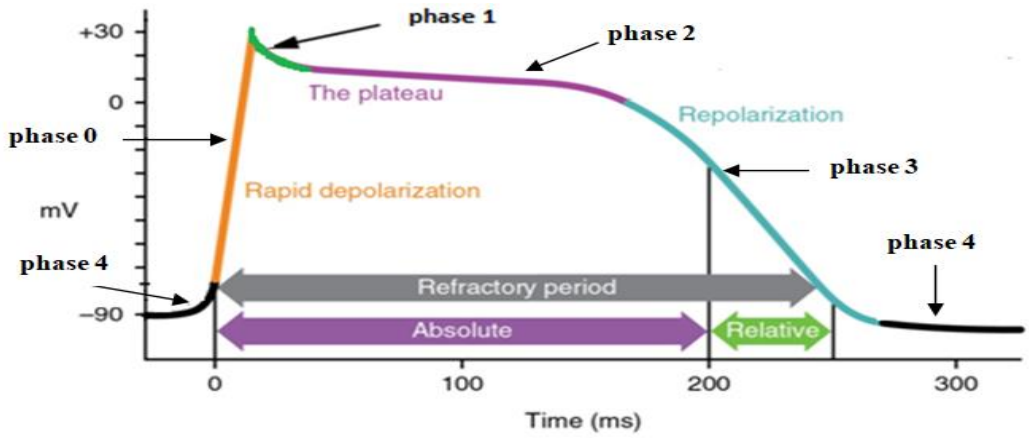

Figure 1.4. Ventricular action potential phases (Adopted from [2]).

During phases 1 and 2 and at the beginning of phase 3, cardiac cells are in their absolute refractory period that takes about 200 ms, and no stimulus can excite them. But, the strong stimulus can depolarize the cells in the second half of phase 3 when the cells are in its relative refractory period that takes 50ms. In phase 4, the membrane potential decreases until it reaches resting levels again and the cell is ready for another stimulus, and the cycle repeats. The whole cycle takes between 250 and 300 milliseconds [2]. The total electrical activity of the heart is the summation in time and space of the primary electrical activities represented by each of the cellular action potentials. It is represented by a trace called an electrocardiogram or ECG.

1.3.3.2 Electrical conduction system pathway

The impulses generated by the SA node are rapidly transmitted throughout the myocardium through a specialized pathway called the conduction system, and thus causing the heart to contract. The conduction system consists of the SA node, the Bachmann bundle, the atrioventricular (AV) node, the Atrioventricular Bundle, and the Purkinje fibers .as shown by figure (1.5).

- **Sinoatrial (SA) Node,** a precise point in the heart known as the heart's main pacemaker, located at the top of the right atrium where the superior vena cava joins the atrial tissue mass. This source is made up of a cluster of cells capable of generating impulses 60 to 100 times per minute. The SA node is able to transmit its impulses as an oil patch to the rest of the two atria to their base through preferential conductive pathways, causing them to contract [18]. The impulses usually can't flow backward because the cells can't respond to a stimulus immediately after depolarization.
- **Bachmann bundle and Inter-nodal Pathways,** The electrical impulses are transmitted from the SA node through the left atrium via the Bachmann's bundle (Interatrial

pathway), on the other hand, through the right atrium; the electrical impulses spread from the SA node to the atrioventricular node (AV) via the internal pathways which are divided into the anterior, middle, and posterior internal pathways (see figure 1.5) [4].

- **Atrioventricular (AV) Node (The slow node),** is a concentrated conductive tissue that lies near the bottom of the right atrium (in medial posterior to the tricuspid valve), although the AV node is also capable of generating an action potential but is slower than that of the SA node. As a result, it operates in response to activity from the SA node. The AV node then delays the impulses it has reached to give enough time to allow the atria to contract. Thus, the ventricles complete the filling phase with the atria contracting. Then the AV node sends the impulses down the atrioventricular bundle into the ventricles [15].
- **The atrioventricular fiber bundle,** or bundle of His, extends into the heart septum from the AV node to the bottom of the septum and is divided into two branches: the right and the left bundle branches, the left bundle feeds the left ventricle and is itself divided into the left anterior fasciculus, which elongates across the anterior portion of the left ventricle, and the left posterior fasciculus, which passes through the lateral portions of the left ventricle, while the right bundle branch feeds the right ventricle [18].
- **Purkinje fibers** are conductive fibers that branch from the His fibers and extend into the wall of the left and right ventricles. These fibers are characterized by a rapid transfer of impulses to the contractile cells in the ventricles in about 75 milliseconds [15] causing them to contract.

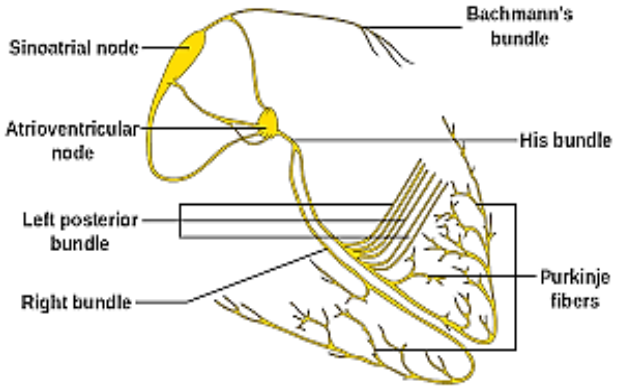

Figure1.5 Normal conduction pathway of the heart (Adopted from [2]).

1.4 The electrocardiogram

The graphic recording of the heart's electrical activity is called an electrocardiogram (ECG), as this recording gives us an electrical signal consisting of a series of ordered and repeated waves and intervals, the height of which represents a millivolt while its width represents a period of time. It is a common non-invasive and painless test performed for people of all ages to detect common heart diseases such as myocardial infarction and monitor its condition such as irregular heartbeat in many situations such as rest or exercise. Electrocardiogram signals are obtained by attaching electrodes (leads) to the patient's skin away from the heart, at the patient's ankles, wrists, and chest. The device used for this examination of the heart is called an electrocardiograph, where the plot then appears on a strip of paper and can be interpreted instantly [5]. The waves and periods originated during depolarization and repolarization expressed by the ECG are distinguished from each other in terms of sharpness of the peak and smoothness. Those resulting from depolarization are sharpest and have a higher peak than the waves associated with repolarization [6].

1.5 The electrocardiogram history

This ECG signal has an ancient history since its first discovery and development, which we summarize as follows:

In 1887, Augustus D Waller recorded the first "electrocardiogram" (ECG) of a healthy human heart using a capillary electrometer. The tracer announced only two deviations described by V1 and V2 to designate ventricular effects [7]. In 1893, the Dutch physician and physiologist Willem Einthoven introduced the term "electrocardiogram" at a meeting of the Dutch Medical Association. He continued to develop it until 1901 when he invented the string galvanometer (series of galvanometers) using a fine silver-coated quartz chain. Then, in 1912 he presented for the first time the famous equilateral triangle consisting of the standard derivations of DI, DII, and DIII, and which was later called the "Einthoven Triangle" [8]. In 1932, Charles Wolferth and Francis Wood described the medicinal use of the V1 - V6 primary derivatives, and it was the first precordial lead in clinical diagnostic cardiology [9]. In 1924, Emmanuel Goldberger added 3 terminal leads, aVR, aVL and aVF, to the leads identified by Einthoven. Combined with the previous six leads, V1 - V6, he was allowed to perform the first 12-channel electrocardiogram [10], which has been widely used in contemporary medicine.

1.6 Generation of the ECG

The propagation of the depolarization and repolarization processes of myocardial cells along the muscle cardiac fibers is represented by the theory of a dipole-vector, The dipole consists of a pair of electrical charges and is associated with a vector that determines the dipole's time-varying position, direction and magnitude, all vectors that are related to specific groups of cells in the myocardium are combined to form one vector that determines the main direction of the electrical pulse and is called a "dominant vector" (see figure 1. 6) [19].

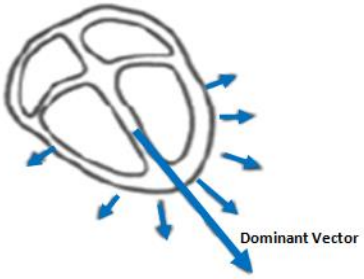

Figure 1.6 The dominant vector [6].

The dominant vector head is situated at the positive pole of a dipole, where an electrode that faces the head of the vector registers a positive deviation [3]. Thus, the vector sequence representation of the different phases of depolarization and repolarization of myocardial cells illustrates how the ECG waves are generated as registered by electrodes (leads) placed on a surface body, The position of electrodes on the body greatly affects the shape and polarity of single waves, and their amplitudes are also affected by the distance between the heart and the electrode [6]. Depolarization- repolarization phases and associated morphology can be summarized as follows:

1.6.1 Atria depolarization

The ECG signal begins with a horizontal line (isoelectric line) that represents the baseline, and this reflects the state of the heart cells that are at rest, see figure 1.7 (a). Then when the SA node fires an impulse, the atria depolarization phase takes place. The dominant vector is orientated to the bottom towards the AV node, and thus an atria wave with positive polarity is created in the registered ECG and called p wave, see figure 1.7 (b). Due to the comparatively small atria muscles, this wave is characterized by low amplitude and usually ranges between 1.5 and 2.5 mm [12]. At the end of the complete depolarization phase of the atria, the depolarization of the AV node and its bundles begins but does not reflect any apparent ECG

waves due to its small muscle masses, and for this, the ECG recovers the isoelectric line upon the complete depolarization of the atria and extends until the depolarization phase begins from ventricles [6], see figure 1.7(c).

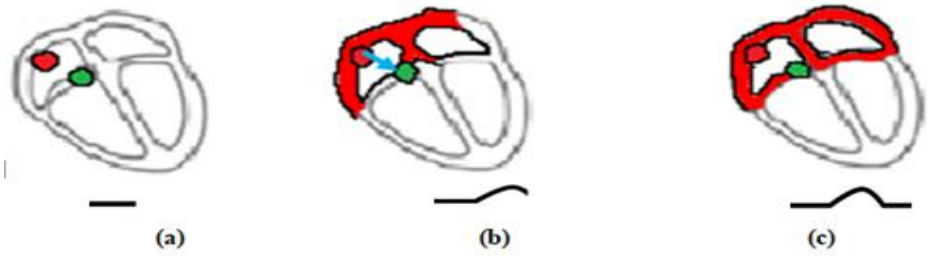

Figure 1.7 .**(a)** All cardiac cells at rest, **(b)** Atrial depolarization, **(c)** Passage of electrical impulse through the AV node (Adopted from [6]).

1.6.2 Septal depolarization

The AV node delays the incoming electrical flow for a short time, then the flow travels rapidly down the bundle of His and through the left and right bundle branches to the septum between the ventricles where its cells begin undergoing depolarization process. The depolarization of the septum leads to a small negative wave reflected on the registered ECG and called Q wave, see figure (1.8). This wave takes of short duration due to the great conduction celerity of the cells in this portion [13].

Figure 1.8 Septal depolarization (Adopted from [6]).

1.6.3 Apical and early ventricular depolarization

Ventricular depolarization takes longer, and this is because the left ventricular wall is thinner compared to the right ventricular wall, and as a result, the dominant vector orientations change progressively downward and to the left, see figures 1.9 (a)-(b). The process of depolarization is almost over, and a wave of a negative polarity is produced that is reflected on the registered ECG and called R wave [2], see figure 1.9 (b).

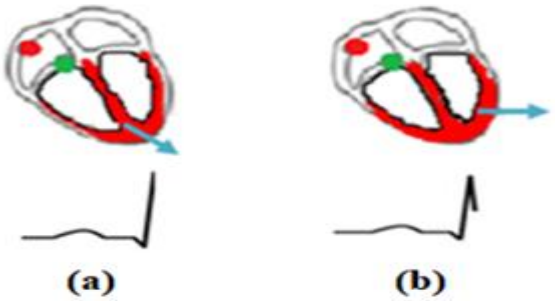

Figure 1.9 (a) Apical, **(b)** Early ventricular depolarization (Adopted from [6]).

1.6.4 Delayed ventricular depolarization

Ventricular depolarization ends when the small spaces at the extremities of the ventricles are depolarized. The electrical stimulation moves, resulting in a longer R wave which represents the right ventricular late depolarization, or a smaller S wave, which represents the left ventricular depolarization [12], see figure (1.10).

Figure 1.10 Delayed ventricular depolarization (Adopted from [6]).

1.6.5 Ventricular repolarization

When the ventricular depolarization phase is completely complete, the cells return to their normal resting state, this is reflected on the ECG as an isoelectric line that remains until the ventricular repolarization occurs. During ventricular repolarization, the dominant vector direction changes from the top to the bottom causing production of wave with positive polarity called T wave [15], see figure (1.11).

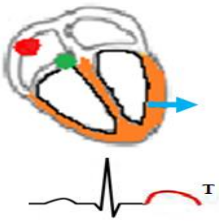

Figure 1.11. Ventricular repolarization (Adopted from [6]).

1.7 ECG Recording Techniques

Since the dominant vector describes the main direction of the electrical wave-front generated during the heart electrical activity, then confirming this direction becomes necessary because it defines the upward or downward deflection of an electrocardiogram waveform, so the ECG records information about these waveforms from diverse viewpoints called 'leads' that have positioned on the skin. In electrical term 'lead' is the voltage difference between a pair of electrodes [4, 5]. The electrocardiogram (ECG) recording requires a set of leads that include unipolar or bipolar leads or both. The unipolar lead records the voltage difference of one electrode and is evaluated in relation to a reference electrode placed so that the voltage stays approximately constant during the whole cardiac cycle; the reference is named the "central terminal." While bipolar lead records the potential difference between two electrodes, for example, between the left and right arm [6]. There are two ECG recordings types, the standard 12-lead ECG and a rhythm strip [2]. Both types provide precious details about heart activity. In this thesis we are interested with the 12-lead ECG.

1.7.1 Standard 12-lead ECG

This system has 12 leads, which are like 12 different angles that simultaneously track the spread of electrical activity. These 12 leads cover much of the heart tissue, and can often be classified as six leads on the frontal plane and six on the horizontal plane.

1.7.1.1 Leads in the frontal plane

The leads on the frontal plane consist of three bipolar limb leads (I, II, III) also called Einthoven leads, and three augmented unipolar limb leads also called Goldberger leads (augmented vector right (aVR), augmented vector left (aVL), and augmented vector foot (aVF)).

a) Regarding bipolar limb leads, lead I measure the potential differences between the left to the right arm, lead II measures the potential differences between left leg and right arm, where lead III measures the potential differences between left leg and left arm. Bipolar limb leads were first defined by Einthoven as a triangle (Einthoven's Triangle in the form of a closed circle, see figure 1.12 (a). Where according to Kirchhoff's law; the voltage in each lead should follow equation II = I+III. By shifting the three sides of the Einthoven triangle toward its center, Bailey derived a reference figure called Bailey’s triaxial system [3].

b) Augmented unipolar limb leads (aVR, aVL, and aVF) are denoted 'augmented' because their voltage is higher than that of the bipolar limb leads (corresponding to Einthoven's law) [3]. they are shifted 30^0 from those of the bipolar limb leads, the space between I and II is covered by -aVR, between II and III by aVF, and between III and I by aVL, i.e. they determine the voltage differences between one angle of the triangle and the average of remaining two angles, see figure 1.12 (b). In augmented limb leads one electrode is detecting while the average of the two other acts as the reference electrode **[6].** Bailey added these three leads to Bailey's triaxial system to obtain Bailey's hex-axial system, see figure 1.12 (c).

The three bipolar limb leads have three positive poles correspond 0^0, $+60^0$, and $+120^0$ respectively, and have three negative poles correspond $\pm180^0$, -120^0, and -60^0 respectively. Thus, they are separated by 60^0. where regarding augmented unipolar limb leads, each has lines going from a positive pole to a negative pole passing across the center of a triangle: the line of aVR extends from positive pole to negative pole corresponding -150^0 to $+30^0$ respectively, that of aVL from the positive pole to negative pole corresponding -30^0 to $+150^0$ respectively and that of aVF from positive pole to negative pole corresponding $+90^0$ to -90^0 respectively, see figure 1.12 (c) [5].

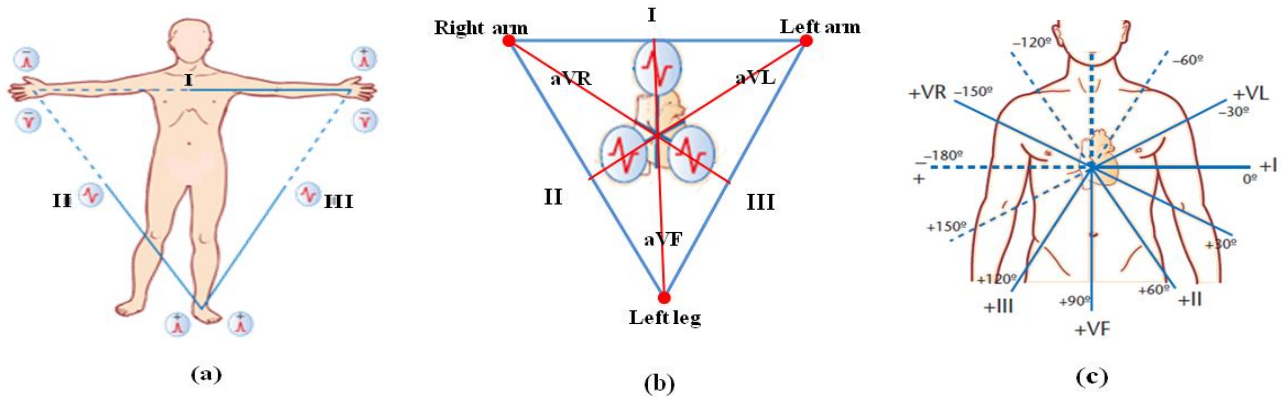

Figure 1.12 (a) Einthoven's triangle, **(b)** Augmented unipolar limb leads and bipolar limb leads, **(c)** Bailey's hexaxial system (Adopted from [3]).

1.7.1.2 Leads in the horizontal plane

In the horizontal plane, there are six chest leads (also known as precordial leads) that named (V1–V6). They are placed on the surface of the chest (the front and left side) through different areas of the heart in order to record the electrical activity of the ventricular areas in a plane perpendicular to the frontal plane [4], see figure (1.13). The activity of the right ventricle (anteroseptal) is reflected by Leads V1 and V2, Leads V3 and V4 mainly explore the front of

the ventricles (interventricular wall and the tip of the heart), while a view of the left ventricle (anterolateral) is explored by V5 and V6. The difference in potential of a chest lead is registered between the relevant chest electrode and a central terminal which is defined as the average potential registered from the three bipolar limb leads [4, 6].

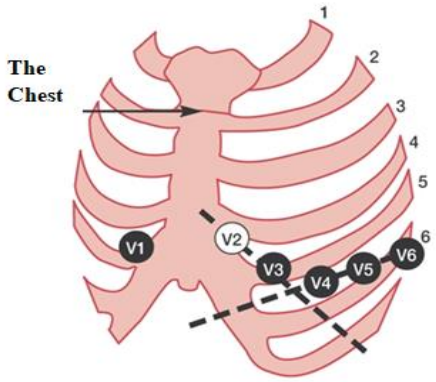

Figure 1.13 Standard attachment sites for chest leads **(**Adopted from [4]).

1.8 Normal Electrocardiogram tracing components

The ECG machine provides a graphical representation of the human heart electrical activity after treating the signals captured from the skin by electrodes, the graphical representation depends on the basic pattern of electrical activity that was first explored more than a hundred years ago which states that electrical activity flowing away from the lead causes a downward deflection, while that flowing towards the lead causes an upward deflection [5, 11]. The ECG signal comprises three waves, which have been by convention named P, QRS complex, and T wave, also consists of segments (the region between two waves), and intervals (includes one segment and one or more waves), see figure (1.14).

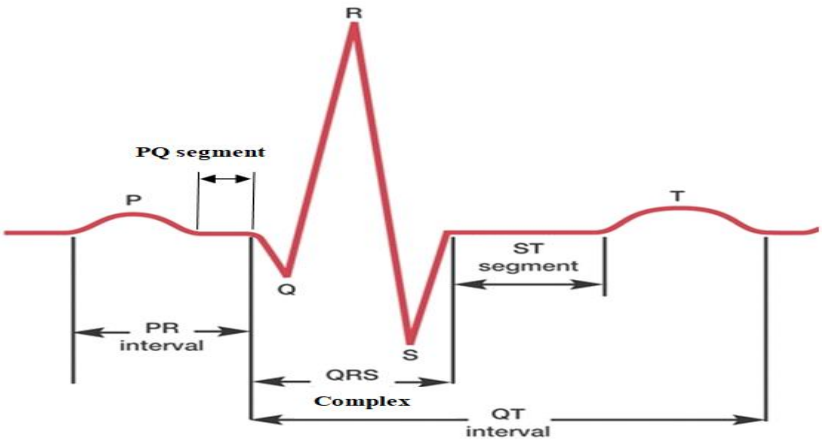

Figure 1.14. ECG normal waveform graphical representations (Adopted from [11]).

1.8.1 P wave

The first upward deflection from the isoelectric line is named the P wave, which represents a sequential atria depolarization wave (Figure 1.14). In general, its shape is rounded, upright has a positive polarity. The amplitude of the P wave is low and less than 300 μV (not exceed 2.5 mm) which is generally masked by concurrent ventricular depolarization (QRS complex), where its duration is less than 120 ms (width) [4, 6]. The spectral characteristic of a normal P wave is generally regarded to be low-frequency, below 10-15 Hz.

1.8.2 PR interval and segment

The PR interval is the time interval that extends from the beginning of atria depolarization (P wave) to the beginning of ventricular depolarization (initiation of the QRS complex). It is more medically appropriate because it reflects the time needed for the electrical impulse to spread from the SA node to the ventricles [3, 6]. The normal PR interval ranges reflected at adult is between 0.12 and 0.2 s (up to 0.22 s at the aged and as short as 0.1 s at the pediatric) [6].

The PQ segment extends from the end of the P wave to the beginning of the QRS (onset) and is generally an isoelectric line (no more electrical current can flow across the myocardium).

1.8.3 QRS wave complex

The three waves of the QRS complex represent ventricular depolarization which in the normal heart takes about 70-110 ms [15]. The first downward deflection from the baseline after the P wave is named Q wave that is narrow and small in amplitude and reflects the depolarization of the inter-ventricular septum, and its duration does not beyond 0.03 second [4]. The first upward deflection after the P wave is named R wave and reflects depolarization of the ventricular mass, this is why it is the largest wave in ECG. The S wave reflects the final stage of depolarization of the ventricles at the base of the heart [5]. The QRS complex has significantly higher frequency content than other waves and is mainly ranged in the interval 10-50 Hz [6].

1.8.4 ST Segment

The ST segment (also known as the ST interval) is the time between the ends of the QRS complex (also known as J point) or from the end of ventricular depolarization and the beginning of the T wave [5]. It reflects the period of zero potential between ventricular depolarization and

repolarization. Generally, the frequency content of the baseline is between 0.5 Hz and 7 Hz [14].

1.8.5 T wave

The T wave reflects the ventricular repolarization (atrial repolarization is obscured by the large QRS complex). This wave becomes narrow and closer to the QRS complex when heart rates are accelerated; the normal T wave is smooth and rounded. In most leads, the T wave is reflected by a single positive peak [6]. another wave named U may follow the T wave, and it is generally of the same polarity as the T wave, which reflects a final stage of the repolarisation of certain ventricular cells in the middle of the myocardium (repolarization of papillary muscles) [4].

1.8.6 QT interval

The QT interval is the time extended from the beginning of the Q wave to the end of the T wave. It reflects the onset of ventricular depolarization to the completion of ventricular repolarization. At more accelerated heart rates, the QT interval becomes shorter [15].

1.9 Noises in the ECG signal

During the recording process, the ECG signal is exposed to the interference of different types of noise that arise from different sources, the range of this noise can be within the frequency range of the ECG signal, which may change its properties and completely overlap their waves and intervals, thus it is difficult for the specialist to interpret the ECG signal if this interference is external or reflects a problem in heart function. The noise is divided into two types: a physiological type that includes muscle noise (MA noise), while the second type is of technical nature and includes baseline wander (BW), electrode motion artifacts (EM), and power line interference (PLI) [6]. ECG and noise signals recordings showed below are digitized at 360 samples per second per channel at 11-bit resolution over a 10-mV range, where the duration of each is 30 minutes.

1.9.1 Muscle noise (EMG noise)

The muscle or electromyographic noise is caused by the contraction of skeletal muscles located near the heart during their electrical activity, this electrical activity reflected as waveforms can be detected and reflected by an ECG during the process of recording (from

using chest leads), and more during exercise. The frequency range of the ECG is overlapping with the spectrum of muscle noises is in between 20-1000 Hz [20], it appears as a narrow and quick spike of ECG and makes the doctor suspicions of shivering and Parkinson's disease [21] (see figure 1.15).The spectral content of muscle activity significantly overlaps that of the PQRST complex and extending into higher frequencies, making cancelling muscle noise from an ECG signal without introducing distortion remains difficult in ECG signal processing.

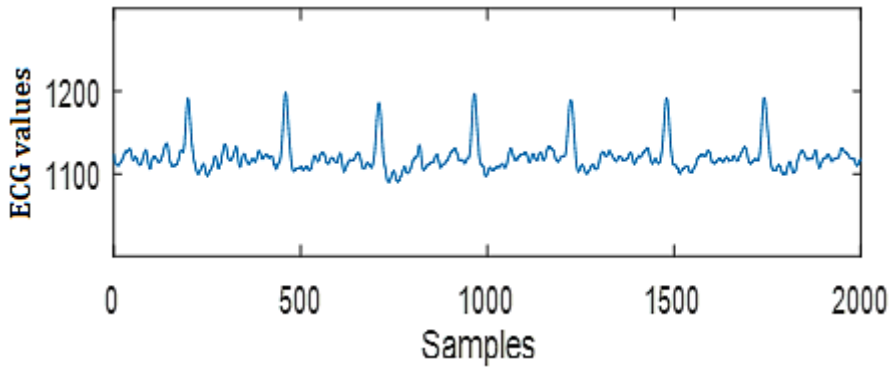

Figure 1.15. Corrupted ECG signal by muscle noise.

1.9.2 Baseline wander (BW) noise

Baseline wander is a low-frequency activity in the ECG picked up in chest-lead ECG signals by coughing or breathing with a great motion of the chest, or when an arm or leg is moved in the case of limb-lead ECG acquisition that leads to the clinical interpretation incorrect and misleading, see figure (1.16). Baseline wander noise is described by a slow wander of the baseline [12]. Its frequency range generally 0.5Hz, but it may contain higher frequencies during vigorous exercise.

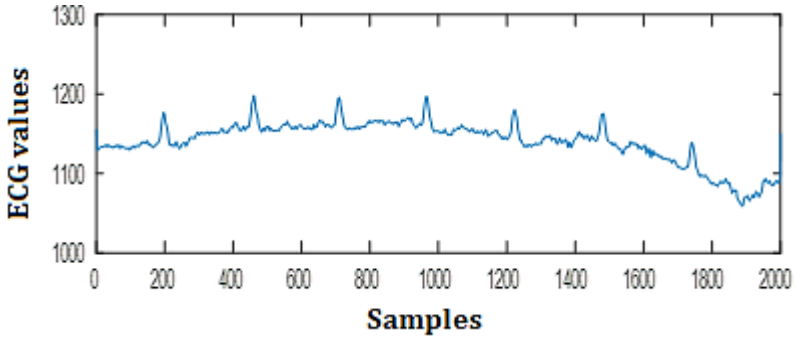

Figure 1.16. Corrupted ECG signal by baseline wander noise

1.9.3 Electrode motion artifacts

Electrode motion artifacts appear roughly in the biomedical signals that are captured by the electrodes. It results from skin stretching which varies the impedance of the skin surrounding the electrode, coughing, and ambulation. The spectral content of the motion artifacts significantly overlaps with the content of the PQRST complex, mostly in the range from 1 to 10 Hz, where it manifests as large amplitude waveforms that are confused with the QRS complex in the ECG (figure 1.17). Electrode motion artifacts are the main source of incorrectly detected heart rhythms recorded from a mobile ECG [21].

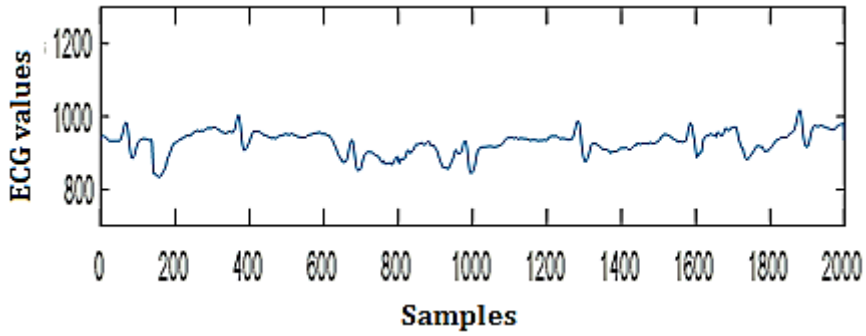

Figure 1.17 Corrupted ECG signal by electrode motion artifacts

1.9.4 Power line interference (50/60 Hz)

Power line interference (50/60 Hz) is resulted from the interference from neighboring equipment because of electromagnetic fields caused by a power line, also resulted from the incorrect grounding of the ECG equipment [12]. It is described by 50 or 60 Hz sinusoidal interference and causes problems in interpreting low amplitude waveform in the ECG signal, see figure (1.18).

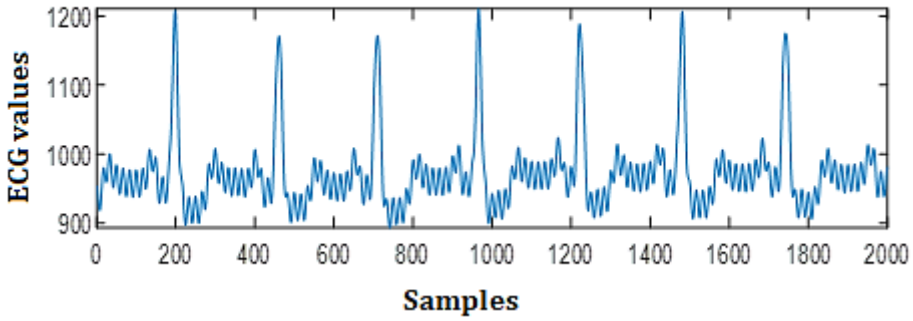

Figure 1.18. Corrupted ECG signal by power line interference.

1.10 Conclusion

An ECG generally offers an important evidence of a heart abnormality, and it also gives to some extent accurate evaluation of the anatomy and physiological importance of that abnormality. Moreover, the ECG is the best way to analyze cardiac arrhythmias, but on the other hand, this signal is a low-frequency electrical signal and has very weak physiology, the maximum amplitude usually does not exceed 5mV, and the signal frequency is between 0.05 and 100Hz, it is subject to interferences with different types of noise that lead to overlapping some of its waves, especially the QRS complex, which reflects ventricular activity responsible for pumping blood either to the lungs or to all parts of the body. Therefore, denoising this signal from annoying interference has become necessary to ensure accurate and non-distorted signal. Many techniques were proposed to overcome this problem as classic and adaptive filtering; the next chapter is exposed to noise canceller adaptive filter theory.

Chapter 2

Adaptive noise cancellation theory

2.1 Introduction

During the recording of the ECG signal, and before its final measurement, it contaminates with various unwanted interference called "noise". The noise rarely appears so distinct from the signal of ECG, which makes it difficult to remove it. Knowing the characteristics that discriminate the ECG signal from noise is imperative in order to apply noise reduction techniques as noise reduction techniques must usually contain a compromise between the quantity of noise to be removed and the quantity of the ECG signal that must be preserved. Many techniques have been achieved for this purpose, some of which are classic and some are adaptive, where some have given satisfactory results, and others showed defects and shortcomings. This chapter deals with adaptive filtering theory that addresses the problem of noise interference with the ECG signal.

2.2 Adaptive filter history

In the 1930s and 1940s, Andrei Kolmogorov, Norbert Wiener, and Norman Levinson began to solve linear estimation problems by proposing the candidate known as Wiener-Kolmogorov is the optimal solution in the sense of square error. Between 1957 and 1960 Howells, APPLEBAUM, and their colleagues at General Electric developed the first adaptive noise cancellation work by designing a side-lobe canceling system for the antenna that uses reference inputs generated from an additional antenna simple two-weight adaptive filter. In 1959, Widrow and Hoff at Stanford University were designing the least-mean square (LMS) adaptive algorithm and the model recognition system known as Adaline (for adaptive linear threshold logic element) [36]. In Great Britain, adaptive filters were developed by GABOR and his colleagues. In the early and middle 1960s, the first application of adaptive filtering at the Bell Laboratories by Lucky was done, where he succeeded in the reduction of inter-symbol interference in high-speed MODEM'S which is designated for digital communication [23]. Two students at Stanford University and in 1965, was designed the first adaptive noise canceling. The goal was to cancel 60-Hz interference at the output of an electrocardiographic amplifier and recorder. Hence, adaptive noise cancellation has been adequately requested to a number of further issues, such as noise removal from ECG signal, periodic interference cancelation, and echo cancellation in long-distance telephone transmission lines [36, 37].

2.3 Adaptive filter definition

The term filter is used to characterize a small piece of physical material embedded in a device or software that is applied to a set of noisy data in order to separate information about a specific amount of the desired signal [23], where an adaptive filter is a digital filter with self-adjusting characteristics. It is able to adjust its linear filter coefficients automatically to adapt the input signal according to optimization or adaptive algorithm. This filter is a central topic in adaptive signal processing which is widely used in telephone echo cancellation, biomedical signal enhancement, noise cancellation, adaptive control systems, equalization of communications channels, and active noise control [32]. There are four basic information processing tasks that an adaptive filter can accomplish:

- **Filtering** means using the data measured up to the current time t and containing it in order to separate information about a specific desired amount of interest [23].
- **Smoothing** is an advanced filtering step i.e. more accurate than filtering. The filtering is performed more accurately because it is used after the current time and before it to extract the information, which causes delays in the output. [24].
- **Prediction**, the aim of which is to extract information about the amount of desired at some future time, using measured data after time t and before [23].
- **Deconvolution** includes the restoration of the filter characteristics given the filter's input and output signals [24].

2.4 Property of the adaptive filter

Adaptive filters have the property that their coefficients change with the input to make the filter converge to an optimal state and improve its performance according to some criterion. If we consider the general structure of an adaptive filtering environment given by the figure (2.1), where n represents the discrete time (n =0, 1…., N-1), X (n) is the input to the digital filter, d (n) is the desired signal, w(n) is the digital filter, y(n) is the filter output, and e(n) is the error signal (the difference between X(n) and y(n)) [29]. The error signals also called estimation error is required to create a cost function or criterion, needed by the adaptation algorithm, there are many criteria that are suggested in the literature like mean square of the estimation error (MSE), an expectation of the absolute value of the estimation error, and expectation of high power of the absolute value of the estimation error [22, 23], where all of them, satisfy the optimization and non-negativity properties, In our case, we will use the MSE. Adaptive filters work mainly

for unknown or time-varying noise, adapting the changing environments, spectral interference between the desired signal and the noise, where the signal and the noise occupy fixed and separate frequency bands [32]. Many conventional linear filters such as low pass filter, notch filter with the fixed filter coefficients are investigated to remove such interferences and extract the signal, but they failed because their coefficients characteristics need to be variable and adapted to changing signal characteristics, where it is needed in some cases such spectral overlapping between signal and noise [22] like ECG signal and muscle noise.

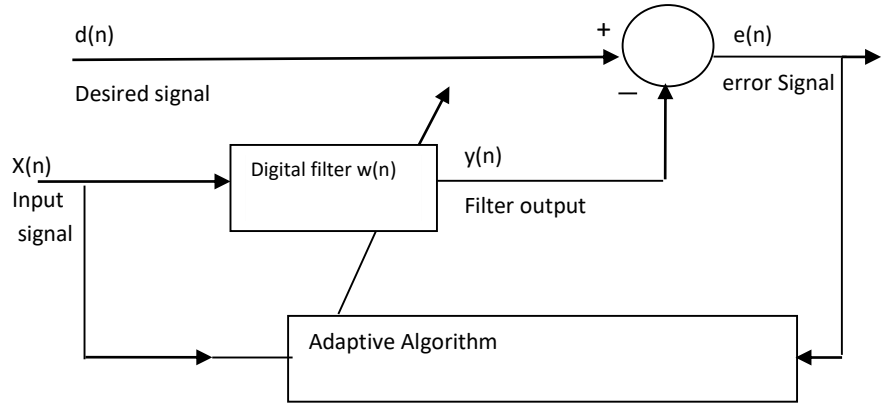

Figure 2.1. General structure of the adaptive filter.

2.4.1 Mean square error (MSE)

In the 1940s, due to research with important applications in communication theory, Norbert Wiener was investigating the problem of filter design that produces optimal signal estimation from a noisy measurement or observation [22]. The discrete form of the Wiener filtering problem, shown in figure (2.2) has basic idea that is to design a filter using a linear combination of the noisy reference X(n) to produces (recover) an estimate y(n) of the desired signal when the MSE function (cost function) is minimized [24, 29, 30]. This filter requires prior information on the statistics of the data to be processed, which is not generally possible in practice. The use of adaptive filtering techniques solves this problem. The cost function defined as the statistical mean squared error (MSE) is given by equation (2.1), which corresponding to the expected value of the squared error loss.

$$J(n) = E[\big(d(n) - y(n)\big)^2] = E[e^2(n)] \qquad (2.1)$$

The mean square error (MSE) leads to simple mathematics and has a special minimum that uniquely determines the optimum statistical filter design [23]. It is always positive, and the closer its value is to zero, it is the better.

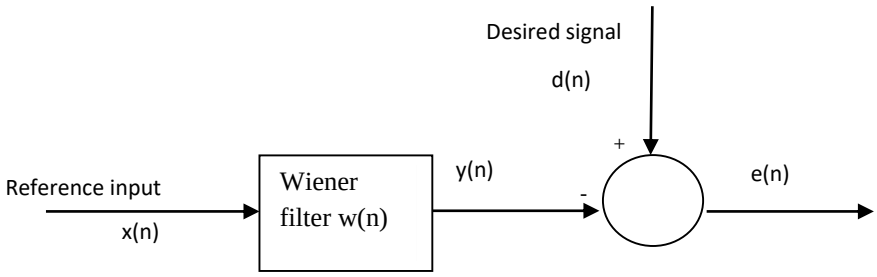

Figure 2.2. Wiener optimum filtering problem block diagram.

2.5 Performance measures in adaptive systems

Developing performance metrics for an adaptive filter is necessary to know how well a particular adaptive system is performing, also to offer comparative performance for diverse filter structures and adaptive algorithms to help in the suitable selection of a good solution in the limitations of the application. Such important features are:

- **Rate of convergence** is a very important performance criterion that must be evaluated; it means how much iteration is required to reach a close optimum Wiener solution [25].
- **Misadjustment**, is a ratio between the finale value and the minimum value of the mean square error obtained by Wiener solution, it measures how much the steady state solution calculated by an adaptive algorithm is away from the Wiener solution [23].
- **Tracking,** capacity to follow the variations in statistical properties of non-stationary environment [25].
- **Robustness**, Whether with regard to algorithmic ill-conditioning and arithmetic quantization error, or with regard to external noise disturbances, means that small disturbances yield only small estimation errors [29].
- **Computational Complexity,** means realistic power requirements, computational operations per iteration, data storage and programming requirements [25].
- **Numerical properties** concerns numerical stability and numerical accuracy, as their numerical is related to the degree of sensitivity of the adaptive algorithm to changes that occur during quantization process [23].

2.6 adaptive filtering configurations

Adaptive filters branch out into four basic configurations that are commonly used to solve practical engineering problems, the configurations are, system identification configuration, adaptive noise canceling configuration, adaptive linear prediction configuration, and inverse system configuration.

2.6.1 System identification configuration

System identification illustrated by the figure (2.3) is an approach for determining mathematical models of dynamic systems using measurements of the input and output signals of the system. By using the structure enforced by the adaptive system, the adaptive filter offers an unknown system model when the adaptive process has formed the optimum estimation in the MSE sense [29].

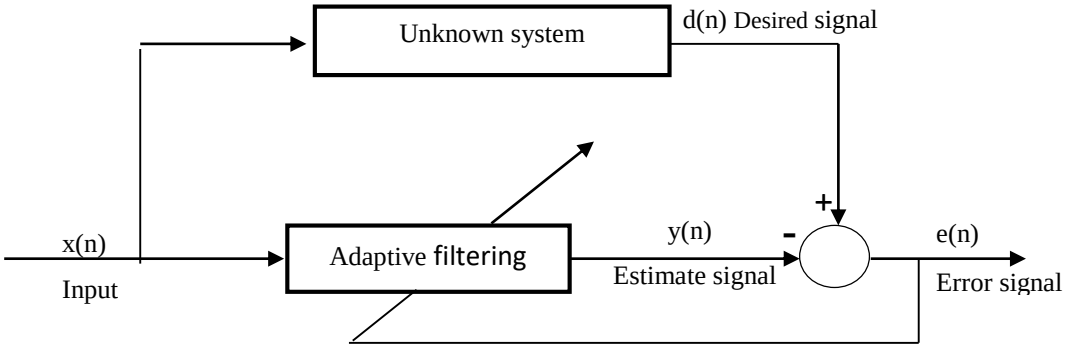

Figure 2.3. System identification configuration (Adopted from [29]).

2.6.2 Adaptive linear prediction configuration

In this configuration, an input vector X(n) is used to predict the output y(n), see figure (2.4), y(n) is the prediction value and strongly correlated with x(n) and e (n), which is used in line enhancement applications, while e(n) represents the prediction error, which is uncorrelated with X(n) is used in different applications like linear predictive coding [38].

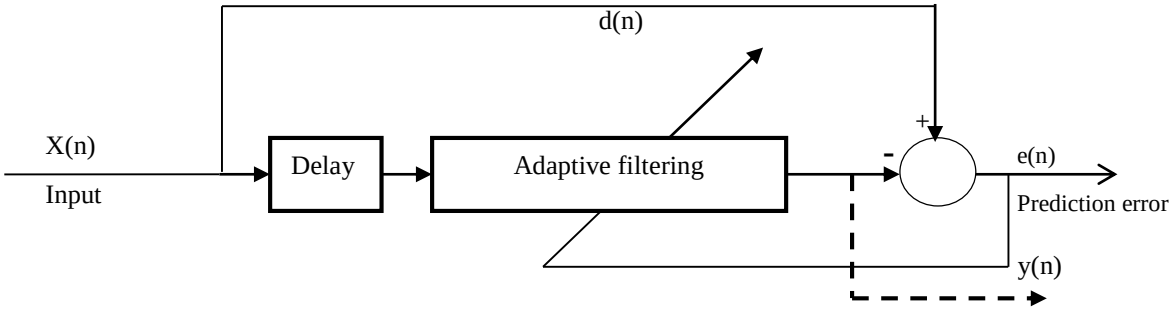

Figure 2.4. Linear prediction configuration (Adopted from [29]).

2.6.3 Inverse system configuration

In this configuration the adaptive filter is placed in series with an unknown system as shown by the figure (2.5), the adaptive algorithm drives the output y(n) to create the best MSE approximation to a delayed input signal. The adaptive algorithm drives the output y(n) to create

the optimum MSE estimation to a delayed of the input signal. This configuration is the basis for adaptive equalization [29], where reduces dispersion and eliminates inter-symbol interference in digital communications systems [38].

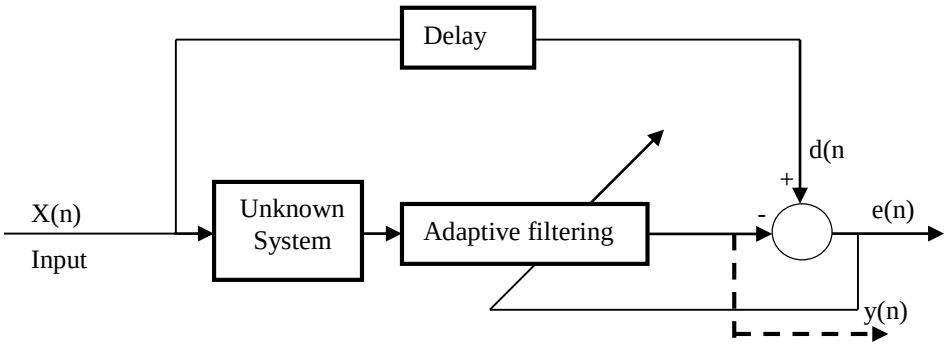

Figure 2.5. Inverse system configuration (Adopted from [29]).

2.6.4 Adaptive noise canceling configuration

An adaptive filter as noise canceller consists of two different components:

1. A filtering process which includes, (a) calculating an output of digital filter that have known special structure, and that have produced by a set of tap of inputs, (b) comparing the output filter to desired response in order to generate an estimation error[22,23].
2. An adaptive process, which includes an automatic adjustment of the filter tap weights according with estimation error.

Two input signals are applied directly and at the same time to the adaptive filter, the primary input, and the reference input, the first one is the noisy input which contains the desired signal d(n) and the noise $v_0(n)$, supposed uncorrelated with each other, the second one is the $v_1(n)$ which is considered as a measure of the noisy signal, assume that $v_0(n)$ and $v_1(n)$ are correlated in some unknown way [36], see figure (2.6) [23]. The reference input passes through a linear digital filter, to produce an output which is an estimate signal y(n) of the noise $v_0(n)$. The filter output is subtracted from the primary input to produce the system output e(n) which is given by equation (2.2).

$$e(n) = d(n) + v_0(n) - y(n) \qquad (2.2)$$

The obtained system output is used in a feedback arrangement to the digital filter in order to adjust the digital filter coefficients through liner adaptive algorithm, thus the system output acts as an estimate of the desired signal, and as an error signal for the adaptive process. The significance of the primary input, reference inputs, and the output system or method they are derived usually depends on the application they are incorporated into [22].

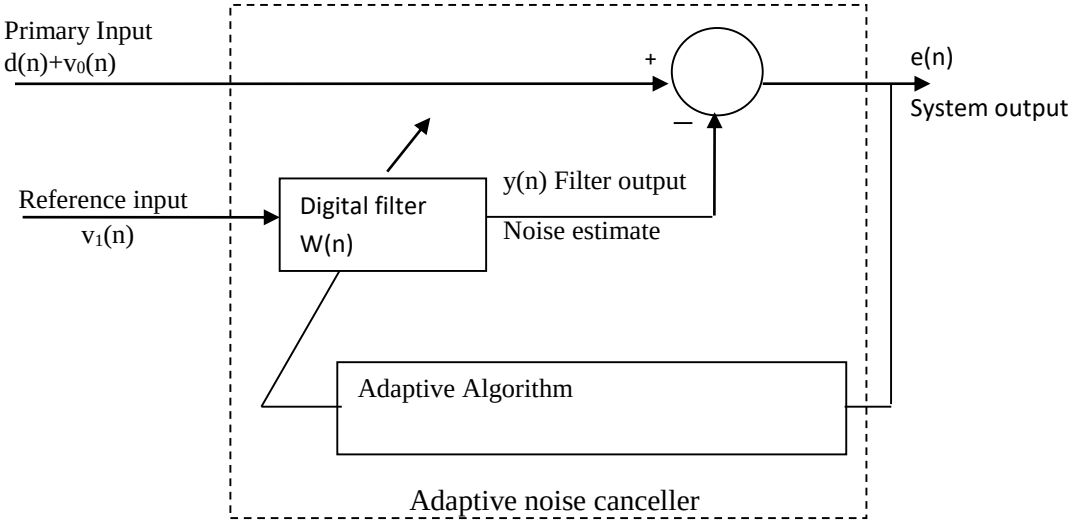

Figure 2.6 Adaptive filter as noise canceller block diagram [29].

Assume that d(n), v_0(n), v_1(n), and y(n) are statistically stationary, where v_0(n) and v_1(n) have zero means. By squaring equation (2.2), we get equation (2.3) as follows:

$$e^2(n) = d^2(n) + (v_0 - y)^2 - 2d(v_0 - y) \qquad (2.3)$$

Taking expectations of both sides of equation (2.2), and since the desired signal d(n) is uncorrelated with v_0(n) and with y(n), thus one obtain

$$E[e^2(n)] = E[d^2(n)] + E[(v_0 - y)^2] - 2E[d(v_0 - y)]$$
$$= E[d^2(n)] + E[(v_0 - y)^2] \qquad (2.4)$$

It is evident in equation (2.4) that if the estimate y(n) replicates $\boldsymbol{v_0}$(n), the output power will contain only the desired signal power $E[d^2(n)]$. When adjusting the adaptive filter towards the optimum solution, the remainder noise power $E[d(v_0 - y)]$ will also be minimized and hence the total output power $E[e^2(n)]$ is minimized, stating that the desired signal power will not be affected as the filter is adjusted to minimize the total output power, since d(n) and $\boldsymbol{v_0}$(n) are uncorrelated. Thus, the minimum output power is given by equation (2.5)

$$min\, E[e^2(n)] = E[d^2(n)] + min\, E[(v_0 - y)^2] \qquad (2.5)$$

It is evident from equation (2.5) that, since the desired signal power is unaffected, and then minimizing the total output power and minimizing the remainder noise power leads to maximize the output signal to noise ratio (SNR).

When the primary input comprises no noise ($\boldsymbol{v_0}(n) = 0$), the adaptive filter turns itself off (at least in theory) by setting all the weights to zero, while when the filter setting is such y(n) = $\boldsymbol{v_0}(n)$, thus the output of the adaptive filter canceller is noise free [22].

2.7 Linear digital filter structure

Since the structure of the digital filter has a deep impact on algorithm operation, the choice of the appropriate filter structure is a very important step in designing an adaptive filter system. There are three basic types of filter structures frequently used, the transversal structure that forms the basis of most used finite impulse response (FIR) discrete-time filter, infinite impulse response (IIR) or lattice predictor (a modular structure with a lattice appearance), and systolic array (a parallel computing network ideally suited for mapping important linear algebra computations) [23]. In this thesis FIR structure is considered.

2.7.1 FIR filters structure

The FIR filter structure is quite regular (also called FIR filter), as shown by figure (2.7); it has an arrow that shows the direction from the input toward the delay unit, but considerably no path exists from the output side back to the input side. It takes the name feed-forward (non-recursive filters) for this reason. A FIR filter that produces the minimum mean-square estimate of a given process d (n) is completely specified by the following system function:

$$w(z) = \sum_{n=0}^{M-1} w_n z^{-n} \qquad (2.6)$$

Where, (M – 1) is the order of the filter (the number of delay elements), and M is the length of the filter (which is equal to the number of coefficients), and w_n are the filter tap weights (coefficients). Assuming that X(n) and d(n) are jointly wide-sense stationary with known both autocorrelations and cross-correlation [24].

From figure (2.7) the FIR filter structure will filter a real-valued stationary process input X (n), to produce an estimate (output) y(n) of a desired real-valued signal d(n) [22]. By assuming that X(n) and y(n) have zero mean values, and filter coefficients do not change with time. Thus, the output y(n) is generated as a linear combination (which is a linear convolution) of the delayed samples of the input sequence X(n) and the filter coefficients according to input-output deference equation (2.7) relationship [30]:

$$y(n) = \sum_{k=0}^{M-1} w_k(n)x(n-k) = w^T X(n) \qquad (2.7)$$

Where, the tap inputs given by equation (2.8) form the elements of the M-by 1 tap input vector for X(n).

$$X(n) = [x(n)\ \ x(n-1)\ \ x(n-2).... x(n-M+1)]^T \qquad (2.8)$$

The tap weights shown by equation (2.9) form the elements of the M-by 1 tap-weight vector w (n)

$$w(n) = [w_0(n)\ \ w_1(n) ..... w_{M-1}(n)]^T \qquad (2.9)$$

Substitute equation (2.7) into equation (2.1), we obtain

$$J(w) = E\left\{\left(d(n) - w^T x(n)\right)^2\right\} \qquad (2.10)$$

$$= E\{\left(d(n) - w^T x(n)\right)\left(d(n) - w^T x(n)\right)\}$$

$$= E\{d^2(n)\} - 2w^T E\{d(n)x(n)\} + w^T E\{x(n)x(n)^T\}w$$

$$J(w) = \sigma_d^2 - 2w^T P_{dx} + w^T R_x w \qquad (2.11)$$

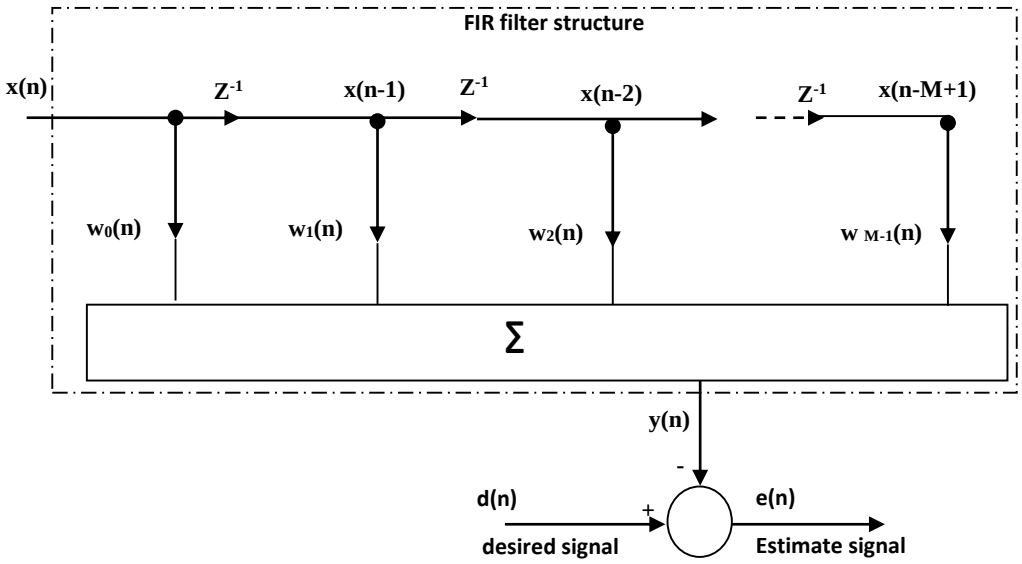

Figure 2.7 Adaptive filters with FIR transversal structure.

Where, $w^T x(n) = x(n)^T w$ (scalar), σ_d is the variance of the desired signal d (n), P_{dx} is M length cross correlation vector between d (n) (scalar) and the tap input vector X(n), and R_x is M x M autocorrelation matrix of the tap input X(n) [22].

Compared to some other filter structures such as IIR filter structures are always stable, quite simple, and can be designed to have a linear phase response, which is suitable in some applications [35]. The structure of the FIR filter includes four forms:

- **Direct form:** In this form the difference equation (2.6) is implemented directly as given (see figure 2.7). Only this form is considered in this thesis.
- **Cascade form:** In this form the system transfer function is factored into 2nd-order factors, which are then implemented in a cascade connection.
- **Linear-phase form:** the impulse response of this form shows particular symmetry conditions.
- **Frequency-sampling form**: A parallel structure obtained from a discrete Fourier transform of the impulse response [35].

2.8 Least mean square (LMS) algorithm

Once a filtering process using the appropriate filter is performed, a mechanism for performing an adaptive control process on the tap weights of the FIR filter is required; the adaptive weights control mechanism called an adaptive algorithm. A recursive adaptive algorithm is used to adjust the coefficients of the digital filter such as MSE according to some criterion. Least mean square (LMS) algorithm, Kalman filter algorithms, and recursive least square (RLS) are various algorithms that have proven effective in many filtering operations in many fields. The least mean square algorithm is the most efficient since it is characterized by numerical stability as other algorithms lack it [23].

The expression of the mean square error (cost function) in equation (2.11) represents a weights quadratic function, which resulted in "a bowl-shaped with unique bottom" when it is plotted versus adjustable filter coefficient w, this shape also known as the error performance surface that never goes negative, see figure (2.8) [23, 36]. To develop a recursive algorithm for adjusting transversal filter coefficients to minimize the error we should: first, perform a process of descending along this surface to get the "bottom of the bowl." this process can be implemented by using a well-known technique called steepest descent that requires the use of gradient vector. The gradient of performance surface (error) is obtained by differentiating equation (2.11) as follows

$$\nabla(J) \triangleq \frac{\partial(J)}{\partial(w)} = -2P_{dx} + R_x w \qquad (2.12)$$

Each set of filter coefficients represents to a point on the error performance surface (see figure 2.8). The optimal weight vector W_{opt} which is known as Wiener weight vector is obtained by setting the gradient of the mean square error function to zero:

$$\mathrm{w}_{\mathrm{opt}} = R_x^{-1} P_{dx} \qquad (2.13)$$

The equation (2.13) is a matrix form of the Wiener-Hopf solution (reflects the minimum point); it depends the correlation matrix of the tap input to the FIR filter, and on the cross-correlation vector between the same input and the desired response. In the second step, the instantaneous values of these correlations are used to drive an estimate for the gradient vector causing it to be stochastic character [23] [36]. The resulting algorithm is known as the least mean square (LMS) algorithm, invented by B. Widrow and M. E. Hoff in 1959. The LMS is a modified system of Wiener- Hopf equations and was used to find close approximate solutions to equation (2.13) in real-time. It is obtained by an implementation of the steepest descent method, where the weight vector is updated from sample to sample as follows:

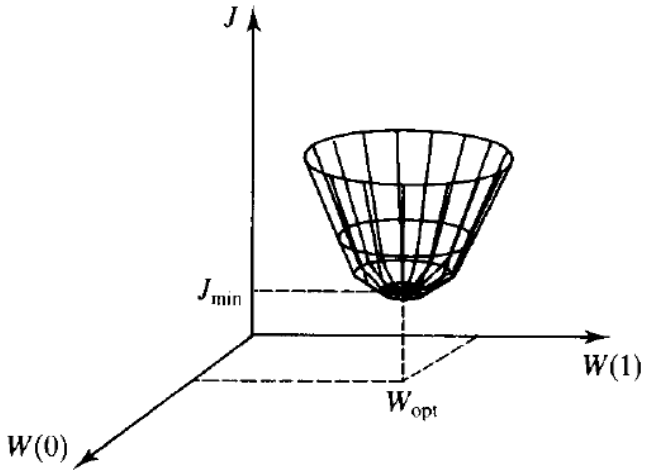

Figure 2.8 Concave hyperparaboloid error function [22].

$$w_{n+1} = w_n - \mu \nabla(J) \qquad (2.14)$$

The parameter μ is the factor that controls the stability and the rate of convergence, w_n and $\nabla(J)$are the weight and the true gradient vectors respectively.

Since the true gradient is derived from equation (2.12), the steepest descent algorithm in equation (2.14) still needs the knowledge on cross correlation vector and autocorrelation matrix. In this case the LMS algorithm seeks to replace the true gradient by the estimate gradient that is given by equation (2.15).

$$\hat{\nabla} = -2 e_n x_n \qquad (2.15)$$

Then by substitute equation (2.15) in equation (2.14), we obtain the Widrow Hopf LMS algorithm for updating the weight from sample to sample as follows:

$$w_{n+1} = w_n + 2\mu e_n x_n \qquad (2.16)$$

The LMS algorithm uses instantaneous estimates of the signal (such correlation and cross-correlation) statistics while it does not need prior information of these statistics. The estimates of weights obtained by the LMS algorithm slowly improve over time as the weight is adjusted and the filter discovers the characteristics of the signal [22]. Filter weights are converging according to the following condition:

$$0 < \mu < \frac{2}{\lambda_{max}} \qquad (2.17)$$

Where, λ_{max} is the maximum eigenvalue of the input data matrix R_x. The algorithm will convergent in the mean square (i.e. the algorithm should satisfy J (∞) =constant) and will remain stable as long as the step size parameter μ is greater than 0 but less than the reciprocal of the largest eigenvalue λ_{max} [23, 32].

The condition convergence (2.17) on μ can be related to the total input power as follows:

$$\lambda_{max} = \sum_{k=0}^{M-1} x^2(n-k) \qquad (2.18)$$

Where, $\sum_{k=0}^{M-1} x^2(n-k)$ is the tap-input power is the sum of the mean square values of all the tap inputs in the transversal filter [37].

The Summary of the LMS recursion algorithm is given by table (2.1)

Table 2.1. Summary of the LMS algorithm

Inputs	**Tap-weight vector w(n).** **Input vector X(n).**
μ, M, N, λ_{max}	Parameters initialization
$0 < \mu < 2/\lambda_{max}$	Set condition
$w(n) = [w_0(n)\ w_1(n) \ldots . w_{M-1}(n)]^T = 0_{Mx1}$	Initialized filter coefficient vector
For n =0, 1…. N-1	Processing
$x(n) = [x(n)\ x(n-1)\ x(n-2) \ldots . x(n-M+1)]^T$	

Output	Filter output, y(n), Tap-weight vector update, w_{n+1}
$y(n) = w^T x(n)$	Filtering
$e(n) = d(n) - y(n)$	Compute error
$w_{n+1} = w_n + 2\mu e_n x_n$	Adaptation
End	

2.8.1 Characteristics of the LMS algorithm

Since the LMS algorithm is simple, easy to implement, performs strong performance according to the independence of its model, involves a step-size parameter that can be selected suitably to control stability and convergence speed of the algorithm, and does not require squaring, averaging, or differentiation, it is still required to reach satisfying performances during adaptation process under appropriate conditions [30]. The LMS only requires (2M +1) multiplications and (2M+1) additions per iteration, where its performance depends on three factors:

- The eigenvalue of the input data matrix R_x,
- The length M of the filter w.
- The adaptation step size μ, where with a small adaptation step, the LMS converges slowly, while with a large adaptation step size, the LMS converges quickly but perhaps less stable around the minimum value. Where the LMS convergence analysis is performed using the convergence of J(n) criterion, i.e. if the $\lim_{n\to\infty} J(n) = J(\infty) =$ constant, or equivalently, $\lim_{n\to\infty} E\{w(n)\} = w_{opt}$, thus the LMS algorithm is said to be convergent in the mean-square, and μ has to satisfy condition (2.17) [23].

2.8.2 Limitation of the LMS algorithm

The main limitation of the LMS algorithm is it suffers from relatively slow convergence and is sensitive to the ratio of the largest to smallest eigenvalue (condition number) of the tap inputs correlation matrix, the higher the ratio, the slower the convergence [25].

A small value of step size achieves the optimum value but results in slow convergence, which is equivalent to the LMS algorithm having a long memory, as a result, the excess mean-squared error after adaptation is small. On the other hand, the large value of step size achieves faster adaptation but leads to an increase in the average excess mean-squared error after adaptation. And therefore; fewer data enter the estimation that leads to lower error estimation performance [30, 22].

Many modified LMS-type algorithms were proposed by researchers over the past years, with the aim to overcome the limitations of the LMS algorithm such as improving convergence behavior, reduce computational requirements. Such modified LMS-type algorithms are the data sign algorithm, error sign algorithm, normalized LMS (NLMS) algorithm, leaky LMS algorithm, variable step-size LMS (VSLMS) algorithm, and error normalized LMS algorithms [30]. In this thesis, we consider only the NLMS algorithm and the leaky LMS algorithm.

2.9 Normalized least mean square (NLMS) algorithm

The NLMS is a modified implementation of an ordinary LMS algorithm that selects a normalized step-size parameter. It has been proposed to make the LMS algorithm less dependent on characteristics of stochastic signals and the convergence rate insensitive to the power level of the input signal; by introducing the normalization of the step size. The implementation of the NLMS is derived from the same steps and the same equations as the LMS [30]. The difference is in the updating of the weights according to the following formulation:

$$w(n+1) = w(n) + \mu(n)\big(x(n)e(n)\big) \qquad (2.19)$$

$$\mu(n) = \frac{\mu}{x^T(n)x(n)} \qquad (2.20)$$

The term $\mu(n)$ is the normalized version of the step size μ also called a time-varying step-size parameter. The normalized LMS algorithm is convergent in the mean square if the adaptation constant satisfies the following condition [23]

$$0 < \mu < 2 \qquad (2.21)$$

In practice, a more relaxed recursion is used that guarantees reliable results. Hence, we write

$$w(n+1) = w(n) + \frac{\mu}{\rho + x^T(n)x(n)}\big(x(n)e(n)\big) \qquad (2.22)$$

Where, $\rho + x^T(n)x(n)$ is the normalization factor and ρ is a small positive constant introduced to preserve the stability in cases where the power of the input is close to zero.

The NLMS algorithm advantageous in reliable complexity of calculations, numerical stability, more suitable in filtering non-stationary signals such ECG signal, stability as well as convergence towards optimal solutions are easier, and most importantly, the normalized

LMS algorithm presents a rate of convergence that is faster than that of the ordinary LMS algorithm for both correlated and uncorrelated input data [30]. While as inconvenient the convergence can become very slow in some cases such as filtering speech. The Summary of the NLMS recursion algorithm is given in table (2.2).

Table 2.2 Summary of the NLMS algorithm.

Inputs	**Tap-weight vector w(n).** **Input vector X(n).**
$\mu, M, N, \rho > 0$	Parameters initialisation
$0 < \mu < 2$	Set condition
$w(n) = [w_0(n)\ w_1(n) \ldots . w_{M-1}(n)]^T = 0_{Mx1}$	initialized filter coefficient vector
For n =0, 1…., N-1	Processing
$X(n) = [x(n)\ x(n-1)\ x(n-2) \ldots . x(n-M+1)]^T$	
Output	Filter output y(n). Tap-weight vector update w_{n+1}
$y(n) = w^T X(n)$	Filtering
$e(n) = d(n) - y(n)$	Compute error
$w(n+1) = w(n) + \frac{\mu}{\rho + x^T(n)x(n)}(x(n)e(n))$	Adaptation
End	

2.10 Leaky least mean square (LLMS) algorithm

The implementation and design of LMS algorithm filtering digitally require a quantization step that is defined as a process converting from infinite precision to finite precision arithmetic, there are three considerations have to quantize, filter coefficients to obtain their finite word-length representations, the input sequence [33], and all internal arithmetic. The process quantization may affect the overall quality of adaptive filter output (round-off error injected into the output of digital filter) by the most known effect called round off error [35]. This error causes a stalling phenomenon that means the digital implementation of LMS stops adapting which occurs when the correction term (quantized element) is too small, also causes the filter driven into an overflow condition which leads the algorithm to be numerically unstable. The impact of the error on the LMS algorithm is further increased when the input data autocorrelation matrix R_x is ill-conditioned (almost singular) [23].

For increasing LMS algorithm robustness, and further stabilize the digital implementation of LMS algorithm; the introduction of leakage coefficient into LMS algorithm was needed to

get leaky least mean square algorithm LLMS [33, 34]. In the Leaky LMS algorithm, the cost function given by equation (2.22) is minimized with respect to the weight vector $w(n)$.

$$J(n) = e^2(n) + \gamma\|w(n)\|^2 \qquad (2.23)$$

Where, $e^2(n)$ is the squared estimation error, $\gamma\|w(n)\|^2$ is the energy in the tap weight vector $w(n)$, and γ is positive control parameter.

The weight update equation of LLMS algorithm obtained after the minimization of equation (2.23) is given by equation (2.24) as follows:

$$w(n+1) = (1 - \mu\gamma)w(n) + \mu\, x(n)\, e(n) \qquad (2.24)$$

The factor$(1 - \mu\gamma)$ is called leakage coefficient that satisfies the follow condition:

$$0 \leq \gamma < \frac{1}{\mu} \qquad (2.25)$$

The leaky LMS algorithm is an intelligent technique that increases the eigenvalues of the underlying correlation matrix by controllable constant [30], and avoids the appearance of the overflow by delivering a compromise between minimizing the square error and containing the energy in the impulse response of the adaptive filter [23]. The Summary of the LLMS recursion algorithm is given in table (2.3).

Table 2.3. Summary of the NLMS algorithm

Inputs	**Tap-weight vector w(n).** **Input vector X(n).**
μ, M, N, γ	Parameters initialisation
$0 \leq \gamma < \frac{1}{\mu}$	Set condition
$w(n) = [w_0(n)\ w_1(n) \ldots . w_{M-1}(n)]^T = 0_{Mx1}$	initialized filter coefficient vector
For n =0, 1…., N-1	Processing
$X(n) = [x(n)\ x(n-1)\ x(n-2) \ldots . x(n-M+1)]^T$	
Output	Filter output y(n). Tap-weight vector update w_{n+1}
$y(n) = w^T x(n)$	Filtering
$e(n) = d(n) - y(n)$	Compute error
$w(n+1) = (1 - \mu\gamma)w(n) + \mu\, x(n)\, e(n)$	Adaptation
End	

2.11 Conclusion

In this chapter, we have presented the working principle of adaptive filtering, how it was derived from Wiener filter solution, its various configurations, its main components with their structure and functions, and the mechanism of filter coefficient adaptation.

Since the adaptive filter is a self-designing filter and does not need a prior knowledge of input characteristics, and more important that it has the ability to track the variations in statistical properties of non-stationary signal such as ECG signal, thus it is the optimum solution to denoise the noisy version of that signal. the following chapter deals with filtering a corrupted ECG signal from unwanted noises using an adaptive filter as noise canceller configuration with multistage and combined algorithms, also filtering theory of ECG signal with other different known technique will presented for the comparison.

Chapter 3

ECG signal filtering

3.1 Introduction

Many methods have been proposed in the literature for removing noise from the heart signal, some of which are classic, and some that are adaptive. In this chapter, we are interested in a detailed presentation of the method that we have proposed to remove noise from the ECG signal which is based on adaptive noise canceller filter, then we provide an overview of the concept of stationary wavelet transform and its basics in filtering the ECG signals as a second method that we have proposed and implemented in this thesis to compare both methods, in addition to mentioning some related work in filtering muscle noise, base wandering noise and electrical motion effect.

3.2 ECG signal filtering

Filtering the noisy ECG signals from unwanted interference is the first step in the processing and analysis of the ECG signal and is necessary for the effectiveness of dependent steps in the processing such as data compression, feature selection, signal classification, and interpretation, to obtain a clear and undistorted signal that helps detect any defects.

3.2.1 Baseline wander filtering

Baseline wander is the slow-varying distortions, in its standard shape it is taken as a reference to study the shape and height of the different heart waves [14]. Typically, frequency content of baseline wander is usually in the range below 0.5 Hz, but increases during the stress test. Removal of baseline wander is needed in order to reduce changes in beat morphology that do not have cardiac source [6].

Several types of methods have been presented in the literature in order to eliminate this type of noise. The methods often rely on high-pass filtering, usually based on finite impulse response filters [38, 39]. The major drawback of these methods is signal distortion due to the spectra overlapping of the ECG and baseline wander. It is not possible to completely remove this type of noise with these filtering methods without causing signal distortion [40]. In [41], the authors proposed a method based on multivariate empirical mode decomposition to remove the baseline wander (BW) from the ECG signal. They estimate the baseline wander by a sum of IMFs numbered N and $N - 1$, then the baseline corrected signal can be obtained by subtracting the estimate from the original ECG signal. The method showed its ability to remove BW of the ECG signals and preserving the morphology of the ECG signals. In [42], the authors took a simulation study between five filtering techniques used in literature, Butterworth high-pass

filter, moving median and subtraction, spline approximation and subtraction, and discrete wavelet transform (DWT); to wander removal considering the preservation of ST changes in the ischemic ECG. The comparison showed the best results when using discrete wavelet transform that. However, the Butterworth high-pass filter is the better choice for medical applications. In [43], the authors propose a methodology based on the eigenvalue decomposition of the Hankel matrix to remove baseline wander and power line interference from ECG signal, these noises were removed simultaneously by eliminating eigenvalues corresponding to noisy constituents. The method achieved better results in comparison with other existing techniques in terms of output SNR, and the percent root mean square difference (PRD). In [44], to remove the baseline wander from ECG signal; the authors proposed a methodology based on the Combination of mathematical morphological filtering (MMF) algorithm and wavelet transformation. The combination overcomes the shortcomings in wavelet transform that introduce distortion in T wave and the shortcomings in MMF method that introduce the rectangular/trapezoidal distortions. The method showed effectiveness in preserving the outline of the BW and avoiding waveform distortions caused by the morphology filter.

3.2.2 Muscle noise filtering

The muscle noise is very difficult to deal with because it behaves like a random wideband spectrum signal, seriously overlapping the ECG spectrum; mainly with the spectrum of the QRS complex. The efforts to remove muscle noise lead to significant distortions of the ECG signal [45]. Many denoising methods were proposed for EMG noise removal from ECG signal, Thakor NV, Zhu YS proposed a recurrent least mean square (LMS) filter structure for obtaining the impulse response of the normal QRS complex and then applied it for arrhythmia detection in ambulatory ECG recordings, they show the effectiveness of such recurrent filter in detecting cardiac arrhythmia by noise reduction. However, the filter does not work adequately when only a single lead is available or when EMG noise arises at all the electrodes [46]. El B'charri et al. investigated the dual-tree wavelet transform (DWT) using tuning threshold to reduce synthetic, realistic, and colored noises in ECG signals; the performance of the method is affected by varying the threshold value, wavelet function, and decomposition level, the method achieved superior results over conventional DWT in removing all kinds of noises. However, wavelet is a non-adaptive tool in denoising ECG signal because of its dependence on the selection of wavelet function and thresholding technique [47]. Venkatesan et al. proposed a delayed error normalized LMS (DENLMS) with pipelined architecture for noise removal from ECG signal;

a comparison with error normalized mean square (NLMS) and delayed NLMS algorithms, the pipelined DENLMS showed an increase in operation speed and reduction in power consumption because of the aspect of latches [48]. Kumar et al. proposed a combination filter between empirical mode decomposition (EMD) with a non-local mean (NLM) to denoise ECG signal; They collected information related to the input noise by calculating the differential standard deviation before passing it to the EMD filter with the aim of reducing noise, then the output obtained is passed through the NLM with aim of preserving ECG signal edges; the method showed superior results in term of mean square error (MSE), mean SNR improvement, and mean of percent root- mean-square difference (PRD). EMD is not ideal in denoising non-stationary signals unless it is combined with another algorithm [49]. Suranai and Xiao-Hua proposed a combination between multi-resolution discrete wavelet transform (DWT) and the adaptive learning potentiality of artificial neural networks for noise removal from ECG signal, the obtained coefficients from the thresholding technique in the DWT step was used as input to the neural network in the initial filtering. Then, the obtained filtered ECG signal after converted to the time domain was used as input to the neural network in final filtering; the neural network in the final filtering accomplishes the inverse DWT to the output. The combination showed satisfactory results to remove the noise with important improvement on SNR [50]. Zia-Ur-Rahman et al. proposed an adaptive noise canceller based on leaky NLMS algorithm for noise removal from ECG signal, by introducing a new variable step size containing the leaky coefficient in the weight update function; the results showed that the performance of the LNLMS based algorithm outperforms LMS based algorithm either in quantitative and qualitative results [51]. M. Liu et al. proposed a guided filter based on Butterworth high-pass filter for EMG and EM-based noises removal from ECG signals; a pre-filtering of ECG signals using Butterworth high-pass filter was used to remove BW, then removed ECG signals whose frequencies are between the BW will be retrieved using the edge-preserving guided filter passing through average template algorithm, The obtained results showed better SNR, root-mean-square error (RMSE), and features edge-preserving compared with other methods. However, the method has the risk of not recovering all the removed information which is important for interpreting the ECG signal [52]. In [53], the authors proposed to remove the muscle noise from ECG signal using the output of wavelet Wiener based filter and to design a variant of NLMS algorithm, where, they conclude that the wavelet functions sym8 for wavelet bank1, rbio1.1 for wavelet bank2, decomposition level of 4, LSMU threshold, and garrote rule combined with NLMS algorithm are suitable of removing muscle noise and gives the best performances compared to other factors.

3.2.3 Electrode motion artifact filtering

Electrode motion artifact causes significant baseline fluctuation, and doubt of large amplitude signals [21], and it is difficult to deal with because its spectral content of the motion artifacts significantly overlaps with the content of the PQRST complex. Several denoising methods were proposed for motion artifact removal from the ECG signal, in [54], authors proposed an adaptive filter to remove the electrode motion artifact from the ECG signal. They used an accelerometer to measure the acceleration signal of the vibrations or movement of the trunk, then this measured signal was considered as the reference input to the adaptive filter, where the least mean square algorithm was chosen to adjust to the weight of the adaptive filter. The Experiments showed the effectiveness in distinction the QRS complex. In [55], the authors proposed an online method based on a feed-forward neural network with three hidden layers to denoise very noisy ECG signal from motion artifacts. This denoising method showed a slight reduction in sensitivity, and an improvement in the positive predictivity. In [56], the authors proposed an online method based on wavelet based threshold methods with grey incidence degree threshold (GID) to remove motion artifacts from ECG signal. This method and according to the noise intensity, the grey incidence degree between approximation coefficients and detail coefficients, sets the thresholds on a different level of decomposition, then the selected thresholds adjust wavelet filter coefficients. The method gives filtered ECG signals with better smoothness and similarity. In [57], the authors proposed a method based on adaptive Fourier decomposition (ADF) for muscle and electrode motion artifacts removal from ECG signals. These noises were filtered by an ADF with the estimated-SNR based decision, and by introduced rules to choose and adjust the best decomposition level. The method outperforms other existing techniques such as Butterworth low pass filter, the EMD, and the wavelet transform. In [58], the authors proposed a Two-stage adaptive filter for motion artifact removal from the ECG signal. In the first stage which is the weighted adaptive noise canceller, the input motion artifact reference is replaced by an acceleration derivative, and the Pearson correlation coefficient between acceleration and ECG was used as the weighting factor. While in the second stage which is a recursive Hampel filter-based estimation method (RHFBE), spatial correlation of the ECG segment constituent that is obtained from sequential ECG signals is used to estimate the ECG signal segments. The method achieved a promising enhancement in the denoising ECG signals. In [59], the authors proposed empirical wavelet transform (EWT) and wavelet thresholding (WT) for motion artifact removal from the ECG signal. The method comprises five steps, spectrum preprocessing and is the first in which a noisy ECG signal is transmitted,

spectrum segmentation, EWT decomposition, wavelet threshold denoising, and EWT reconstruction. The method showed in either simulation ECG signals or practical non-contact ECG monitoring systems, effectiveness in filtering out the motion artifact.

3.3 Proposed approach

In this work, an adaptive filter based on the noise canceller configuration and a combined adaptive algorithm is proposed to remove three kinds of noises that may interfere with ECG signal (in the original paper only the EMG noise was considered). The structure of the proposed filter consists of three distinct parts; inputs, self-correcting ECG noise adaptive canceller, and the outputs.

3.3.1 First input to the adaptive filter

Our proposed adaptive method has been validated using diverse real free noise ECG signal recordings with a large collection of wave morphologies from MIT-BIH arrhythmia database [60], and three real noises, baseline wander (bw), muscle (EMG) artifact (ma), and electrode motion artifact ('em'), are taken from MIT-BIH noise stress test database (NSTDB) [61]. Then, we perform the addition process the add any noise signal (under various signal to noise ratio level (SNR_{inp})) to the clear ECG signal to get the noisy ECG signal which is the input to the digital filter, the desired signal here is the clear ECG signal.

3.3.2 Self-correcting ECG noise adaptive canceller

The self-correcting [62] ECG noise adaptive canceller is multistage of one adaptive noise canceller, in the first stage, the first input which is the contaminated ECG signal passes through the digital FIR Wiener filter described by equation (2.7) to get the first filtered output, this later is subtracted from the clear ECG signal to get the first error signal which is needed to perform the adaptive algorithm required to update the filter coefficients. In the second stage, we will apply the same process as we did in the first stage, but the input to the FIR Wiener filter is the previous filtered output. The number of stages depends on the reached maximum SNR, minimum MSE, and the observed i^{th} output filters. The output of the i^{th} stage is related to the previous one by equation (3.1) as follows:

$$y_{i+1}(n) = y_i * w_{i+1} \tag{3.1}$$

Where, i=1… I, is the number of stages.

3.3.3 Leaky normalized least mean square adaptive algorithm

After obtaining the error signal e(n), it is used to perform the adaptive algorithm proposed in [51], the leaky normalized least mean square algorithm (LNLMS) is introduced by combining LLMS and NLMS algorithms in the aim to improve both stability and filtering capability because of the normalization factor and leaky coefficient. The weights update relation for LNLMS algorithms is given by equation (3.2) as follows:

$$w(n+1) = w(n) + \frac{(1-\mu\gamma)}{\rho + x^T(n)x(n)}\, x(n)\, e(n) \qquad (3.2)$$

The new time varying step size parameter normalized with every new sample according to input power in equation (3.2) and leakage parameter is given by equation (3.3), As the input signal power changes, the algorithm computes the input power and adjusts the step size to preserve an adapted value. Thus the step size changes with time and hence the LNLMS improves the convergence performance.

$$\mu(n) = \frac{(1-\mu\gamma)}{\rho + x^T(n)x(n)} \qquad (3.3)$$

The weights update equation (3.2) is applied in the first stage only, where in the following stages we propose to apply the weights update equation (3.4) given as follows

$$w_i(n+1) = w_i(n) + \frac{1-\mu_i\gamma_i}{\rho + x_i^T(n)\, x_i(n)}\, x_i(n)\, e_i(n) \quad (3.4)$$

Where, i=1... I, is the number of stages, and $x_i(n)$ here is the new input which corresponds to the previous filtered output i.e.

$$x_i(n) = y_{i-1}(n) \qquad (3.5)$$

In equation (3.4) we proposed that the time varying step size also changes according to the variable value of the expression $(1-\mu_i\gamma_i)$ form stage to stage, which means that the parameters $\mu, \mu_i, \gamma, \gamma_i \ldots \mu_I, \gamma_I$ are different from stage to stage. The proposed approach is represented by figure (3.1).

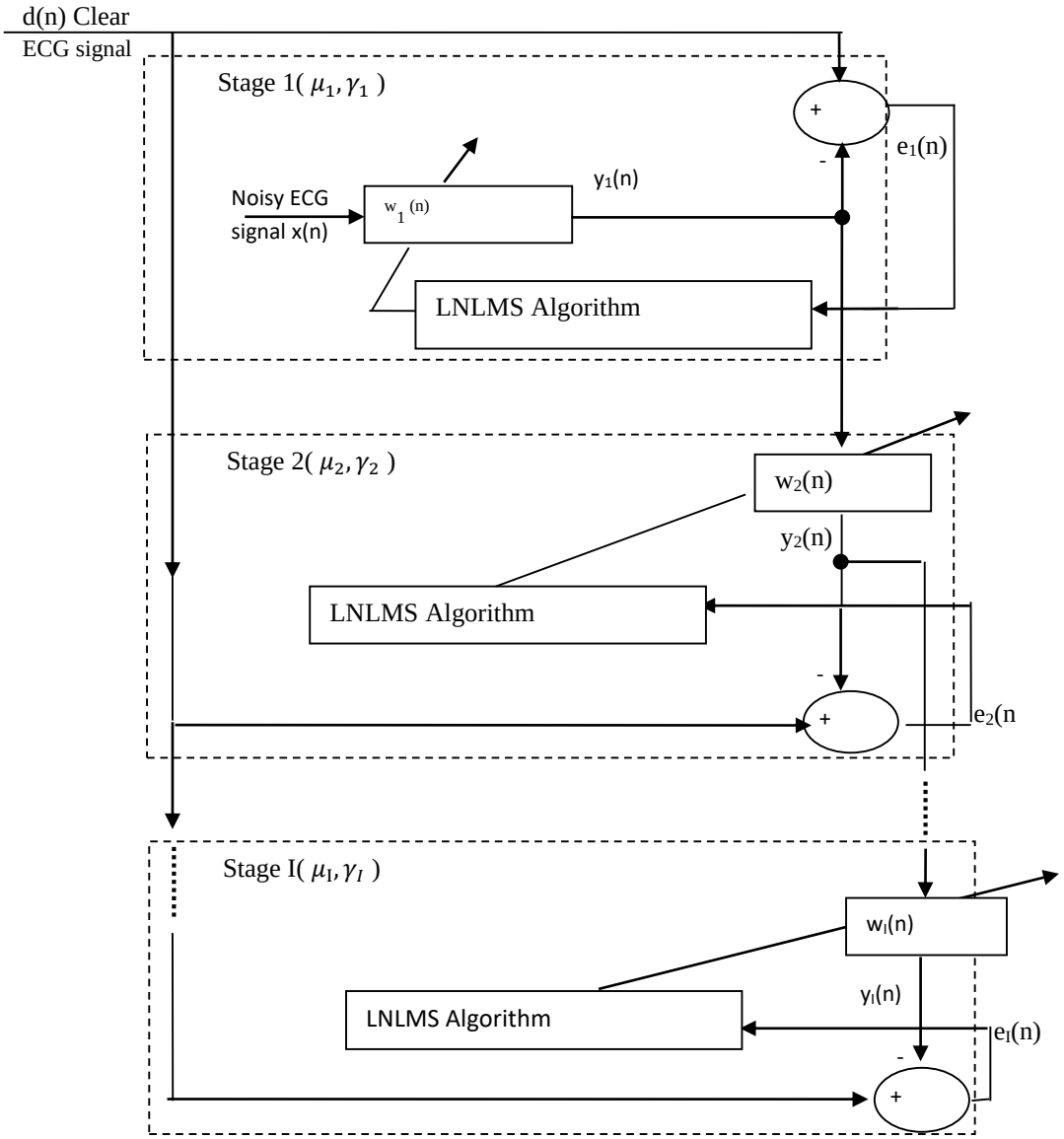

Figure 3.1 Block diagram of the self-correcting adaptive filtering (SCAF) based on SC-LNLMS algorithm

3.3.4 Outputs from the adaptive filter

The number of the adaptive filters is equal to the number of stages used during the filtration, where we determine the number of stages according to the reached maximum SNR, minimum MSE, and observed i^{th} output filter with taking care to preserve the standard shape of the ECG signal with all its waveforms, intervals, and segments. The output of the i^{th} stage is given by equation (3.6) as follows:

$$y_{i+1}(n) = y_i * w_{i+1} \qquad (3.6)$$

Where, $y_i$is the previous filtered output.

3.4 Comparative study

3.4.1 Stationary wavelet transforms approach

The wavelet transform (WT) is an effective tool in the ECG signal denoising and it is the best choice then classical filtering, as is local in both frequency/scale and time, which does not happen in typical filter design [63][64], see figure (3.2). Wavelet transform has two main concepts, scaling (frequency) and shifting (time);

- Scaling means stretching or shrinking the signal in time, the scaling factor which is a positive value corresponds to how much a signal is scaled in time, a larger scale factor results in a stretched wavelet, which corresponds to a lower frequency, while a smaller scale factor results in a shrunken wavelet, which corresponds to a high frequency. A stretched wavelet helps in catching the slowly varying changes in a signal while a compressed wavelet helps in catching abrupt changes [65].
- Shifting means advancing or delaying the onset of the wavelet along the length of the signal. Shifting the wavelet is needed to align with the feature we are looking for in the signal [66] [67].

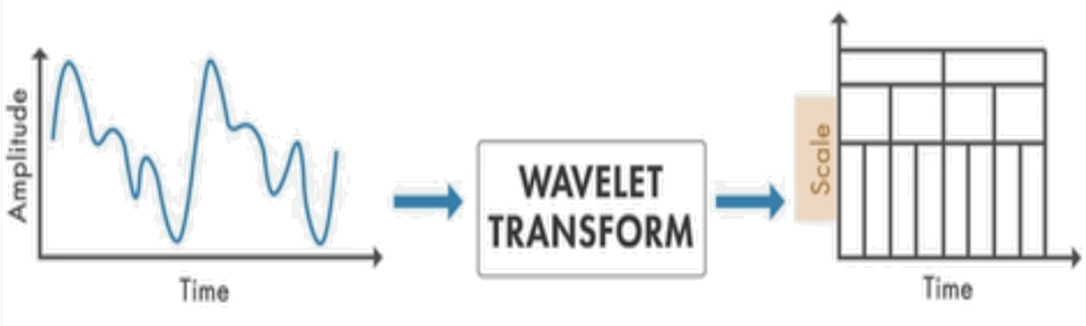

Figure 3.2 Concepts of wavelet transform.

The scaling and shifting concepts are combined to generate the mother wavelet (wavelet function) described by equation (3.7), the conjugate of the mother wavelet is used to be convolved with the original signal in order to transform this later in the wavelet domain and to extract needed coefficients. The most known wavelet transform are continuous wavelet transform (CWT) given by equation (3.8), discrete wavelet transform (DWT) described by equation (3.9) which is the discrete version of the CWT, and the Stationary wavelet transforms (SWT). The SWT is an offshoot of the conventional discrete wavelet transform (DWT), where it was introduced to restore translation invariance (stability), which classic DWT lacked [63] [65]. When using SWT, the signal is never sub-sampled, and the filters are up-sampled at each

level of decomposition, i.e. the obtained coefficients have the same length as the original signal, also the energy of a signal is conserved. In terms of the equations the slight difference between DWT and SWT lies in the parameter, called ε decimated DWT [65]. SWT is widely used for several applications such as breakdown points detection, where denoising a corrupted signal is its main application [66].

$$\varphi_{a,b}(t) = \frac{1}{\sqrt{b}}\,\varphi\left(\frac{t-a}{b}\right) \qquad (3.7)$$

Where the parameter a, is the scale of wavelet (dilatation) and the parameter b is the translation of the wavelet and indicates the time localization [68].

$$C(a,b) = \int_{-\infty}^{+\infty} x(t)\,\varphi^{*}_{a,b}(t)d(t) \qquad (3.8)$$

$x(t)$, is the signal, and $\varphi^{*}_{a,b}(t)$ is the conjugate of the mother wavelet. By different discretize of the scale and the translation parameters as $b = 2^{-s}$ and $a = 2^{-s}\tau$, we obtain the dyadic DWT equation as follows:

$$W(\tau, s) = 2^{\left(\frac{s}{2}\right)} x(n)\varphi(2^{s}n - \tau) \qquad (3.9)$$

Where s, τ are the scale and the shifting factors respectively (s=0, 1,…, $\tau = 0,1, \ldots..$)
The general SWT based method for denoising the corrupted signal is to transform the data into the wavelet domain by decomposing the signal into many levels, thresholding the wavelet coefficients, and invert the transform to reconstruct the signal.

3.4.1.1 Multilevel stationary wavelet decomposition step

The idea is to transform the corrupted signal into the wavelet domain by performing multilevel (scale) wavelet decomposition to obtain two types of coefficients; approximate and detail coefficients. For each level, the two coefficients can be obtained by convolving the corrupted signal with the appropriate filters, where approximate coefficients often resemble the signal itself and are obtained by convolution with a low pass filter named *h*, while detail coefficients are obtained by convolution of the signal with a high pass filter named g, see figure (3.3). In conventional DWT decomposition at level *l*, the approximate coefficients at level *l* (cAP^{l}) [63], and detail coefficients at level *l* (cDT^{l}) are given by equation (3.10) as follows:

$$\begin{cases} cAP^{l} = (h)\,cAP^{l-1}, & l = 1,2,\ldots,L \\ cDT^{l} = (g)\,cDT^{l-1}, & l = 1,2,\ldots,L \end{cases} \qquad (3.10)$$

L is the maximum decomposition level; and $\boldsymbol{cA^0}$ is the original signal. The parameter ε in equation (3.10) is always 0, shifted by 0, and then the SWT decomposition at level l can be written by equation (3.11) as follows:

$$\begin{cases} scAP^{l}_{\varepsilon_{1,\dots}\epsilon_l} = \left(h^{l-1}\right) cAP^{l-1}_{\varepsilon_{1,\dots}\epsilon_{l-1}} & ,l = 1,2..L \\ scDT^{l}_{\varepsilon_{1,\dots}\epsilon_l} = (g^{l-1})\, cDT^{l-1}_{\varepsilon_{1,\dots}\epsilon_{l-1}} & ,l = 1,2..L \end{cases} \quad (3.11)$$

In equation (3.11) $\varepsilon = [\varepsilon_1, \dots \varepsilon_l]$, and are selected 0 and 1 respectively, h^l , g^l are low pass and high pass filters respectively and satisfied the condition given by equation (3.12) as follows:

$$\begin{cases} h^l \uparrow 2 = h^{l+1}, & h^0 = h \\ g^l \uparrow 2 = g^{l+1}, & g^0 = g \end{cases} \quad (3.12)$$

Thus in SWT, the approximate coefficients ($scAP^{l}_{\varepsilon_{1,\dots}\epsilon_l}$), and the detail coefficients ($scDT^{l}_{\varepsilon_{1,\dots}\epsilon_l}$) have the same length of the original signal ($scAP^{0}_{\varepsilon}$), where the length of the signal must be divided by 2^L. in this step the decomposition of the corrupted signal is based on the suitable level and suitable wavelet function [63].

The low pass filter and high filter must have equal length.

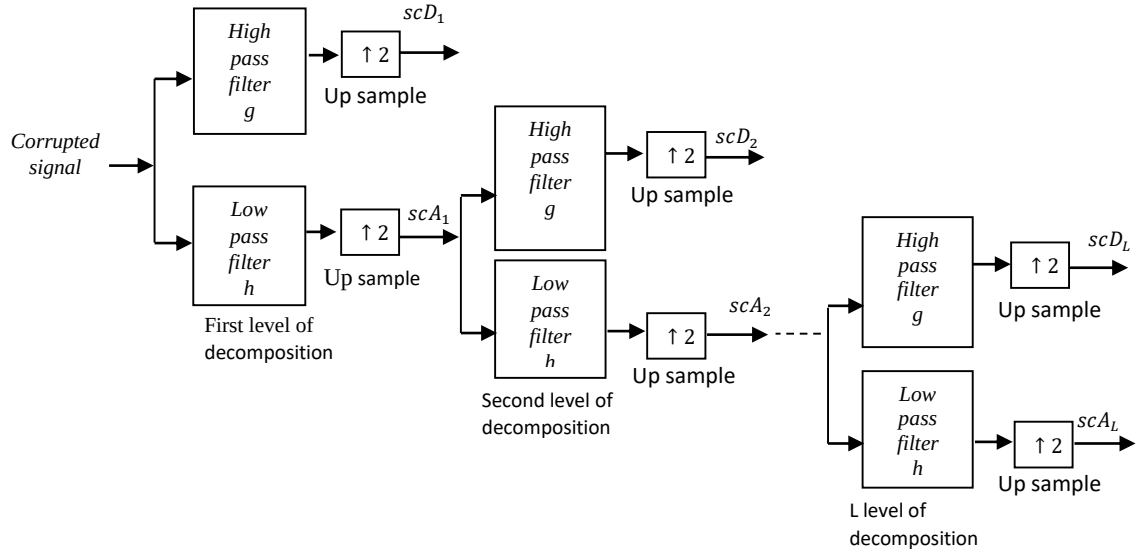

Figure 3.3 SWT decomposition at level L.

3.4.1.1.1 Wavelet function (mother wavelet)

A wavelet is a rapidly decaying, that has zero mean, and exists for a finite duration unlike sinusoids, which extend to infinity, and has different sizes and shapes. The wavelet has chosen according to the signal characteristics and the filtering method. The wavelet selection must satisfy the following criteria:

- Existence of a scaling function.
- Regularity, smoother wavelets provide sharper frequency resolution
- Symmetry or anti-symmetry of the wavelet
- Vanishing moments, where the wavelet with increasing numbers of vanishing moments results in sparse representations for a large class of signals.
- Compactly supported wavelets (in time and frequency and rate of decay) [68].

Some of the well-known orthogonal and biorthogonal that are used in discrete wavelet transform are illustrated in table (3.1).

Table 3.1 Orthogonal and biorthogonal wavelet function

Wavelet family name	Wavelet family short name
Daubechies	'db1' or 'haar', 'db2', ..., 'db10', ..., 'db45'
Coiflets	'coif1', ..., 'coif5'
Symlets	'sym2', ..., 'sym8', ...,'sym45'
Discrete Meyer	'dmey'
Biorthogonal	'bior1.1', 'bior1.3', 'bior1.5' 'bior2.2', 'bior2.4', 'bior2.6', 'bior2.8' 'bior3.1', 'bior3.3', 'bior3.5', 'bior3.7' 'bior3.9', 'bior4.4', 'bior5.5', 'bior6.8'
Reverse Biorthogonal	'rbio1.1', 'rbio1.3', 'rbio1.5' 'rbio2.2', 'rbio2.4', 'rbio2.6', 'rbio2.8' 'rbio3.1', 'rbio3.3', 'rbio3.5', 'rbio3.7' 'rbio3.9', 'rbio4.4', 'rbio5.5', 'rbio6.8'

- **Haar** is the oldest and simplest wavelet. The Haar wavelet is discontinuous and resembles a step function. It represents the same wavelet as Daubechies db1 [69].
- **Daubechies** compactly supported orthonormal wavelets that make discrete wavelet analysis practicable. Its family short name presented by dbN, where N is the number of vanishing moments or as referred in the literature by the number of filter [67] taps, and db the “surname” [69].
- **Coiflets** was built by Daubechies, it has 2*N* moments equal to 0 and the scaling function has 2*N*-1 moments equal to 0. The two functions have a support of length 6*N*-1[67].
- **Symlets** are nearly symmetrical wavelets proposed by Daubechies as modifications to the db family. The properties of the two wavelet families are similar. Symlet wavelet reassembles the QRS complex [69] [63].
- **Meyer** wavelet and scaling function are defined in the frequency domain.

- **Biorthogonal** exhibits the property of linear phase, which is needed for signal and image reconstruction [63].

3.4.1.1.2 Decomposition level

The choice of decomposition level is important in the process of wavelet transformation, the decomposition in the first level results in primer both approximation coefficient and detail coefficient, then the primer approximation coefficient will undergo the same decomposition process to produce the second both approximate and detail coefficients, and so on. All obtained coefficients are the same length as the original signal, where the length of the signal must be divided by two squares the total number of levels. When more levels are needed, the signal must be extended.

3.4.1.2 Identify a thresholding technique step

This step has proposed by Donoho and Johnstone [70] that applied on detail coefficients, it is varied based on types and rules to obtain the estimated wavelet coefficients that are calculated from 1 to level L, this step needs to choose and estimate the suitable thresholding algorithms and the suitable threshold value.

3.4.1.2.1 Selection of threshold value

The threshold value is one of the accurate parameters that alter the quality of noise suppression, there are many methods used to estimate the optimal threshold values [71]. According to the selected threshold value, if it was small or extremely large, the denoised signal may have some distortion and discontinuities or maintain some interference [47]. The common threshold values used in the literature [72] are illustrated in the table (3.2) as follows:

Table 3.2. Thershold functions.

Thershold name	Corresponding expression	Equation number
Universal threshold	$th = \sigma\sqrt{2\log(N)}$	(3.13)
Universal threshold level dependent	$th = \sigma_l\sqrt{2\log(n_l)}$	(3.14)
Universal modified threshold level dependent	$th = \sigma_l \frac{\sqrt{2\log(n_l)}}{\sqrt{n_l}}$	(3.15)
Exponential threshold	$th = (2^{(\frac{l-L}{2})})\ \sigma_l\sqrt{2\log(N)}$	(3.16)

Exponential threshold level dependent	$th = (2^{(\frac{l-L}{2})})\sigma_l\sqrt{2\log(n_l)}$	(3.17)
Minimax threshold	$th = 0.3936 + 0.1829 \times (\frac{\log n_l}{\log 2})$	(3.18)
The Log Scale modified unified threshold [73]	$\mathrm{TSH_{LSMU}} = \sigma_l \frac{\sqrt{2\log(\mathrm{N})}}{\log(l+1)}$	(3.19)

Where, N is the length of the signal, n_l is the length of the signal at l th scale, while σ_l is the standard deviation of the noise on l th decomposition level which can be estimated using the median parameter [71] The standard deviation is expressed by equation (3.20) as follows:

$$\sigma_l = \frac{median(|DT_l|)}{0.6745} \quad (3.20)$$

Where: $\frac{1}{0.6745}$ is a constant scale factor, it depends on distribution of the noise.

3.4.1.2.2 Selection of thresholding algorithm

The details wavelet coefficients are scaled or shrunken using the selected thresholding rule in order to reduce the noise in the corrupted signal, the most known thresholding rules are: hard and soft thresholding proposed in [74], hyperbolic, nonnegative garrote and firm thresholding [75] which they are derived from the mainly soft thresholding, see figure (3.4). The function of each one is expressed below:

- **Soft thresholding,** first setting to zero the coefficient absolute values below the threshold and then shrinking the coefficients absolute values greater or equal the threshold towards zero. The soft routine is a continuous function but induces a biased estimation of large coefficients [70].

$$f^{soft}(DT, th) = \begin{cases} sign(DT)(|DT| - th), & |DT| \geq th \\ 0, & |DT| < th \end{cases} \quad (3.21)$$

- **Hard thresholding**, the coefficient absolute values below the threshold are set to zero. The hard rule creates discontinuities [66].

$$f^{Hard}(DT, th) = \begin{cases} DT, & |DT| \geq th \\ 0, & |DT| < th \end{cases} \quad (3.22)$$

- **Garrote thresholding** is an intermediate between soft and hard. It acts like soft thresholding for small data values and approximates hard thresholding for large data values [76] [77].

$$f^{garr}(DT, th) = \begin{cases} sign(DT)\left(|DT| - \frac{th^2}{|DT|}\right), & |DT| \geq th \\ 0, & |DT| < th \end{cases} \quad (3.23)$$

- **Firm thresholding** (semi soft) requires two threshold values (threshold-high and threshold-low) acts as soft thresholding for values below threshold-low and the same as hard thresholding for values above threshold-high. For intermediate values, the thresholded value is in between that corresponding to hard or soft thresholding. Firm is a continuous function as soft thresholding, but is unbiased for large values as hard thresholding [47].

$$f^{Firm}(DT, th) = \begin{cases} DT, & |DT| < th_2 \\ sign(DT)\left(\frac{(DT - th_1) * th_2}{th_2 - th_1}\right), & th_2 < |DT| \leq th_1 \\ 0, & |DT| < th_1 \end{cases} \quad (3.24)$$

Where, th_2 is the maximum threshold value, and th_1 is the minimum threshold value.

- **Hyperbolic thresholding** can be obtained by soft thresholding energies of the wavelet coefficients [75].

$$f^{Hyperb}(DT, th) = \begin{cases} sign(DT)\sqrt{DT^2 - th}, & |DT| \geq th \\ 0, & |DT| < th_1 \end{cases} \quad (3.25)$$

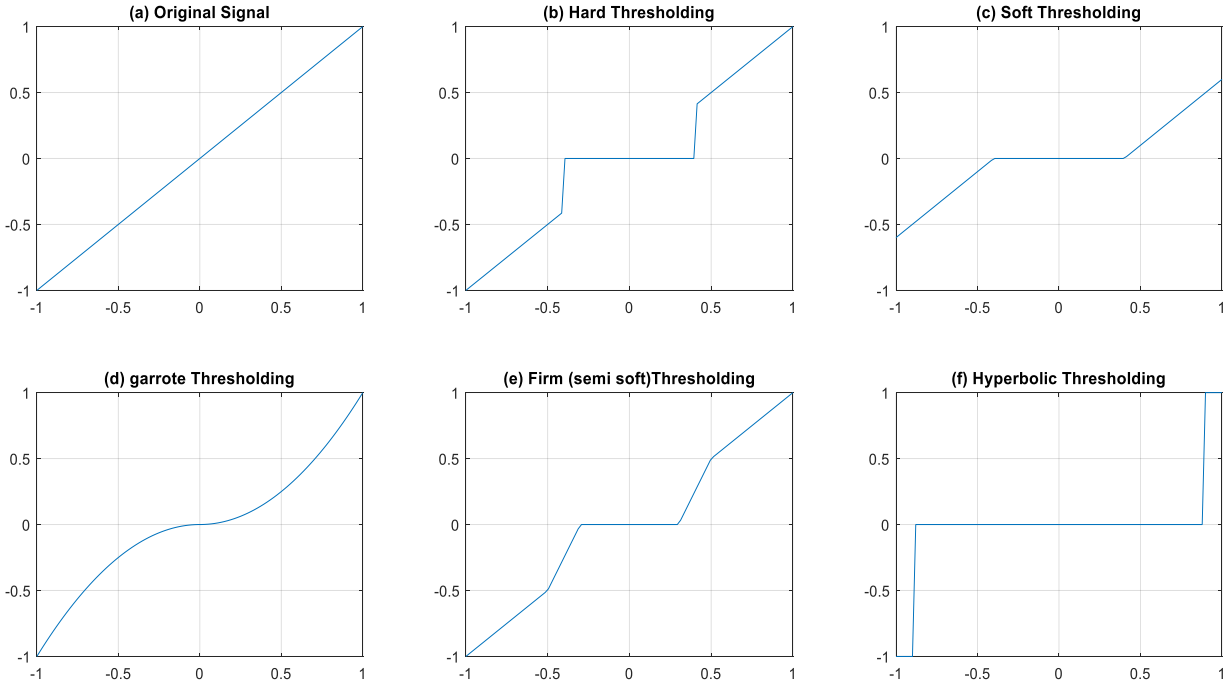

Figure 3.4 Threshold responses applied to linear test signal (**a**) Original signal, (**b**) Hard, (**c**) Soft, (**d**) Garrote, (**e**) Semi-soft, (**f**) Hyperbolic.

3.4.1.3 Reconstruction step

The reconstruction step is the last in the process of wavelet transformation; also called the synthesis process, the synthesis is achieved mathematically by using inverse stationary wavelet transform (ISWT), where all the thresholded details coefficients and the approximate coefficient of the last level are used to reconstructing the free noise signal. Generating the denoised signal will undergo the same process as the analysis step but with inverted operation as illustrated by the figure (3.5), which represents the reconstruction of the denoised signal at level L.

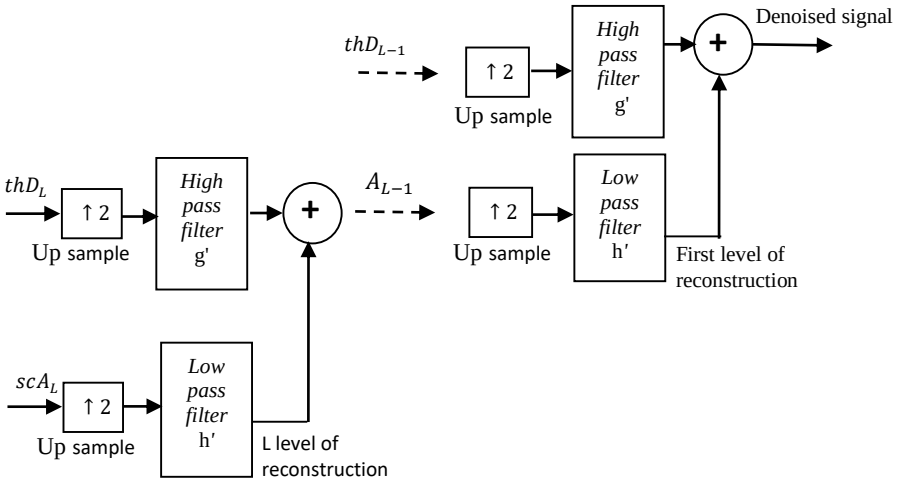

Figure 3.5 SWT reconstructions at level L.

g' and h′ are high pass and low pass, respectively.

3.4.1.4 Denoising ECG signal using SWT and NLMS algorithm

Since the main application of the SWT is to denoise corrupted signal and image, in this thesis, we have applied this algorithm to the corrupted ECG signal with the aim to do a comparative study with the SC-NLMS algorithm that we have proposed in the context of noise reduction from the ECG signal without introducing distortion. We added a block of the NLMS algorithm as the second stage of denoising in order to smooth out the ECG signal and get the best results. The evaluation study using the SWT and the block of the NLMS algorithm is realized according to the diagram given in figure (3.6).

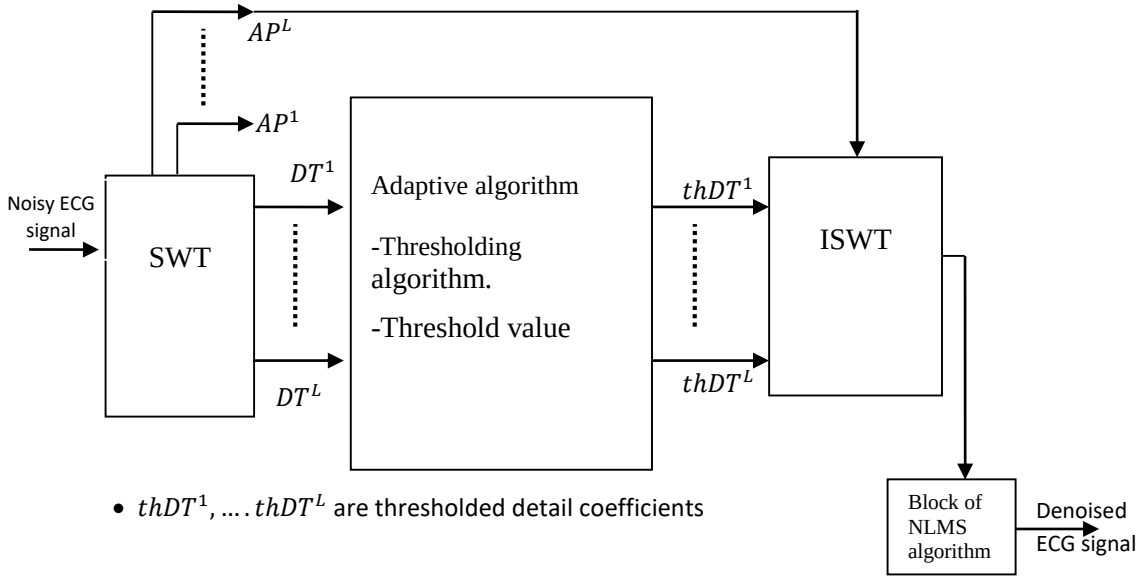

Figure 3.6 SWT plus NLMS evaluation diagram to denoise corrupted ECG signal.

The noisy ECG signal passes through the stationary wavelet transform where it will be decomposed into several levels, and then the detailed coefficients obtained during the splitting process pass into the thresholding process using several algorithms. Then we use the smoothed coefficients and the approximation coefficient of the last decomposition level to carry out the inverse stationary wavelet process. Then we pass the obtained denoised signal back through the NLMS filter to get a more distinct and smooth ECG signal

3.4.2 Suggested other techniques for comparison

The other five methods that we have suggested for the comparison, we have chosen them among the best methods that were used in noises removal from the ECG signal.

- Method one is based on dual-tree wavelet transform (DT-WT) using the tuning threshold to reduce synthetic, realistic, and colored noises in ECG signals. The base wander noise, muscle noise, and motion artifacts were generated using Matlab [47].
- Method two based on empirical mode decomposition (EMD) and non-local mean (NLM) technique, using added white and color gaussian noise [49].
- Method three based on discrete wavelet transform (DWT) and the adaptive learning potentiality of artificial neural networks technique, the base wander noise, muscle noise, and motion artifact were taken from MIT-BIH noise stress test database [50].
- Method four is based on constructing a guided filter by exploiting the butterworth Filter, the base wander noise, muscle noise, and motion artifact were taken from MIT-BIH noise stress test database [52].
- Method five is based on adaptive noise canceller to remove power line interference and baseline wander noise [51].

3.5 Conclusion

Denoising ECG signals from unwanted noises using either adaptive noise canceller or wavelet transform are considered an important step in ECG signal processing. Both of them have been proposed to overcome some limitations when using conventional filtering. Mentioning some of the methods that have been used for filtering and reviewing their advantages and disadvantages helps in understanding the reasons for proposing adaptive cancellation, and the overview study that was conducted in this chapter made it possible to understand the theoretical foundations and characteristics of stationary wavelet transform in filtering ECG signal. In the following chapter, the application of the proposed adaptive filter and the stationary wavelet transforms for the denoising and edges preserving of the ECG signal is carried out, they constitute the contribution for this thesis.

Chapter4

Results and Discussion

4.1 Introduction

In this chapter, we present the results that we obtained after applying the two methods we proposed to remove noise from the ECG signal. For the first proposed method, which is based on a self-correcting leaky normalized least mean square algorithm, we used the same parameters as we used in the original paper in denoising muscle noise [78], and we added in this thesis the simulation of removing baseline wander noise and electro motion artifact. While for the second method that is based on the combination between the SWT and block of NLMS algorithm, it was simulated to remove all kinds of noise.

4.2 Evaluation ECG Database

Specialized cardiology laboratories and hospitals have created reference databases by storing a variety of electrocardiograms that contain both normal and rarely observed conditions in mainstream clinics [79]. In this thesis, and for the evaluation and comparison purposes, we used ECG signals from the MIT-BIH database available on physionet. The MIT-BIH database is a universal database that contains several categories [60]. Among these categories, we adopted the category of MIT-BIH arrhythmia database for clean ECG signals. As for noise, we adopted the category of MIT-BIH noise stress test database (NSTDB) [61] [80].

4.2.1.1 MIT-BIH arrhythmia database

The MIT-BIH Arrhythmia Database contains 48 half-hour segments of two-channel mobile ECG recordings; the recordings are numbered at 360 samples per second per channel at 11-bit resolution over a 10-mV range, where the duration of each of the 48 recordings is 30 minutes. The 23 records numbered between 100 and 124 for the first group are intended to serve as a representative sample of the variety of waveforms that an arrhythmia detector might encounter in routine clinical use, while the remaining and 25 records numbered between 200 and 234 for the second group are chosen to include a variety of pathological cases [79] [60]. In this work, we present the results of the quantitative evaluation of a set of data from eight records: 100, 105, 107, 118, 200, 205, 213, 217, and only four of them (105, 118, 205, and 217) that achieved the best results are presented for the evaluation of graphics.

4.2.1.2 MIT-BIH noise stress test database

The recordings were digitized at 360 samples per second per channel with 11-bit resolution over a 10 mV range. The database contains samples for three types of noise; that were assembled from the recordings by selecting intervals that contained predominantly baseline wander (in record 'BW'), muscle (EMG) artifact (in record 'MA'), and electrode motion artifact (in record 'EM'). In this work, all of three types of noises were used for the evaluation.

4.2.1.3 Noise addition

The noises were directly added to the aforementioned original ECGs, where two levels of SNR_{inp} of 5 and 10dB were performed. The process of addition is illustrated by the following equation [61] [82] [81].

$$Necg(n) = Cecg(n) + (n * V(n)) \qquad (4.1)$$

Where, $Necg$ is the noisy ECG signal, V(n) is the noise, $Cecg(n)$ is the clean (noise free) ECG signal, and n is a coefficient that has been tuned to control the input signal to noise ratio (SNR_{inp}) that is given by the following equation:

$$SNR_{inp} = 10log_{10}\frac{P_{signal}}{n^2 X P_{noise}} \qquad (4.2)$$

Where, P_{signal} denotes the signal power, and P_{noise} denotes the noise power.

4.3 Evaluation metrics

To validate the efficiency of the suggested methods in noise reduction from corrupted ECG signal, and for a significant comparison with other existing techniques; the output SNR_{out}, the mean square error MSE, and the improvement SNR have been calculated and compared, their equations are given as follows:

$$SNR_{out} = 10log_{10}\left(\frac{\sum_{n=0}^{N-1}[Cecg(n)]^2}{\sum_{n=0}^{N-1}[Fecg(n)-Cecg(n)]^2}\right) \qquad (4.3)$$

$$MSE = \frac{1}{N}\sum_{n=0}^{N-1}\left(Cecg(n) - Fecg(n)\right)^2 \qquad (4.4)$$

$$SNR_{Imp} = SNR_{out} - SNR_{inp} \qquad (4.5)$$

4.4 Evaluation results

This section is subdivided into two subsection namely qualitative results and discussion, quantitative results and discussion, respectively.

4.4.1 Qualitative results and discussion

4.4.1.1 Filtering ECG signal using the first proposed method (SC-LNLMS)

In qualitative sub section, the simulation results of the proposed filtering methodology based on self-correcting leaky NLMS adaptive filter, and filtering methodology based on stationary wavelet transform and NLMS to remove noises from free ECG signal are shown, We applied both methods to 48 clean signals taken from MIT-BIH database, then we presented the signals that achieved the best results. Signal of data number 105 is added to muscle noise (MA), the signal of data number 217 is added to the baseline wander (BW) noise and motion artifact (EM) to represent the results of the first proposed method, while signal of data number 118 is added to muscle noise, the signal of data number 205 is added to the baseline wander noise and motion artifact to represent the results of the second method.

- **Removing muscle noise added at 5 and 10dB**

Figure (4.1) displays the outputs of the proposed filtering for noise cancelation from the noisy ECG signal created by using added MA noise at 10 dB input SNR level. Figure 4.1 (a) shows noise free ECG signal of data number 105. Figure 4.1 (b) shows the noisy ECG signal. Figure 4.1(c) shows the output of the first stage. Figure 4.1 (d) shows the output of the second stage, and figure 4.1 (e) shows the output of the last stage [78].

Figure (4.2) displays the outputs of the proposed filtering for noise cancelation from the noisy ECG signal created by using added MA noise at 5 dB input SNR level. Figure 4.2(a) shows the noise free ECG signal of data number 105. Figure 4.2(b) shows the noisy ECG signal. Figure 4.2(c) shows the output of the first stage. Figure 4.2(d) shows the output of the second stage, and figure 4.2 (e) shows the output of the third stage.

As we can see in figure (4.1) and figure (4.2), whatever the added noise signal is weak or large; the proposed method can successfully remove major components of MA noise from the ECG signal, and even into the outputs of the first and second stages (Figure 4.1(c)),

figure 4.1 (d), figure 4.2 (c), and figure 4.2 (d)) there are a little noise components in Q waves and isoelectric line but the signals still keep the details, and all of the ECG features are distinct contrasted with the conventional filters which can remove most of the MA noise, but also filtrate the details. Although the PQST region in figure 4.1 (b), and the PQRST region in figure 4.2 (b), are completely overlap with the noise, the filter that we have proposed has achieved success in removing noise to a large extent from these sensitive areas without distorting the original signal [78].

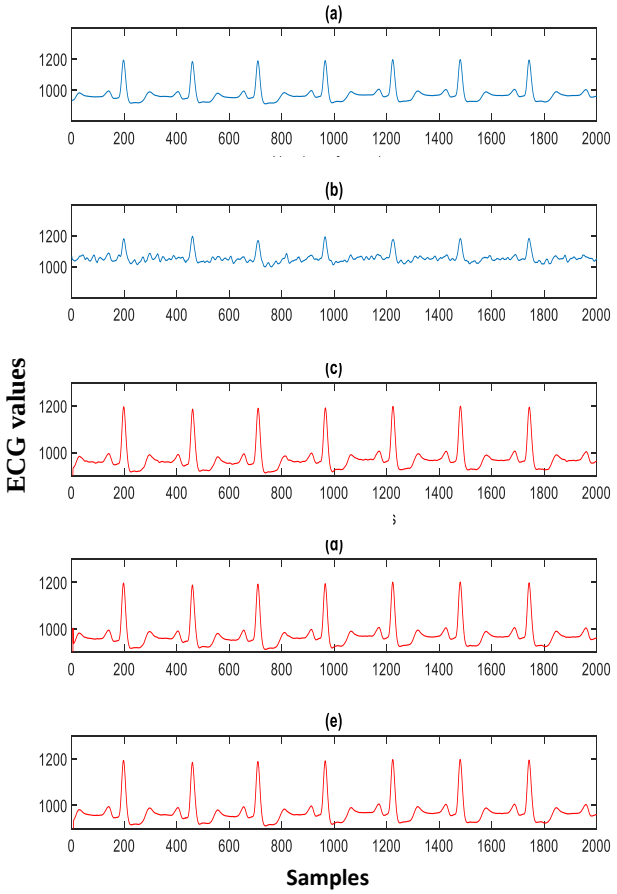

Figure 4.1 Outputs of ECG denoising using proposed method, (a)Noise free ECG signal (record 105 from MIT-BIH), (b) Noisy ECG signal with added MA noise at 5 dB, (c)First stage of denoised ECG signal, (d) Second stage of denoised ECG signal, (e) Third stage of denoised ECG signal.

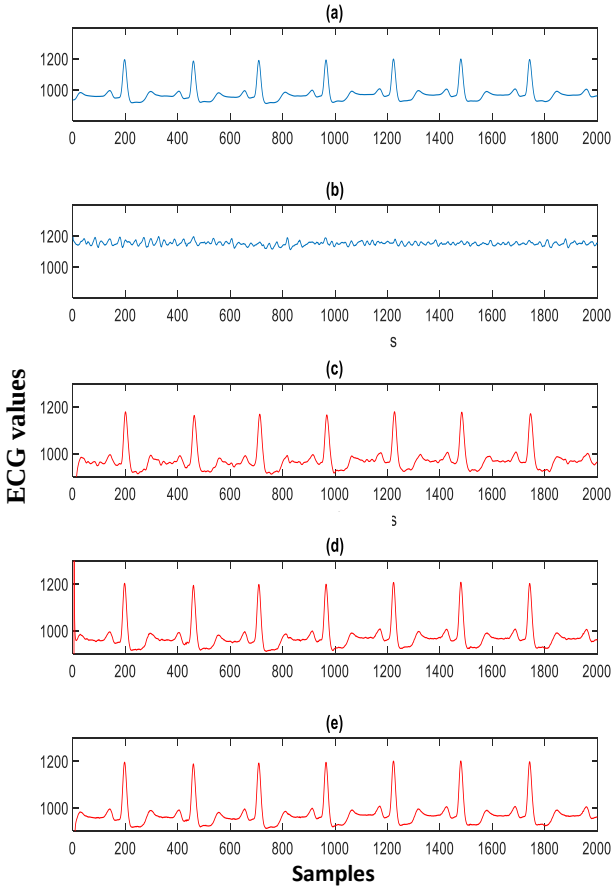

Figure 4.2 Outputs of ECG denoising using proposed method, (a)Noise free ECG signal (record 105 from MIT-BIH), (b) Noisy ECG signal with added MA noise at 10 dB, (c) First stage of denoised ECG signal, (d) Second stage of denoised ECG signal, (e) Third stage of denoised ECG signal

During applying the proposed denoising technique to many corrupted ECG signals to remove a realistic muscle noise, we found that the best length for filter M for some signals is 3 and for others it is 4, and we found that most signals do not need more than three stages in order to reduce a largest amount of noise without distorting small wavelets such P and T waves. Besides,

we adjust the step size and leakage coefficient different from one stage to another, but also different from one signal to another [78].

- **Removing baseline wander noise added at 5 and 10dB**

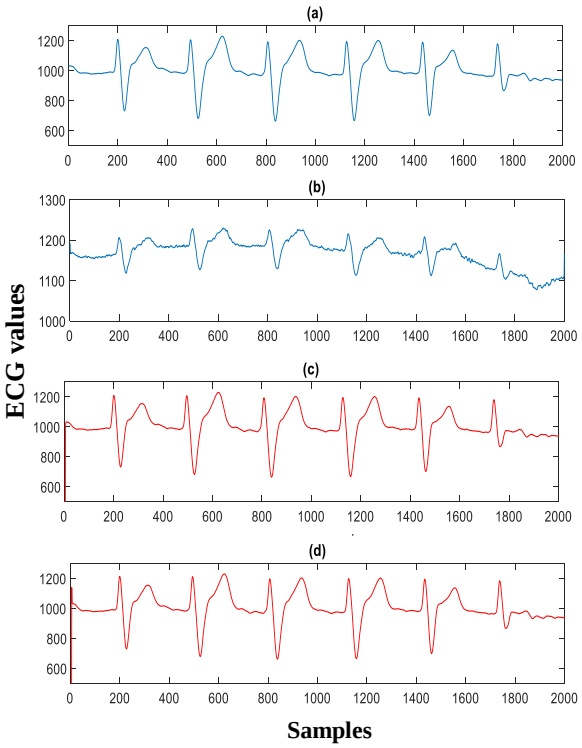

Figure 4.3 Outputs of ECG denoising using proposed method, (a)Noise free ECG signal (record 217 from MIT-BIH), (b) Noisy ECG signal with added BW noise at 10 dB, (c)First stage of denoised ECG signal, (d) Second stage of denoised ECG signal, (e) Third stage of denoised ECG signal.

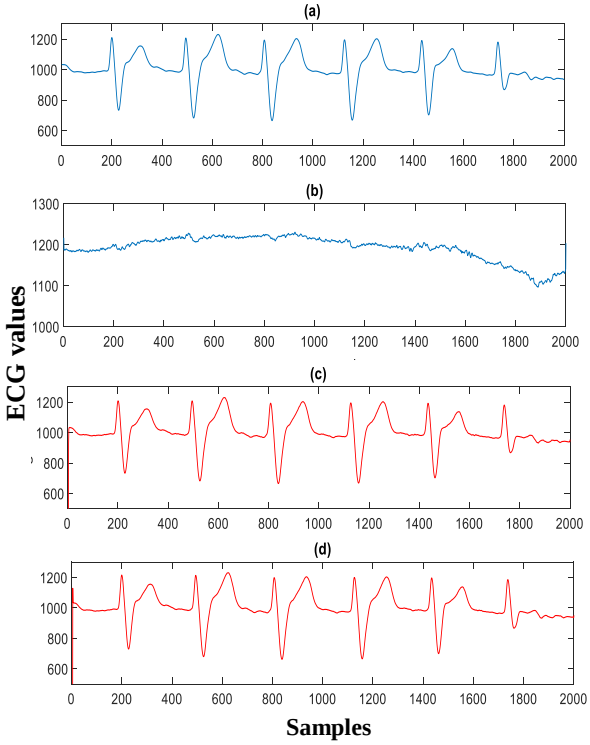

Figure 4.4 Outputs of ECG denoising using proposed method, (a)Noise free ECG signal (record 217 from MIT-BIH), (b) Noisy ECG signal with added BW noise at 5 dB, (c) First stage of denoised ECG signal, (d) Second stage of denoised ECG signal, (e) Third stage of denoised ECG signal

Figure (4.3) displays the outputs of the proposed filtering for noise cancelation from noisy ECG signal created by using added BW noise at 10 dB input SNR level. Figure 4.3 (a) shows noise free ECG signal of data number 217. Figure 4.3 (b) shows the noisy ECG signal. Figure 4.3(c) shows the output of the first stage. Figure 4.3 (d) shows the output of the second stage.

Figure (4.4) displays the outputs of the proposed filtering for noise cancelation from noisy ECG signal created by using added BW noise at 5 dB input SNR level. Figure 4.4 (a) shows noise free ECG signal of data number 217. Figure 4.4 (b) shows the noisy ECG signal. Figure 4.4 (c) shows the output of the first stage, and figure 4.4(d) shows the output of the second stage.

The noisy signal in figure 4.3 (b) shows a slow wandering of the baseline resulting in an increased width of the R and S waves, while figure 4.4 (b) shows a rapid wandering at baseline where the ECG signal is completely distorted, however, the technique we proposed was able to successfully eliminate wandering at baseline, regardless of how quickly or slowed the resulting wandering, as the figure 4.3 (d) and figure 4.4 (d) have shown respectively, noting that there are still very few narrow ripples around samples 1600 and 1400 in relation to figure 4.4 (d), and around sample 1400 with respect to figure 4.3 (d). For removing baseline wander noise, only two stages were required.

By applying the proposed denoising technique to remove realistic baseline wander, we found that the best selected filter length M for some signals is 3 for a small amount of BW noise, while for a large amount of BW noise they need the length of 4. We also concluded that whenever the value of ג is very small than 1/μ, i.e. close to the value of μ, gives better results in removing BW noise. All the methods tested in the literature proved to be better if leaving baseline wander unfiltered, where none of the methods was able to reconstruct the original ECG signal without distorting the ST segment [42]. However, our proposed method has proven superior performance in removing BW noise from ECG signal without modifying the ST segment.

- **Removing electro motion artifact added at 5 and 10dB**

Figure (4.5) displays the outputs of the proposed filtering for noise cancelation from noisy ECG signal created by using added EM noise at 10 dB input SNR level. Figure 4.5 (a) shows noise free ECG signal of data number 217. Figure 4.5 (b) shows the noisy ECG signal. Figure 4.5 (c) shows the output of the first stage, and figure 4.5 (d) shows the output of the second stage.
Figure (4.6) displays the outputs of the proposed filtering for noise cancelation from noisy ECG signal created by using added EM noise at 5 dB input SNR level. Figure 4.6 (a) shows noise free ECG signal of data number 217. Figure 4.6 (b) shows the noisy ECG signal. Figure 4.6 (c) shows the output of the first stage. Figure 4.6 (d) shows the output of the second stage, and figure 4.6 (e) shows the output of the third stage.

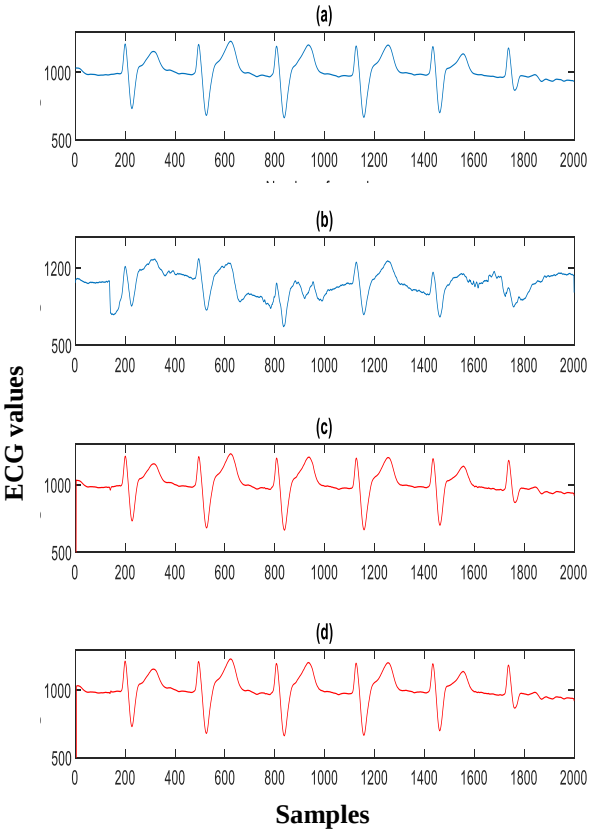

Figure 4.5 Outputs of ECG denoising using proposed method, (a)Noise free ECG signal (record 217 from MIT-BIH), (b) Noisy ECG signal with added EM noise at 10 dB, (c)First stage of denoised ECG signal, (d) Second stage of denoised ECG signal.

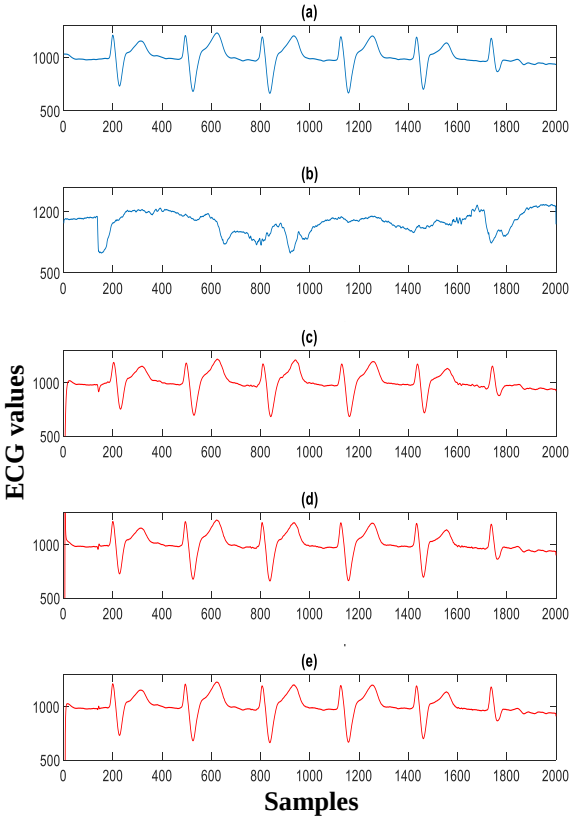

Figure 4.6 Outputs of ECG denoising using proposed method, (a)Noise free ECG signal (record 217 from MIT-BIH), (b) Noisy ECG signal with added EM noise at 5 dB, (c) First stage of denoised ECG signal, (d) Second stage of denoised ECG signal, (e) Third stage of denoised ECG signal

The noisy signal in figure 4.5 (b) shows that half of QRS complexes were distorted, while figure 4.6 (b) shows that all of the QRS complexes were distorted and became with large amplitude and wide waveform. Nevertheless, the technique we proposed was able to separate electro motion noise from ECG signal and preserving all its features, especially since the motion effect was reported as the most difficult type of noise to be removed from the ECG signals because its spectrum completely overlaps the ECG signal. Its morphology is similar to that of the P, QRS, and T waves.

4.4.1.2 Filtering ECG signal using SWT and NLMS algorithm

Five thresholding rules were selected to perform the thresholding technique: hard, soft, firm (semi-soft), hyperbolic, and garrote, where the universal threshold level-dependent (see table 3.2) was used to compute the threshold values.

- **Removal muscle noise (MA) added at 10 dB**

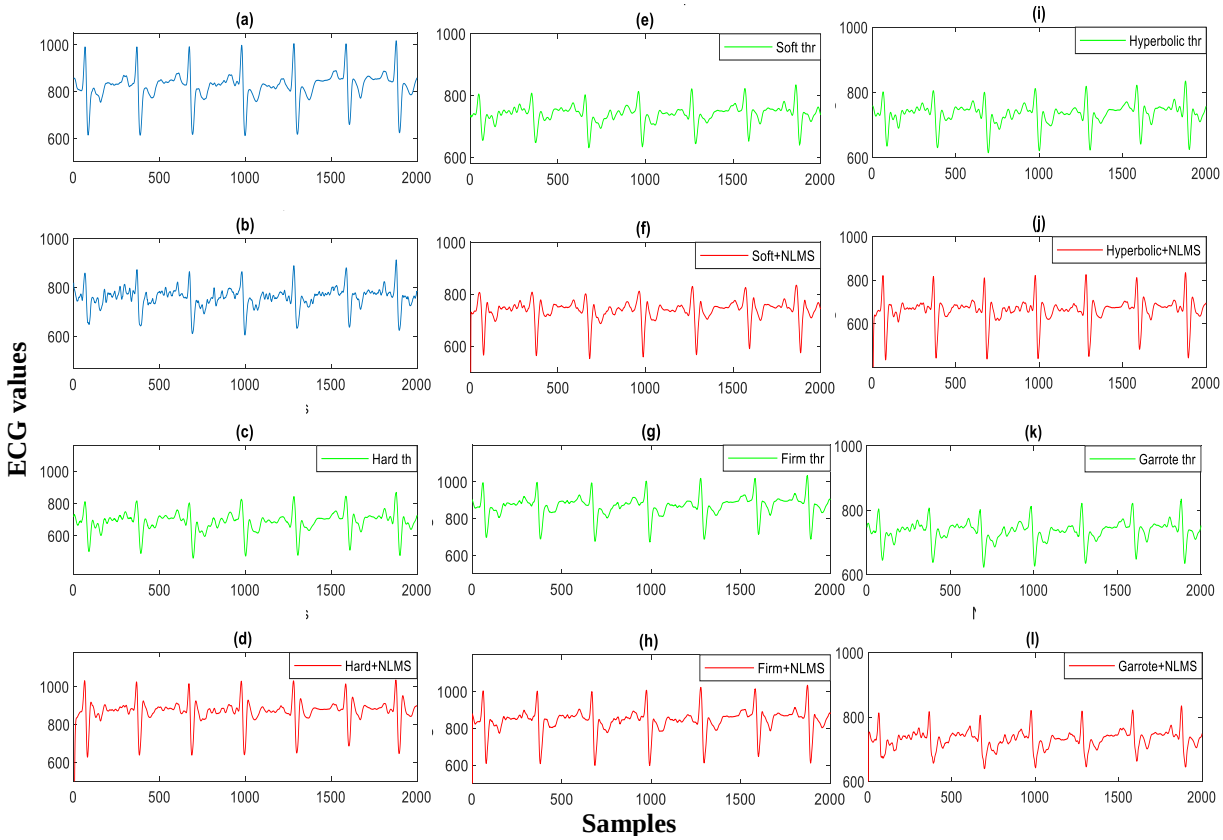

Figure 4.7 Outputs of ECG denoising using SWT+NLMS method, (a)Noise free ECG signal (record 118 from MIT-BIH), (b) Noisy ECG signal with added MA noise at 10 dB, (c)Denoised ECG using hard thr, (d) Denoised signal using hard thr+NLMS,(e) Denoised ECG using soft thr, (f)Denoised signal using soft thr+NLMS, (g) Denoised ECG using firm thr, (h) Denoised signal using firm thr+NLMS, (i)Denoised ECG using hyperbolic thr, (j) Denoised signal using hyperbolic thr+NLMS, (k)Denoised ECG using garrote thr, (l) Denoised signal using garrote thr+NLMS.

Figure (4.7) displays the denoised outputs after using five thresholding rules; hard, soft, firm, hyperbolic, and garrote thresholding to remove realistic muscle noise from ECG signal that is added at 10dB to free ECG signal to data number 118, and then displays their corresponding outputs after using the selected thresholding rule plus NLMS algorithm.

Figure 4.7(d) shows the denoised signal resulted after using hard rule and NLMS, figure 4.7(f) shows the denoised signal resulted after using soft rule and NLMS, figure 4.7(h) shows the denoised signal resulted after using firm rule and NLMS, figure 4.7(j) shows the denoised signal resulted after using hyperbolic rule and NLMS, figure 4.7(l) shows the denoised signal resulted by using garrote and NLMS. The SWT decomposition level that was selected for each rule is L=4.

- **Removal muscle noise added at 5dB**

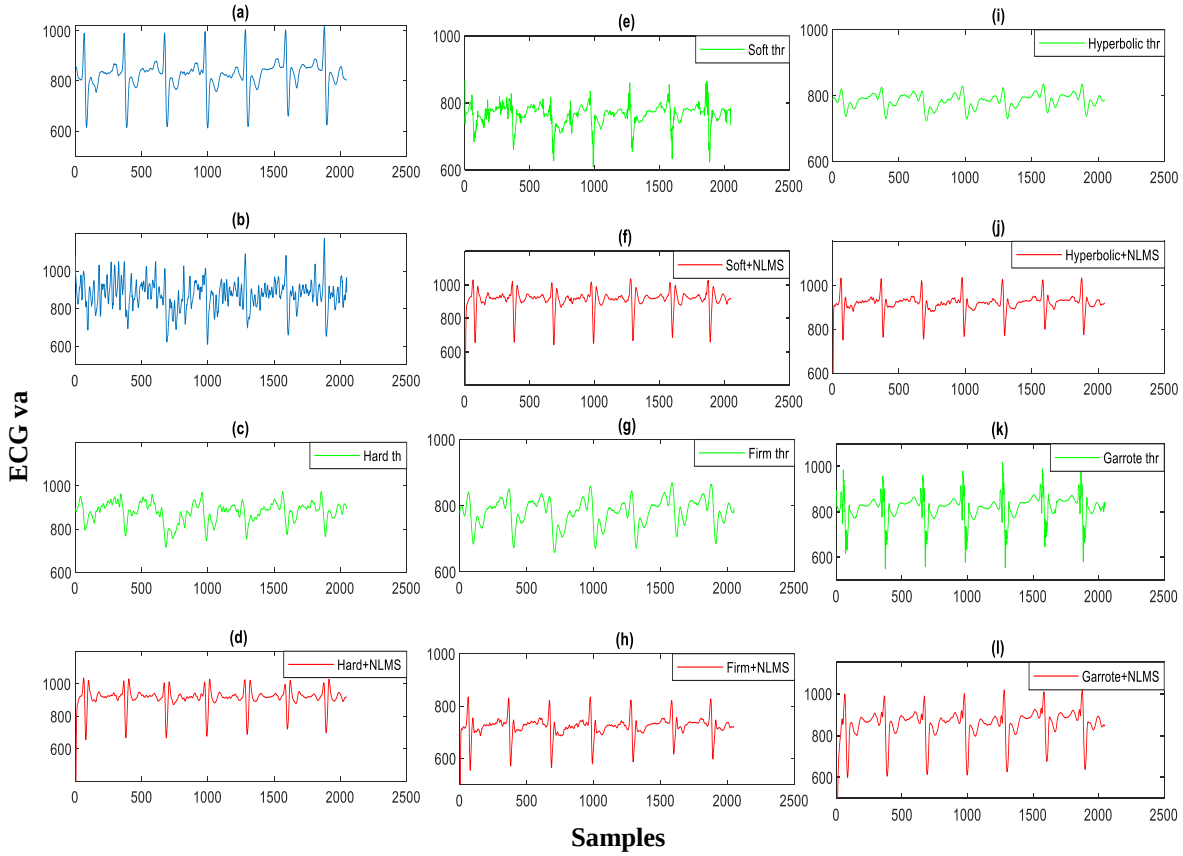

Figure 4.8 Outputs of ECG denoising using SWT+NLMS method, (a)Noise free ECG signal (record 118 from MIT-BIH), (b) Noisy ECG signal with added MA noise at 5 dB, (c)Denoised ECG using hard thr, (d) Denoised signal using hard th+NLMS,(e) Denoised ECG using soft thr, (f)Denoised signal using soft th+NLMS, (g) Denoised ECG using firm thr, (h) Denoised signal using firm th+NLMS, (i)Denoised ECG using hyperbolic thr, (j) Denoised signal using hyperbolic th+NLMS, (k)Denoised ECG using garrote thr, (l) Denoised signal using garrote th+NLMS.

Figure (4.8) displays the denoised outputs after using five thresholding rules; hard, soft, firm, hyperbolic, and garrote thresholding to remove realistic muscle noise from ECG signal that is added at 5dB to free ECG signal of data number 118, and then displays their corresponding outputs after using the selected thresholding rule plus NLMS algorithm.

Figure 4.8(d) shows the denoised signal resulted after using hard rule and NLMS, figure 4.8(f) shows the denoised signal resulted after using soft rule and NLMS, figure 4.8(h) shows the denoised signal resulted after using firm rule and NLMS, figure 4.8 (j) shows the denoised signal resulted after using hyperbolic rule and NLMS, figure 4.8(l) shows the denoised signal

resulted after using garrote and NLMS. The SWT decomposition level that was selected for each rule is L=5.

As we can see from figures (4.7) and (4.8), the second proposed method that is based on SWT and NLMS algorithm was largely successful in removing the added muscle noise at 10 dB using a firm thresholding technique and decomposition level of 4 (figure 4.7(h)) but some ST interval remained distorted. Also, it succeeded in removing the MA noise when it was added at 5 dB by using the garrote thresholding technique and decomposition level of 5 (figure 4.8(l)), as the latter was able to remove noise while still leaving the distortion of the QRS complex which is the most important feature in the ECG signal because it reflects depolarization of the ventricular mass. NLMS was added in order to refine and restore this complex, but it succeeded only recovered QS waves. However, the proposed technique based on SC-LNLMS remains the best in eliminating muscle noise.

- **Removal of baseline wander added at 5 and 10 dB**

Figure (4.9) displays the denoised outputs after using five thresholding rules; hard, soft, firm, hyperbolic, and garrote thresholding to remove realistic baseline wander noise from ECG signal that is added at 5dB to free ECG signal of data number 205, and then displays their corresponding outputs after using the selected thresholding rule plus NLMS algorithm.

Figure 4.9(d) shows the denoised signal resulted by using hard rule and NLMS. Figure 4.9(f) shows the denoised signal resulted by using soft rule and NLMS, figure 4.9(h) shows the denoised signal resulted by using firm rule and NLMS, figure 4.9(j) shows the denoised signal resulted by using hyperbolic rule and NLMS, figure 4.9(l) shows the denoised signal resulted by using garrote and NLMS. The SWT decomposition level that was selected for each rule is L=5.

Figure (4.10) displays the denoised outputs after using five thresholding rules; hard, soft, firm, hyperbolic, and garrote thresholding to remove realistic baseline wander noise from ECG signal that is added at 10dB to free ECG signal of data number 205, and then displays their corresponding outputs after using the selected thresholding rule plus NLMS algorithm.

Figure 4.10(d) shows the denoised signal resulted after using hard rule and NLMS, figure 4.10(f) shows the denoised signal resulted after using soft rule and NLMS, figure 4.10(h) shows the denoised signal resulted after using firm rule and NLMS, figure 4.10(j) shows the denoised signal resulted after using hyperbolic rule and NLMS, figure 4.10(l) shows the denoised signal

resulted after using garrote and NLMS. The SWT decomposition level that was selected for each rule is L=5.

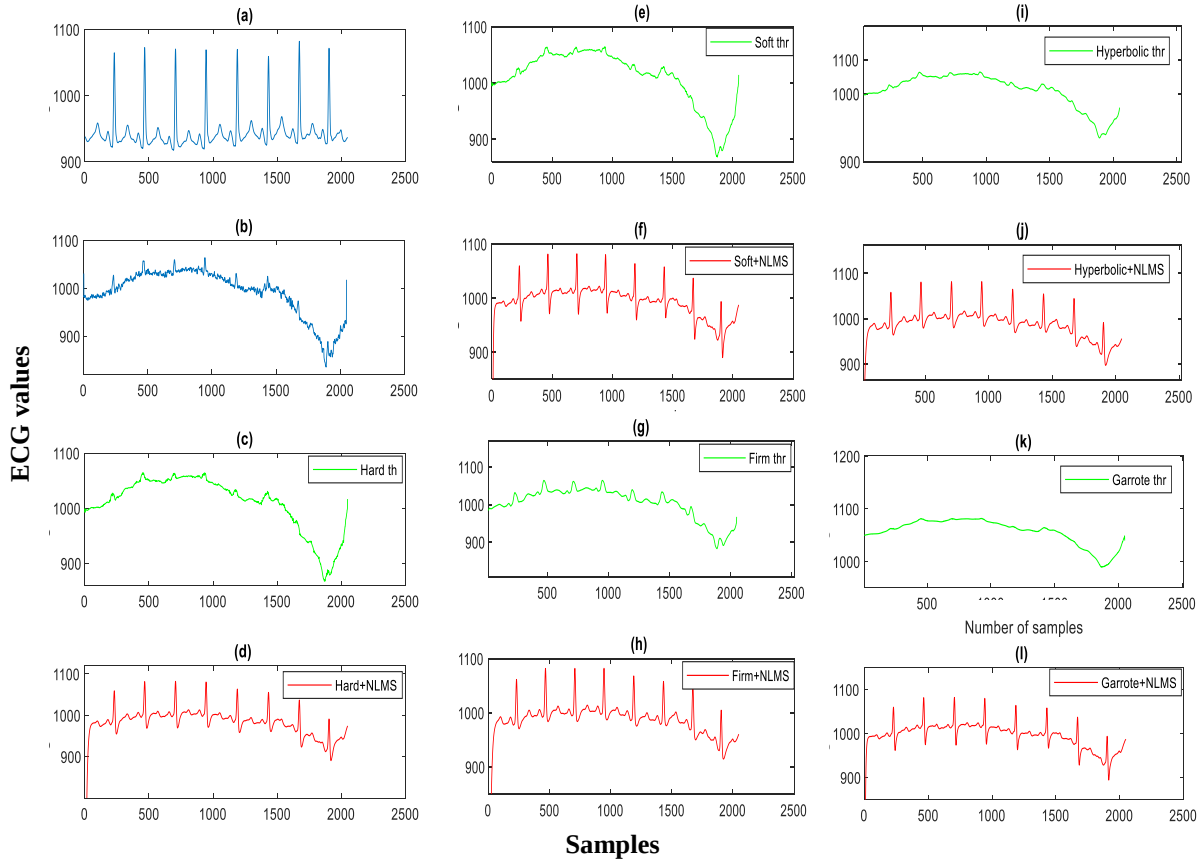

Figure 4.9 Outputs of ECG denoising using SWT+NLMS method, (a)Noise free ECG signal (record 205 from MIT-BIH), (b) Noisy ECG signal with added BW noise at 5 dB, (c)Denoised ECG using hard thr, (d) Denoised signal using hard th+NLMS,(e) Denoised ECG using soft thr, (f)Denoised signal using soft th+NLMS, (g) Denoised ECG using firm thr, (h) Denoised signal using firm th+NLMS, (i)Denoised ECG using hyperbolic thr, (j) Denoised signal using hyperbolic th+NLMS, (k)Denoised ECG using garrote thr, (l) Denoised signal using garrote th+NLMS

As we can see from figures (4.9) and (4.10), the second proposed method based on the SWT and NLMS algorithm was able to a small extent to remove BW in two cases, in the case of the additive BW noise at 5 dB using the firm threshold technique and decomposition level of 5 (figure. 4.9(f)), then in the case of added BW noise at 10 dB using garrote threshold technique and decomposition level of 5(figure. 4.10(l)), in the first case, nearly every ST segments remained distorted, and in the second case all Q waves were deformed by widening in its width and increasing in its amplitude, and this, of course, will stand as a barrier to the doctor's diagnosis of this case, especially the Q wave reflects the depolarization of the septum between the two ventricles and ST segment reflects the period of zero potential between ventricular

depolarization and repolarization. Compared to the proposed SC-LNLMS-based technique for eliminating BW noise from the ECG signal, the latter remains the best.

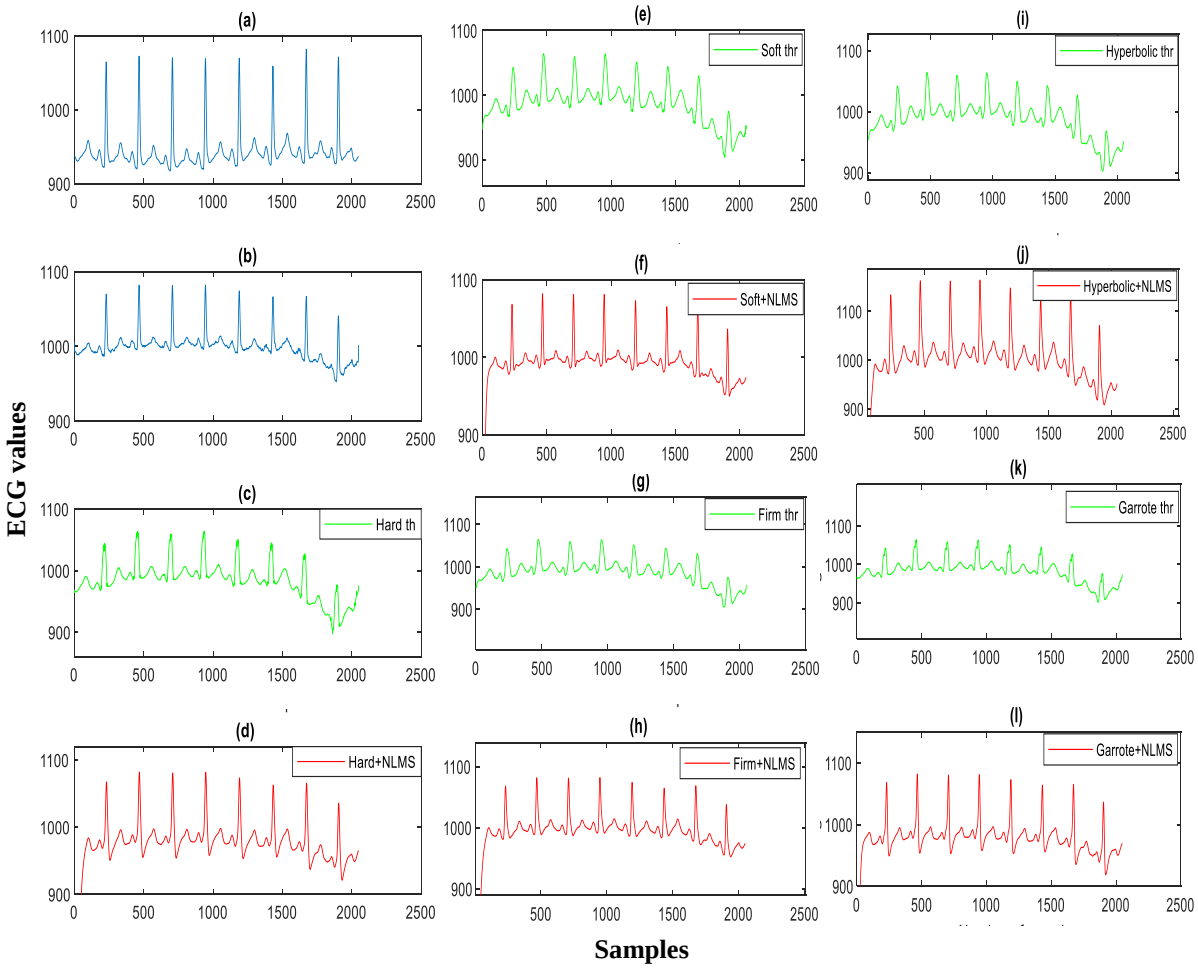

Figure 4.10 Outputs of ECG denoising using SWT+NLMS method, (a)Noise free ECG signal (record 205 from MIT-BIH), (b) Noisy ECG signal with added BW noise at 10 dB, (c)Denoised ECG using hard thr, (d) Denoised signal using hard th+NLMS,(e) Denoised ECG using soft thr, (f)Denoised signal using soft th+NLMS, (g) Denoised ECG using firm thr, (h) Denoised signal using firm th+NLMS, (i)Denoised ECG using hyperbolic thr, (j) Denoised signal using hyperbolic th+NLMS, (k)Denoised ECG using garrote thr, (l) Denoised signal using garrote th+NLMS

Figure (4.11) displays the denoised outputs after using five thresholding rules; hard, soft, firm, hyperbolic, and garrote thresholding to remove realistic electro motion artifact from ECG signal that is added at 5dB to free ECG signal of data number 205, and then displays their corresponding outputs after using the selected thresholding rule plus NLMS algorithm.

Figure 4.11(d) shows the denoised signal resulted after using hard rule and NLMS, figure 4.11(f) shows the denoised signal resulted after using soft rule and NLMS, figure 4.11(h) shows the denoised signal resulted after using firm rule and NLMS, figure 4.11(j) shows the denoised

signal resulted after using hyperbolic rule and NLMS, figure 4.11(l) shows the denoised signal resulted after using garrote and NLMS. The SWT decomposition level that was selected for each rule is L=8.

- **Removal of electro motion added at 5dB**

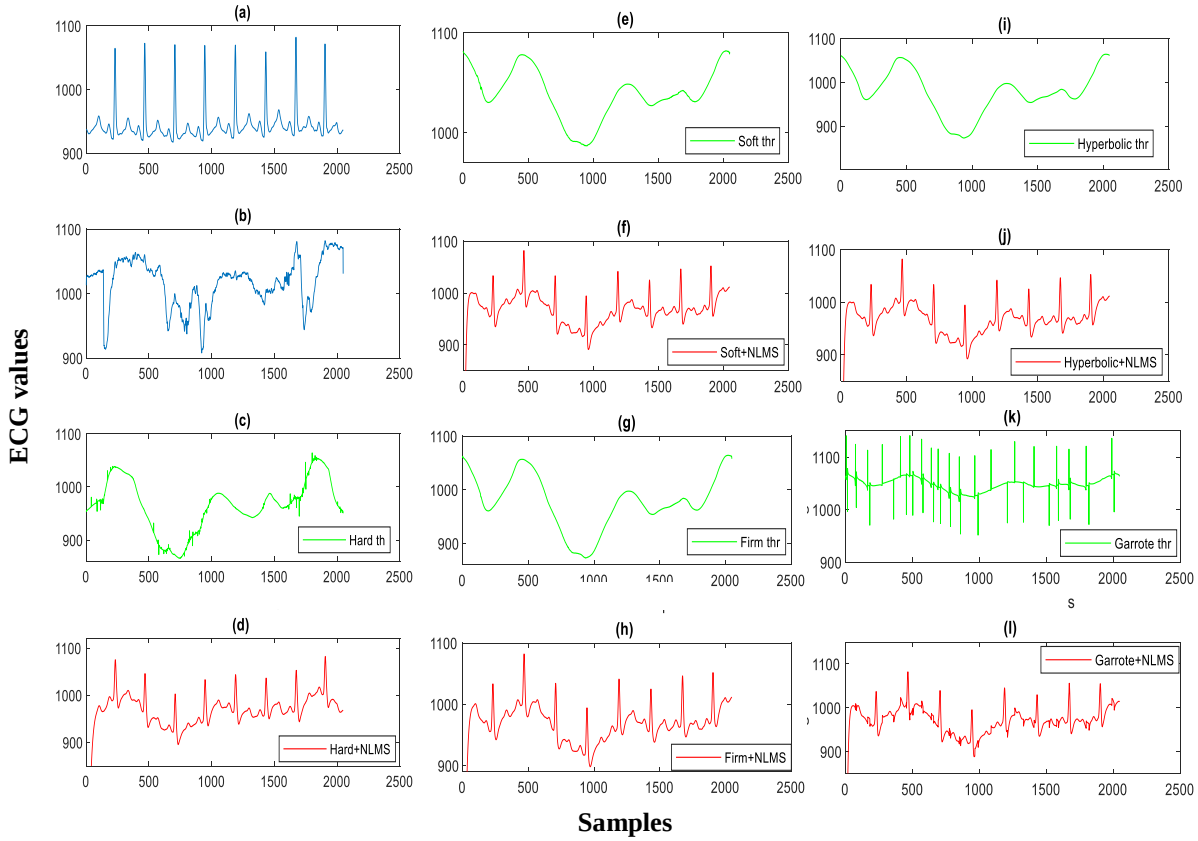

Figure 4.11 Outputs of ECG denoising using SWT+NLMS method, (a)Noise free ECG signal (record 205 from MIT-BIH), (b) Noisy ECG signal with added EM noise at 5 dB, (c)Denoised ECG using hard thr, (d) Denoised signal using hard th+NLMS,(e) Denoised ECG using soft thr, (f)Denoised signal using soft th+NLMS, (g) Denoised ECG using firm thr, (h) Denoised signal using firm th+NLMS, (i)Denoised ECG using hyperbolic thr, (j) Denoised signal using hyperbolic th+NLMS, (k)Denoised ECG using garrote thr, (l) Denoised signal using garrote th+NLMS

Figure (4.12) displays the denoised outputs after using five thresholding rules; hard, soft, firm, hyperbolic, and garrote thresholding to remove realistic electro motion artifact from ECG signal that is added at 10dB to free ECG signal of data number 205, and then displays their corresponding outputs after using the selected thresholding rule plus NLMS algorithm.

figure 4.12(d) shows the denoised signal resulted after using hard rule and NLMS, figure 4.12(f) shows the denoised signal resulted after using soft rule and NLMS, figure 4.12(h) shows

the denoised signal resulted after using firm rule and NLMS, figure 4.12(j) shows the denoised signal resulted after using hyperbolic rule and NLMS, figure 4.12(l) shows the denoised signal resulted after using garrote and NLMS. The SWT decomposition level that was selected for each rule is L=5.

- **Removal of electro motion added at 10 dB**

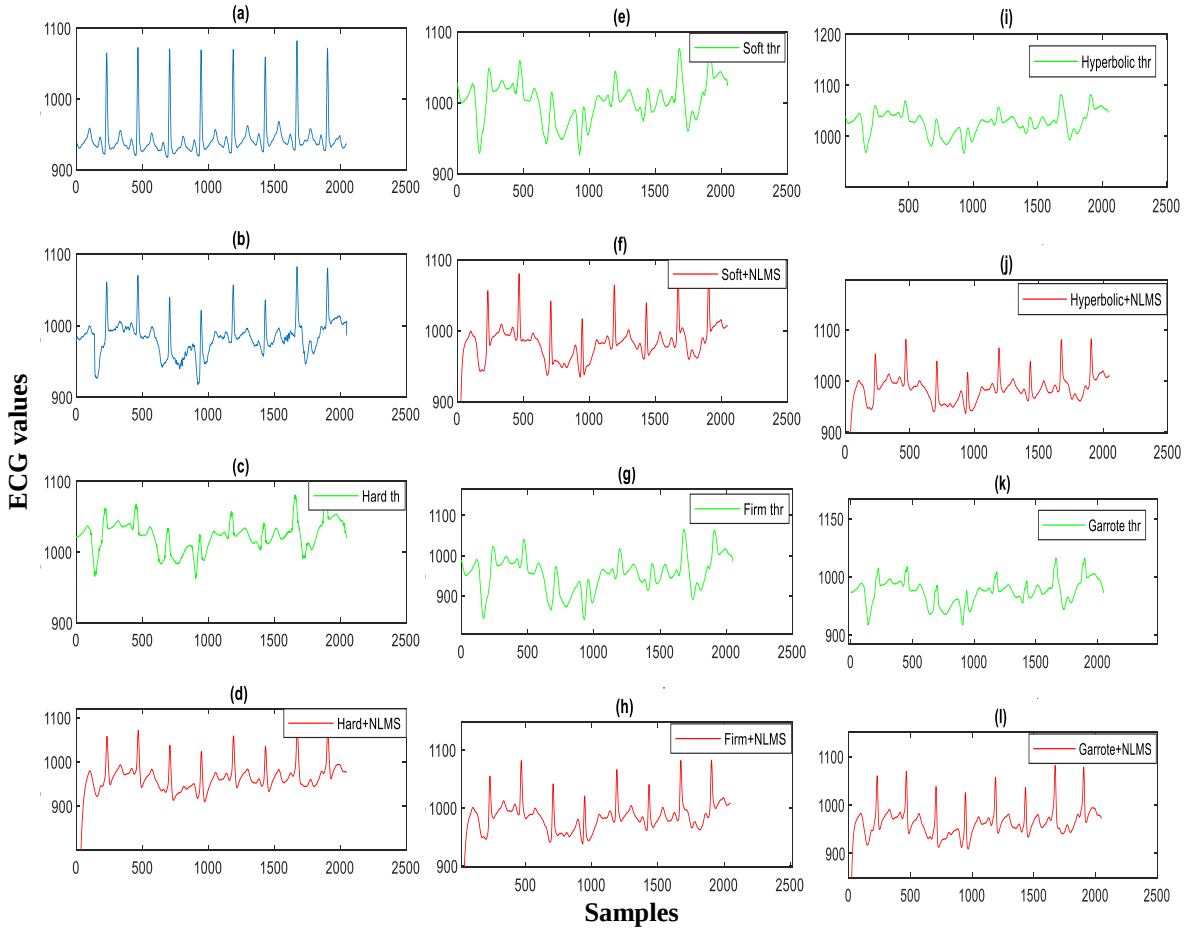

Figure 4.12 Outputs of ECG denoising using SWT+NLMS method, (a)Noise free ECG signal (record 205 from MIT-BIH), (b) Noisy ECG signal with added EM noise at 10 dB, (c)Denoised ECG using hard thr, (d) Denoised signal using hard th+NLMS,(e) Denoised ECG using soft thr, (f)Denoised signal using soft th+NLMS, (g) Denoised ECG using firm thr, (h) Denoised signal using firm th+NLMS, (i)Denoised ECG using hyperbolic thr, (j) Denoised signal using hyperbolic th+NLMS, (k)Denoised ECG using garrote thr, (l) Denoised signal using garrote th+NLMS

We conclude from figures (4.11) and (4.12) that the second proposed method based on the SWT and NLMS algorithm did not succeed in removing EM noise except for a slight improvement in two cases, in the case of EM noise added at 5 dB using the firm threshold technique and decomposition level of 8 (figure. 4.11(h)), then the case of EM noise added at 10

dB using the garrote threshold technique and decomposition level of 5 (figure. 4.12(l)), in both cases the signal is completely distorted except for the retrieval of the R waves, This technique was unable to eliminate significant abrupt swing in the baseline and the appearance of large amplitude in the ECG signal. In contrast, the proposed method based on SC-LNLMS filtering has been shown significant improvement in removing EM artifacts.

In this work, based on the overall experiment of filtering the ECG signal from MA, BW, and EM noise using the second proposed method based on the SWT and NLMS algorithm, we concluded that garrote is the best thresholding to deal with contaminated ECG signal with one of the aforementioned noise, followed by the firm, then the soft thresholding, as for the appropriate wavelet function, we found that the family of symlet and db are more suitable in denoising ECG signals, while the decomposition level depends on the amount of added noise. On the other hand, we increased the length of the filter up to 44 which creates a longer delay and a greater calculation load which is not recommended for real time signal filtering.

4.4.2 Quantitative results and discussion

In the quantitative subsection, output SNR (SNR_{out}), SNR improvement, and mean square error (MSE) of the proposed filtering methodology based on SC-LNLMS and the methodology based on SWT and NLMS algorithm are shown and compared with other existing techniques.

4.4.2.1 Obtained results after using SC-LNLMS method

Table 4.1 SNR_{out} and MSE results after using SC-LNLMS method for removing MA noise.

Added noise= muscle noise (MA)						
	SNR in=10dB			**SNR in=5dB**		
Signals	**SNR_{out} First stage**	**SNR_{out} (last stage)**	**MSE at last stage**	**SNR_{out} (First stage)**	**SNR_{out} (last stage)**	**MSE at last stage**
100	17.15	21.87	0.0001200	14.64	18.82	0.0005801
105	20.87	28.56	5.059e-7	16.40	20.86	0.0001032
107	18.19	22.59	0.0000461	15.09	19.63	0.0002840
118	19.01	22.14	0.0000987	15.01	19.60	0.0001970
200	19.97	24.10	0.0000053	14.72	20.14	0.0002800
205	18.05	21.66	0.0003125	13.81	17.73	0.0010141
213	18.01	21.30	0.0003462	13.22	16.53	0.0033742
217	19.98	25.09	0.0000099	16.39	20.82	0.0001210

Table (4.1) illustrates the performances of MSE and SNR_{out} of the SC-LNLMS filtering method when dealing with MA noise added at 5 and 10 dB input SNR for the first and the last stage. The results of processing the data number 100, 105, 107, 118, 200, 205, 213, and 217 show that the SNR_{out} is improved from first stage to the last stage, for example, SNR_{out} of the first stage for data number 105 is 20.87 dB while it achieves 28.56 dB for the last stage when considering added MA at 10 dB, and when considering added MA at 5 dB it is 16.40 dB and 20.86 dB for first and last stage respectively. The proposed denosing technique also achieves the best MSE at the last stage that alternating from 0.0003462 to 5.059e-7 when considering added MA at 10 dB, and when considering added MA at 5 dB it alternates from 0.0033742 to 0.0001032 [78].

Table 4.2 SNR_{out} and MSE results after using SC-LNLMS method for removing BW noise

Added noise= baseline wander noise (BW)						
	SNR in=10dB			**SNR in=5dB**		
Signals	**SNR_{out} First stage**	**SNR_{out} (last stage)**	**MSE at last stage**	**SNR_{out} (First stage)**	**SNR_{out} (last stage)**	**MSE at last stage**
100	17.90	22.53	0.0027836	15.71	16.81	0.0612400
105	18.39	24.41	0.0037331	15.70	17.92	0.0153233
107	18.50	21.29	0.0021202	15.76	17.98	0.0151211
118	18.53	23.09	0.0017439	16.02	18.18	0.0086163
200	20.01	21.70	0.0053245	18.07	20.82	9.016843e-04
205	18.21	24.50	0.00110588	16.35	18.01	0.01308033
213	16.69	20.86	0.00580477	15.22	16.47	0.08219667
217	22.20	27.28	2.86755e-06	20.12	22.15	1.857011e-05

Table (4.2) illustrates the performances of MSE and SNR_{out} of the SC-LNLMS filtering method when dealing with BW noise added at 5 and 10 dB input SNR for the first and the last stages. The results of processing the data number 100, 105, 107, 118, 200, 205, 213, and 217 show that the SNR_{out} is improved from the first stage to the last stage, for example, SNR_{out} of the first stage for data number 217 is 22.20 dB while it achieves 27.28 dB for the last stage when considering added BW noise at 10 dB, and when considering added BW noise at 5 dB it is 20.12 dB and 22.15 dB for first and last stage respectively. The proposed denoising technique also achieves the best MSE at the last stage that alternating from 0.00580477 to 2.86755e-06

when considering added BW at 10 dB, and when considering added BW at 5 dB it alternates from 0.08219667 to 0.0001032.

Table (4.3) illustrates the performances of MSE and SNR_{out} of the SC-LNLMS filtering method when acting with EM noise added at 5 and 10 dB input SNR for the first and the last stages. The results of processing the data number 100, 105, 107, 118, 200, 205, 213, and 217 show that the SNR_{out} is improved from the first stage to the last stage, for example, SNR_{out} of the first stage for data number 217 is 22.59 dB while it achieves 27.97 dB for the last stage when considering added EM at 10 dB, and when considering added EM artifact at 5 dB it is 17.18 dB and 22.21 dB for first and last stage respectively. The proposed denoising technique also achieves the best MSE at the last stage that alternating from 1.4462883e-04 to 1.5454146e-06 when considering added EM artifact at 10 dB, and when considering added EM at 5 dB it alternates from 0.0332111 to 2.44956e-05.

Table 4.3 SNR_{out} and MSE results after using SC-LNLMS method for removing EM noise.

Added noise= electro motion (EM)						
	SNR in=10dB			**SNR in=5dB**		
Signals	**SNR_{out} First stage**	**SNR_{out} (last stage)**	**MSE at last stage**	**SNR_{out} (First stage)**	**SNR_{out} (last stage)**	**MSE at last stage**
100	19.59	23.76	4.425398e-05	15.69	18.54	0.00846643
105	20.98	25.93	5.187104e-06	15.52	18.73	0.0069406
107	20.70	23.82	4.378119e-05	14.64	19.21	0.0044294
118	19.78	22.27	1.4462883e-04	15.99	18.71	0.00506461
200	22.20	24.93	1.478135e-05	17.05	22.36	2.01149e-04
205	19.32	23.05	8.682866e-05	15.83	18.29	0.0101219
213	18.90	22.87	1.0349422e-04	13.81	17.08	0.0332111
217	22.59	27.97	1.5454146e-06	17.18	22.21	2.44956e-05

Figure 4.13 displays the performance SNR improvement of the SC-LNLMS filtering method to remove MA noise. Figure 4.13(a) displays SNR improvement between the first and the last stage when acting with MA noise added at 10dB input SNR level. Figure 4.13(b) displays SNR improvement between the first and the last stage when acting with MA noise added at 5 dB input SNR level. We see from figure 4.13(b) that the improvement of SNR alternates from 3.31

dB resulting from processing data number 213 to 5.42 dB was resulting from processing data number 200, and from figure 4.13(a) the SNR improvement alternates from 3.13 dB was resulting from processing data number 118 to 7.69 dB was resulting from processing data number 105. It is clear that the improvement of SNR is significantly improved from the first stage to the last stage due to varied both step size and leakage coefficient in each stage that are controllable to achieve better SNR without distorting the shape of the original ECG signal.

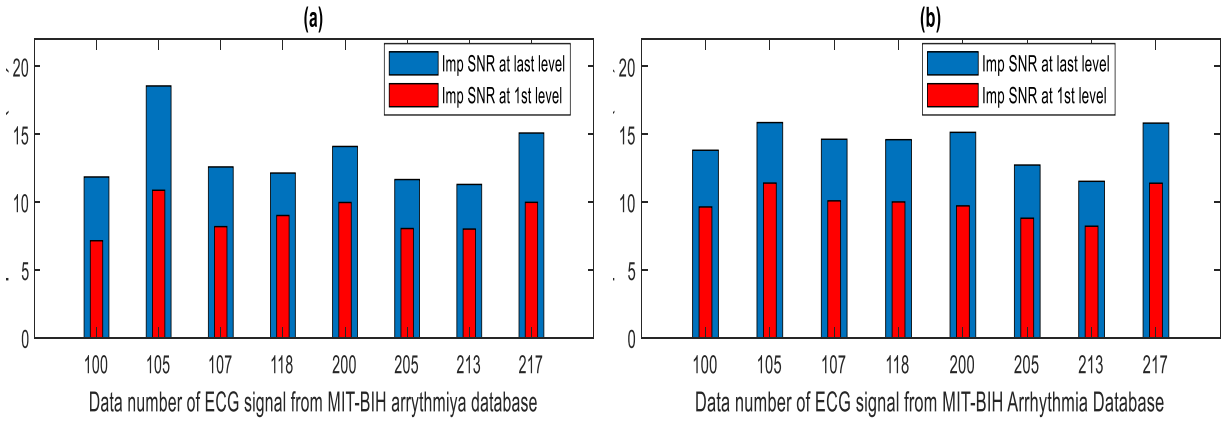

Figure 4.13 SNR improvements of SC-LNLMS filtering method for MA removing, (a) SNR improvement for MA removing at 10 dB, (b) SNR improvement for MA removing at 5 dB.

Figure (4.14) displays the performance SNR improvement of the SC-LNLMS filtering method to remove BW noise. Figure 4.14(a) displays SNR improvement between the first and the last stage when acting with BW noise added at 10dB input SNR level. Figure 4.14(b) displays SNR improvement between the first and the last stage when dealing with BW noise added at 5 dB input SNR level. We see from figure 4.14(a) that the improvement of SNR alternates from 1.69 dB was resulting from processing data number 200 to 6.29 dB was resulting from processing data number 205, and from figure 4.14(b) the SNR improvement alternates from 1.1 dB was resulting from processing data number 105 to 2.16 dB was resulting from processing data number 217. It is clear that the improvement of SNR is significantly improved from the first stage to the last stage, which indicates the effectiveness of the SC-LNLMS method.

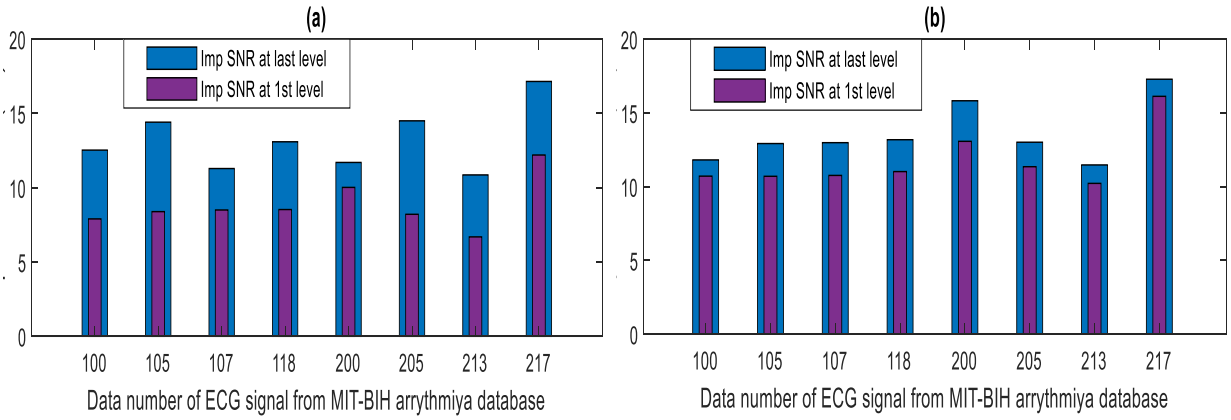

Figure 4.14 SNR improvements of SC-LNLMS filtering for BW removing, (a) SNR improvement for BW removing at 10 dB, (b) SNR improvement for BW removing at 5 dB.

Figure (4.15) displays the performance SNR improvement of the SC-LNLMS filtering method to remove EM noise. Figure 4.15(a) displays SNR improvement between the first and the last stage when acting with EM artifact added at 10dB input SNR level. Figure 4.15(b) displays SNR improvement between the first and the last stage when acting with EM artifact added at 5 dB input SNR level. We see from Figure 4.15(a) that the improvement of SNR alternates from 2.49 dB was resulting from processing data number 118 to 4.95 dB was resulting from processing data number 105, and from figure 4.15(b) the SNR improvement alternates from 2.46 dB was resulting from processing data number 205 to 5.79 dB was resulting from processing data number 217. It is clear that the improvement of SNR is significantly improved from the first stage to the last stage, which indicates the effectiveness of the SC-LNLMS method.

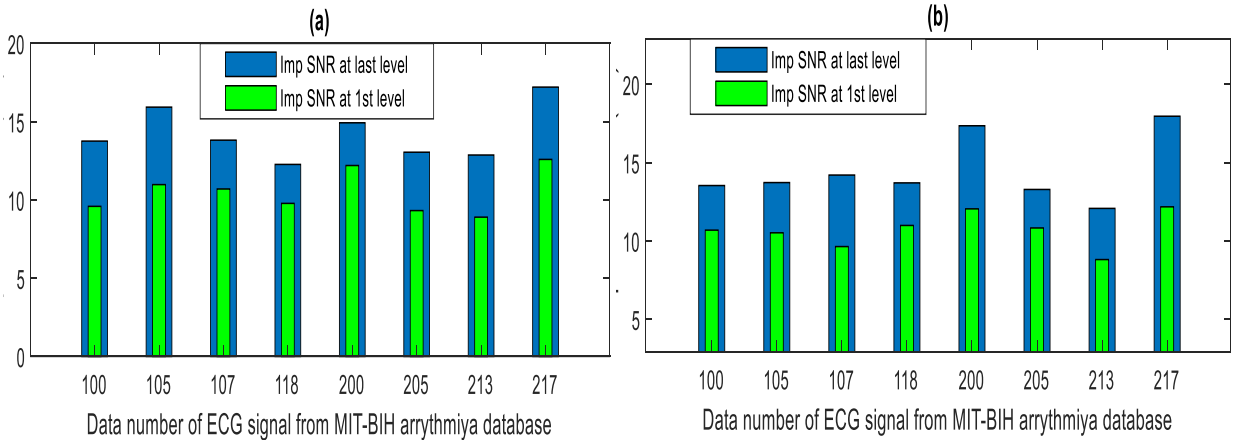

Figure 4.15 SNR improvements of SC-LNLMS filtering for EM artifact removing, (a) SNR improvement for EM artifact removing at 10 dB, (b) SNR improvement for EM removing at 5 dB.

4.4.2.2 Obtained results after using SWT and NLMS method

Table (4.4) illustrates the performances of MSE and SNR_{out} of the SWT plus NLMS filtering method when dealing with MA noise added at 5 and 10 dB input SNR to the free ECG signal of data number 118. The results show that the best SNR_{out} of 27.90 dB and MSE of 1.10009e-6 were obtained by selecting db1 for filter bank 1, rbioi1.1 for filter bank 2, firm thresholding, and NLMS algorithm when dealing with added MA noise at 10 dB, while when dealing with added MA noise at 5 dB the best SNR_{out} of 20.11 dB and MSE of 7.3046e-04 were obtained by selecting db2 for filter bank 1, rbioi1.1 for filter bank 2, garrote thresholding, and NLMS algorithm. The SWT and NLMS method achieved sufficient and satisfactory results when dealing with the removal of muscle noise from ECG signal.

Table 4.4 SNR_{out} and MSE results after using SWT and NLMS method for removing MA noise.

Added noise = muscle noise (MA)								
SNR in=10 dB					**SNR in=5 dB**			
Threshol ding rule	**Filter bank 1 (SWT)**	**Filter Bank 2 (ISWT)**	**SNR out**	**MSE**	**Filter bank1 (SWT)**	**Filter Bank2 (ISWT)**	**SNR_{out}**	**MSE**
Garrote	db2	db1	27.40	2.99801e-6	db2	Bior1.1	20.11	7.3046e-04
Soft	Sym4	Sym2	27.01	4.04244e-06	db1	dmey	19.66	1.88732e-3
Hard	Sym8	rbio1.1	22.21	0.0001259	db1	db1	16.70	0.0413812
Semi soft	db1	Bior1.1	27.90	1.10009e-6	Sym1	rbio2.2	19.82	1.00691e-3
Hyperbolic	dmey	bior4.4	26.93	9.24721e-5	Sym2	Coif1	19.54	2.3700e-03

Table (4.5) illustrates the performances of MSE and SNR_{out} of the SWT plus NLMS filtering method when acting with BW noise added at 5 and 10 dB input SNR to the free ECG signal of data number 205. The results show that the best SNR_{out} of 15.91 dB and MSE of 0.0303022 were obtained by selecting Sym1 for filter bank 1, Sym1 for filter bank 2, soft thresholding, and NLMS algorithm when dealing with added BW noise at 10 dB, while when dealing with added BW noise at 5 dB the best SNR_{out} of 8.54 dB and MSE of 0.113611 were obtained by selecting sym1 for filter bank 1, db1 for filter bank 2, firm thresholding and NLMS algorithm. The SWT and NLMS method achieved rather acceptable results when dealing with

input SNR of 10 dB of added BW noise, while for input SNR of 5dB it achieved insufficient and unsatisfactory results to remove BW noise.

Table 4.5 SNR_{out} and MSE results after using SWT and NLMS method for removing BW noise.

Added noise= Base wander (BW)								
SNR in=10dB					**SNRin=5dB**			
Thresholding rule	**Filter bank1 (SWT)**	**Filter Bank2 (ISWT**	**SNR_{out}**	**MSE**	**Filter bank1 (SWT)**	**Filter Bank2 (ISWT**	**SNR_{out}**	**MSE**
Garrote	Sym1	Sym4	15.91	0.0377840	bior1.1	Rbio3.7	8.10	0.254287
Soft	Sym1	Sym1	15.54	0.0303022	Dmey	Coif1	7.72	0.548752
Hard	db4	dmey	14.75	0.0700205	Sym4	Coif5	7,22	0.860540
Firm	db1	db1	15.65	0.0386886	Sym1	db1	8,54	0.113611
Hyperbolic	Sym4	db4	14.89	0.1004717	db2	db2	7,12	0.914756

Table 4.6 SNR_{out} and MSE results after using SWT and NLMS method for removing EM artifact

Added noise= electro motion (EM)								
SNR in=10dB					**SNRin=5dB**			
Thresholding rule	**Filter bank1 (SWT)**	**Filter Bank2 (ISWT)**	**SNR_{out}**	**MSE**	**Filter bank1 (SWT)**	**Filter Bank2 (ISWT)**	**SNR_{out}**	**MSE**
Garrote	Sym1	db1	14.71	0.2010796	Sym1	db1	8.02	0.2542873
Soft	Bior1.1	Bior1.1	14.14	0.6490395	Bior1.1	Bior1.1	7.09	0.8231081
Hard	Sym1	db1	14.44	0.3002106	Coif2	Rbio1.1	6.98	0.9974547
Semi soft	Bior1.1	Bior1.1	14.22	0.3409551	Sym1	db1	8.20	0.2172143
Hyperbolic	dmey	Sym2	13.87	0.8278035	Bior1.1	Bior1.1	7.03	0.8875487

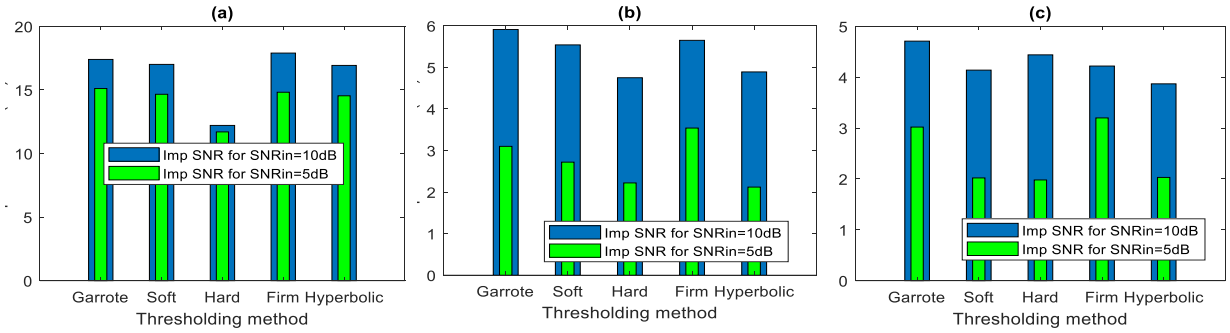

Figure 4.16 SNR improvement after using SWT and NLMS method for noises removing, (a) SNR improvement for MA artifact removing at 10 and 5dB, (b) SNR improvement for BW removing at 10 and 5 dB, SNR improvement for EM removing at 10 and 5 dB.

.

Table (4.6) illustrates the performances of MSE and SNR_{out} of the SWT plus NLMS filtering method when acting with EM artifact added at 5 and 10 dB input SNR to the free ECG signal of data number 205. The results show that the best SNR_{out} of 14.71 dB and MSE of 0.2010796 were obtained by selecting Sym1 for filter bank 1, db1 for filter bank 2, garrote thresholding and NLMS algorithm when dealing with added EM artifact at 10 dB, while when dealing with added EM artifact at 5 dB the best SNR_{out} of 8.20 dB and MSE of 0.2172143 were obtained by selecting Sym1 for filter bank 1, db1 for filter bank 2, firm thresholding and NLMS algorithm. The SWT and NLMS method achieved insufficient and unsatisfactory results to remove EM artifact from ECG signal.

Figure (4.16) displays the performance of SNR improvement after using SWT and NLMS filtering. Figure 4.16(a) shows SNR improvement achieved when dealing with MA noise added at 10dB and 5dB input SNR level. Figure 4.16(b) shows SNR improvement achieved when dealing with BW noise added at 10dB and 5dB input SNR level. Figure 4.16(c) displays SNR improvement achieved when dealing with EM artifact added at 10dB and 5dB input SNR level. We see from figure 4.16(a) that the best improvement SNR resulted from removing MA from data number 118 added at 10dB is 17.9dB, while when dealing with added MA noise at 5 dB, the best resulted improvement SNR is 15.11 dB. Figure 4.16(b) illustrates the best improvement SNR resulted from removing BW from data number 205 added at 10dB is 5.91 dB, while when dealing with added BW noise at 5 dB, the best resulted improvement SNR is 3.54 dB. Figure 4.16(c) illustrates the best improvement SNR resulted from removing EM artifact from data number 205 added at 10 dB is 4.71 dB, while when acting with added EM noise at 5 dB, the resulted best improvement SNR is 3.2 dB. It is clear that the SWT and NLMS filtering method did not succeed in removing EM noise from the ECG signal.

4.4.2. 3 Compare results with different techniques

Table (4.7) and table (4.8) illustrate the performances of the two proposed filtering in terms of SNR improvement and MSE compared with dual tree wavelet transform [47], empirical mode decomposition (EMD) with non-local mean (NLM) technique [49], neural networks technique [50], leaky normalized least mean square technique [51], and constructing a Guided Filter [52] in aim of noises reduction from corrupted ECG signal.

- **After filtering MA noise**

Table 4.7 improvement SNRs (in dB) for MA, BW, and EM noise removal compared with other existing technique

Type of added noise	**MA noise**		**BW noise**		**EM artefact**	
Input SNR (dB)	**10dB**	**5dB**	**10dB**	**5dB**	**10dB**	**5dB**
Denoising methods	**SNR imp (dB)**	**SNR imp (dB)**	**SNR imp (dB)**	**SNR imp (dB)**	**SNR imp (dB)**	**SNR imp (dB)**
Proposed method based on SC-LNLMS	18.56	15.86	17.28	17.15	17.97	17.21
Proposed method based on SWT and NLMS	17.90	15.11	5.91	3.54	4.71	3.20
Reference [49]	<12	<11	/	/	/	/
Reference [50]	5.19 (SNRinp =22.9)	/	11.56 (SNRinp= 19.18)	/	9.64 (SNRinp= 15.65)	/
Reference [51]	11.8843	/	9.8429	/	/	/
Reference [52]	/	11.53	/	/	/	14.28
Reference [47]	/	7.2195 3	/	5.65466	/	15.24564

The SNR improvement and MSE on MA noise after using SC-NLMS approach and SWT and NLMS are the most significant (18.56 dB and 5.059e-7, 17.90dB and 1.10009e-6 respectively); when dealing with added MA noise at 10 dB. While, the resulted SNR improvement and MSE achieved when using reference [49], and reference [51] are the moderate one (less then12 dB and 0.000472, 11.8843dB respectively). Also when dealing with added MA at 5 dB, the resulted

improvement SNR and MSE after using SC-NLMS approach and SWT and NLMS are the most significant (15.86 dB and 1.032e-4, 15.11 and 7.3046e-04). While, the SNR improvement and MSE achieved when using the reference [49], reference [52] achieved moderate results (less than 11 dB and 0.001021, 11.53 dB and 0.0625), reference [47] achieved the lowest one (7.21953 dB and 0.00277).

Table 4.8 Resulted MSE for MA, BW, and EM noises removal compared with other existing technique

Type of added noise	**MA noise**		**BW noise**		**EM artefact**	
Input SNR (dB)	**10dB**	**5dB**	**10dB**	**5dB**	**10dB**	**5dB**
Denoising methods	**MSE**	**MSE**	**MSE**	**MSE**	**MSE**	**MSE**
Proposed method based on SC-LNLMS	**5.059e-7**	**1.032e-4**	**2.86755e-06**	**1.85701 1e-05**	**1.5454146 e-06**	**2.44956e-05**
Proposed method based on SWT and NLMS	**1.10009e -6**	**7.3046e -04**	0.030302 2	0.11361 1	0.2010796	0.2172143
Reference [49]	0.000472	0.0010 21	/	/	/	/
Reference [50]	/	/	/	/	/	/
Reference [51]	/	/	/	/	/	/
Reference [52]	/	0.0625	/	/	/	0.0441
Reference [47]	/	0.0027 7	/	0.00044	/	0.00397

- **After filtering BW noise**

The SNR improvement and MSE on BW noise after using SC-NLMS approach is the most significant (17.28 dB and 5.059e-7) when dealing with added BW noise at 10 dB. While, the SNR improvement and MSE achieved when using and SWT and NLMS is the lowest one (5.91 dB and 0.0303022), reference [50] and reference [51] achieved the moderate one (11.56 dB, 9.8429 respectively). Also when dealing with added BW at 5 dB, the resulted improvement SNR and MSE after using SC-NLMS approach is the most significant (17.15 dB and 1.857011e-05). Where, when using the SWT plus NLMS approach and reference [47] are the lowest one (3.54dB and 0.113611, 5.65466dB and 0.00044 respectively).

- **After filtering EM noise**

The SNR improvement and MSE on EM noise after using SC-NLMS approach is the most significant (17.97 dB and 1.5454146e-06) when dealing with added EM noise at 10 dB, then the SNR improvement and MSE achieved when using and SWT and NLMS is the lowest one (4.71 dB and 0.2010796). Also when dealing with added EM at 5 dB, the resulted improvement SNR and MSE after using SC-NLMS approach is the most significant (17.21 dB and 2.44956e-05). Where, when using the SWT plus NLMS approach is the lowest one (3.20 dB and 0.2172143), the references [52] and [47] gave the moderate one (0.0441, 0.00397 respectively)

As shown in table (4.7) and table (4.8), the proposed SC-NLMS approach can successfully reduce various types of noise, improve the SNR and reduce the MSE, and outperforms the method of SWT plus NLMS, dual tree wavelet transform [47], empirical mode decomposition (EMD) with non-local mean (NLM) technique [49], neural networks technique [50], leaky normalized least mean square technique [51], and constructing a guided filter [52].

4.5 Conclusion

This chapter includes presenting the results, discussing, and then comparing them. The results are divided into two sections, the results of the first section that we obtained by applying the SC-LNLMS technique that we proposed on the contaminated ECG signal with either muscle noise (MA), Baseline wander (BW) noise, or electro motion (EM) noise. The SC-LNLMS technique is based on a self-correcting leaky normalized least mean square algorithm with varied step size and leakage coefficient. As for the results of the second section, we obtained by applying the second technique, which is based on SWT and the NLMS algorithm. Finally, we provide a comparison with other existing techniques in the literature. The experimental results have shown the effectiveness of the first proposed method (SC-LNLMS) in improving the output SNR and reducing MSE to obtain clean ECG records that contains all its distinctive features without introducing distortion on the original signal compared to the method of SWT plus NLMS algorithm and compared with other existing techniques like dual-tree wavelet transform, empirical mode decomposition (EMD) with non-local mean (NLM) technique, neural networks technique, leaky normalized least mean square technique and, constructing a guided filter by exploiting the Butterworth filter for ECG signal enhancement. The success achieved by our method is due to relying first on leakage coefficient, which interferes with the difficulty of controlling the step size coefficient, and secondly on the self-correction of the filter

who gave interval to change both step size and leakage coefficients from one stage to a stage according to the abrupt changes of the signal, and on the other hand speed up the treatment process. The second method of SWT plus NLMS also can successfully remove major components of muscle noise from the ECG signal. However, it gave moderate results to eliminating BW noise, but it did not give sufficient and satisfactory results to eliminate EM noise, as it produced an ECG signal with blurred detail.

General conclusion

General conclusion

ECG is a low-frequency variable signal, which presents a number of challenges while recording and processing it. It has distinctive characteristics which include its non-stationarity, diversity between personals, and its high susceptibility to different types of noise. The frequency spectrum of the noise interferes with the frequency spectrum of the ECG signal, distorting the original signal, thus misleading an accurate diagnosis of a heart function.

Noise cancellation from the ECG signal is a typical application of adaptive filtration. Adaptive filtering is the most appropriate solution to varying the signal voltage over time in an iterative manner, as the filter parameters are updated by the adaptive algorithms. For this purpose and as the first contribution to this thesis, we proposed an adaptive technique to remove three types of noise MA, BW, and EM noise(each separately) from the contaminated ECG signal, as this technique depends on adaptive noise canceller using the algorithm based on leaky normalized least means square with varied step size and leakage coefficients, the variation of these two coefficients from stage to stage allowed a good compromise between the amount of noise to be removed and the amount of ECG signal to be preserved. As a second contribution, we proposed another technique to remove noises from the ECG for the purpose of comparing it with the first method and showing the efficiency of the first method. The second method is based on the SWT plus NLMS algorithm. With this method; the decomposition level, wavelet function threshold value, and thresholding algorithm are all factors that must be carefully selected taking into account the nature and the amount of the noise to be removed. Finally, we added a comparative study with some of the techniques found in the literature.

The experimental application of these two algorithms was carried out using a large number of real ECG signals contaminated with real noise that helped to give more realistic results and analyzes than those signals and noises that were created artificially. The results confirmed the efficiency and reliability of SC-LNLMS in reducing three types of noise while maintaining the standard shape of the ECG signal. SC-LNLMS outperforms all the methods proposed in the comparison section, while the SWT and NLMS method also gave the best results in removing MA noise and outperforming the rest of the proposed comparison technique after the SC-LNLMS method, but it was only able to remove a little bit of the BW noise and EM noise and keep the ECG signal distorted.

References

[1] NAJARIAN, KAYVAN; SPLINTER, ROBERT. (2012). BIOMEDICAL SIGNAL AND IMAGE PROCESSING. CRC PRESS.

[2] JESSICA COVEILLO. ECG INTERPRETATION MAKE INCREDIBLY EASY. (2016) SIXTH EDITION. CLINICAL EDITOR. WOLTERS KLUWER.

[3] A JOHN CAMM THOMAS F. LÜSCHER PATRICK W. SERRUYS. (2006). CARDIOVASCULAR MEDICINE. WILEY- BLACKWELL.

[4] NOBLE RJ, HILLIS JS, ROTHBAUM DA. (1990). ELECTROCARDIOGRAPHY. IN: WALKER HK, HALL WD, HURST JW, EDITORS. CLINICAL METHODS: THE HISTORY, PHYSICAL, AND LABORATORY EXAMINATIONS. 3RD EDITION. BOSTON: BUTTERWORTHS; CHAPTER 33.

[5] ASHLEY EA, NIEBAUER J. CARDIOLOGY EXPLAINED. LONDON: REMEDICA; 2004. CHAPTER 3, CONQUERING THE ECG.

[6] Sornmo, L., Laguna, P. (2005). Bioelectrical Signal Processing in Cardiac and Neurological Applications. Academic press

[7] Hurst JW. (1998). Naming of the waves in the ECG with a brief account of their genesis. Circulation. Nov 3;98 (18):1937-42

[8] wilhelm einthoven, m.d., of leyden. (1912). The different forms of the human electrocardiogram and their signification. Volume 179, issue 4622, p853-861. doi:https://doi.org/10.1016/s0140-6736(00)50560-1

[9] Wolferth CC, Wood FC. (1932). The electrocardiographic diagnosis of coronary occlusion by the use of chest leads. Am J Med Sci; 183:30-35

[10] Burch GE. (1978). History of precordial leads in electrocardiography. Eur J Cardiol.; 8(2): 207-36.

[11] Andrew R Houghton. (2020). Making sense of the ECG; A hands on guide; fifth edition, by Taylor & Francis Group, LLC.

[12] Asma BOUNOUARA. (2015).QRS Detection in ECG Signals, MAGISTER thesis in Electronics, Hadj Lakhdar Batna University Faculty of Technology Department of Electronics

[13] TCHP Education Consortium. ECG Rhythm Interpretation Primer. 2004-2007.

[14] Abdelhaq OUELLI. (2015).Contributions to the analysis and processing of non-stationary biomedical signals Applications to electrocardiograms and electroencephalograms. Doctoral thesis in Computer Science and Signal Processing. Sultan Moulay Slimane University, Faculty of Sciences and Techniques, Béni Mellal, Morocco.

[15] Openstax college; (2013). Anatomy and Physiology. 1st Edition, Rice University.

[16] Sutanto H and Heijman J. (2019).The Role of Calcium in the Human Heart: With Great Power Comes Great Responsibility. Front. Young Minds. 7:65. doi: 10.3389/frym.2019.00065.

[17] ALI OSTADFAR (2016). BIOFLUID DYNAMICS IN HUMAN ORGANS. CHAPTER4. BIOFLUID MECHANICS PRINCIPLES AND APPLICATIONS, PAGES 111-204. HTTPS://DOI.ORG/10.1016/B978-0-12-802408-9.00004-1

[18] Aleksander Sizarov, Antoon F.M. Moorman, Arthur S. Pickoff. (2013). Development and Functional Maturation of the Cardiac Conduction System. Electrophysiology. Chapter 18_p523-546.

[19] Antoun khawaja. (2009). Automatic ECG analysis using principle component analysis and wavelet transformation. Karslurhe transactions on biomedical engineering. Vol3

[20] Saif Eddine Hadji, Mazleena Salleh,MohdFoad Rohani, Maznah Kamat . (2016). Wavelet-based Performance in Denoising ECG Signal. Faculty of Computing Universiti Teknologi Malaysia, DOI: http://dx.doi.org/10.1145/3015166.3015212.

[21] Sivaraks, Haemwaan, Ratanamahatana, Chotirat Ann. (2015). Robust and Accurate Anomaly Detection in ECG Artifacts Using Time Series Motif Discovery. Computational and Mathematical Methods in Medicine, DOI: 10.1155/2015/453214.

[22] Emmanuel C. Ifeachor, Barrie W. Jervis. (1993). Digital Signal Processing_ A Practical Approach (Electronic Systems Engineering) -Addison-Wesley.

[23] Haykin, S., Totterdill, P. (2001). Adaptive filter theory. Prentice Hall.

[24] Hayes MH (1996) Statistical digital signal processing and modelling. John Wiley & Sons, Inc.

[25] Anthony Zaknich. (2005). Principles of adaptive filters and self-learning systems. Advanced textbooks in control and signal processing Springer London.

[26] Radenkovic, Miloje; Bose, Tamal. (2001) Adaptive IIR filtering of nonstationary signals. Signal Processing 81(1):183-195. DOI: 10.1016/S0165-1684(00)00196-1

[27] Karthick, S.; Valarmathy, S.; Prabhu, E. (2015). Low Power Systolic Array Based Digital Filter for DSP Applications. The Scientific World JOURNAL, volume 2015. DOI: 10.1155/2015/592537.

[28] KALLMANN, H. J. (1940). "Transversal filters," Proc. IRE, vol. 28, pp. 302-310.

[29] W. Kenneth Jenkins, Andrew W. Hull, Jeffrey C. Strait, Bernard A. Schnaufer, Xiaohui Li. (1996). Advanced Concepts in Adaptive Signal Processing. The Springer International Series in Engineering and Computer Science 365. Springer US.

[30] Behrouz Farhang-Boroujeny. (2013). Adaptive Filters_ Theory and Applications-Wiley.

[31] R.J. O'Dowd. (1990). A study of Ill-conditioning in Linear Techniques with emphasis on some applications in the Earth Sciences. A thesis for the degree Of Doctor of Philosophy. University of Adelaide Department of Geology and Geophysics November.

[32] Jiang, Jean_ Tan, Li. (2019). Digital signal processing. Fundamentals and applications-Elsevier.

[33] Gitlin, R.D. Meadors, H.C., Weinstein, S.B. (1982). The tap-leakage algorithm: An algorithm .for the stable operation of a digitally implemented, fractionally adaptive spaced equalizer. Bell System Technical Journal, 61(8): 1817-1839. https://doi.org/10.1002/j.1538-7305.1982.tb03086.x

[34] Zahm, C. L. (1973). Applications of adaptive arrays to suppress strong jammers in the presence of weak signals. IEEE Transactions on Aerospace and Electronic Systems, 9(2): 260-271. https://doi.org/10.1109/taes.1973.309794

[35] Vinay K. Ingle, John G. (2011). Proakis-Digital Signal Processing Using MATLAB-Cengage Learning.

[36] Widrow, B., Glover, J.R., McCool, J.M., Kaunitz, J., Williams, C.S., Hearn, R.H., Zeidler, J.R., Eugene Dong, Jr., Goodlin, R.C. (1975). Adaptive noise cancelling: Principles and applications. Proceedings of the IEEE. Vol: 63 (12), pp: 1692—1716. DOI: 10.1109/PROC.1975.10036.

[37] B. Widrow, P. Mantey, L. Griffiths;and B. Goode. (1967). Adaptive antenna systems," *Proceeding of IEEE*, vol. 55, pp. 2143-2159.

[38] S. CANAN, Y. ÖZBAY AND B. KARLIK. (1998). A METHOD FOR REMOVING LOW VARYING TREND FROM ECG SIGNAL. PROCEEDINGS OF THE INTERNATIONAL CONFERENCE IN BIOMEDICAL ENGINEERING DAYS, PP 144–146.

[39] M.L. RICCIO.; J.C. BELINA. (1992). A VERSATILE DESIGN METHOD OF FAST, LINEAR-PHASE FIR FILTERING SYSTEMS FOR ELECTROCARDIOGRAM ACQUISITION AND ANALYSIS SYSTEMS. COMPUTERS IN CARDIOLOGY, PP 147–150.

[40] J.M. LESKI; N. HENZE. (2005). ECG BASELINE WANDER AND POWERLINE INTERFERENCE REDUCTION USING NONLINERA FILTER BANK. SIGNAL PROCESSING, 85, PP 781–793.

[41] Sharma, Kamalesh Kumar; Gupta, Praveen; Joshi, Shiv Dutt. (2015). Baseline wander removal of electrocardiogram signals using multivariate empirical mode decomposition. Healthcare Technology Letters. Volume 2, issue 6, pp: 164—166.. DOI: 10.1049/htl.2015.0029.

[42] Lenis, Gustavo; Pilia, Nicolas; Loewe, Axel; Schulze, Walther H. W.; Dössel, Olaf. (2017). Comparison of Baseline Wander Removal Techniques considering the Preservation of ST Changes in the Ischemic ECG: A Simulation Study. C mputational and Mathematical Methods in Medicine. Volume 2017, pp: 1—13. DOI: 10.1155/2017/9295029

[43] Sharma, Rishi Raj; Pachori, Ram Bilas. (2018). Baseline wander and power line interference removal from ECG signals using eigenvalue decomposition. Biomedical Signal Processing and Control volume 45, pp: 33-49. DOI: 10.1016/j.bspc.2018.05.002.

[44] Wan, Xiang-kui; Wu, Haibo; Qiao, Fei; Li, Feng-cong; Li, Yan; Yan, Yue-wen; Wei, Jia-xin. (2019). Electrocardiogram Baseline Wander Suppression Based on the Combination of Morphological and Wavelet Transformation Based Filtering. Computational and Mathematical Methods in Medicine volume 2019, pp: 1-7. DOI: 10.1155/2019/7196156.

[45] Jarosław Wasilewski, Lech Poloński, Adam Gacek, Witold Pedrycz. (2012). ECG Signal Processing, Classification and Interpretation_ A Comprehensive Framework of Computational Intelligence-Springer.

[46] Thakor, N.V., Zhu, Y.S. (1991). Applications of adaptive filtering to ECG analysis: noise cancellation and arrhythmia detection. IEEE Transaction Biomedical Engineering, 38(8): 785–794. https://doi.org/10.1109/10.83591.

[47] Oussama, E.B, Rachid, L., Khalifa E., Abdenbi, A., Wissam, J. (2017). ECG signal performance denoising assessment based on threshold tuning of dual-tree wavelet transform. BioMedical Engineering OnLine. https://doi.org/10.1186/s12938-017-0315-1.

[48] Venkatesan, C., Karthigaikumar, P., Varatharajan, R. (2018). FPGA implementation of modified error normalized LMS adaptive filter for ECG noise removal. Cluster Computing. https://doi.org/10.1007/s10586-017-1602-0.

[49] Kumar, S., Panigrahy, D., Sahu, P.K. (2018). Denoising of Electrocardiogram (ECG) signal by using empirical mode decomposition (EMD) with non-local mean (NLM) technique. Biocybernetics and Biomedical Engineering. https://doi.org/10.1016/j.bbe.2018.01.005.

[50] Suranai, P., Xiao-Hua, Yu. (2013). An adaptive filtering approach for electrocardiogram (ECG) signal noise reduction using neural networks. Neurocomputing, 117(6): 206-213. https://doi.org/10.1016/j.neucom.2013.02.010.

[51] Sk, Nore Johny Basha., Mohammad, Zia-Ur-Rahman., B V Rama Mohana, Rao. (2011). Noise Removal from Electrocardiogram Signals using Leaky and Normalized version of Adaptive Noise Canceller. International Journal of Computer Science & Communication Networks, 1(1): 81-84.

[52] Ming, Liu., HuaQing, Hao., Peng, Xiong., Feng Lin, ZengGuang Hou., Xiuling, Liu. (2017). Constructing a Guided Filter by Exploiting the Butterworth Filter for ECG

Signal Enhancement. Journal of Medical and Biological Engineering. https://doi.org/10.1007/s40846-017-0350-1

[53] Khiter, A., Mitiche, A.B.H.A., Mitiche, L. (2020). Denoising electrocardiogram signal from electromyogram noise using adaptive filter combination. Revue d'Intelligence Artificielle, Vol. 34, No. 1, pp. 67-74. https://doi.org/10.18280/ria.340109.

[54] Shin g-Hong Liu Hong Liu. (2009). Motion Artifact Reduction in Electrocardiogram Using Adaptive Adaptive Filter Filter. Journal of Medical and Biological Engineering, 31(1): 67-72.

[55] Rodrigues, Rui & Couto, Paula. (2012). A Neural Network Approach to ECG Denoising. Departamento de Matem_atica da Faculdade de Ciencias e Tecnologia da UNL, 2829-516 Caparica, Portugal.

[56] umamaheswara redy, m. muralidhar. (2012). Removal of electrode motion artifact in ecg signals using wavelet based threshold methods with grey incidence degree. International journal of electrical and electronics engineering (ijeee) issn (print): 2231 – 5284, vol-2, issue-1.

[57] Wang, Ze; Wong, Chi Man; da Cruz, Janir Nuno; Wan, Feng; Mak, Pui-In; Mak, Peng Un; Vai, Mang I. (2014). Muscle and electrode motion artifacts reduction in ECG using adaptive Fourier decomposition. IEEE International Conference on Systems, Man and Cybernetics, pp: 1456—1461. DOI: 10.1109/SMC.2014.6974120

[58] Ghaleb FA, Kamat MB, Salleh M, Rohani MF, Abd Razak S. (2018) Two-stage motion artifact reduction algorithm for electrocardiogram using weighted adaptive noise cancelling and recursive Hampel filter. PLoS ONE 13(11): e0207176. https:// doi.org/10.1371/journal.pone.0207176.

[59] Xu X, Liang Y, He P, Yang J. (2019). Adaptive Motion Artifact Reduction Based on Empirical Wavelet Transform and Wavelet Thresholding for the Non-Contact ECG Monitoring Systems. Sensors. Vol:
19(13):2916. doi: 10.3390/s19132916. PMID: 31266226; PMCID: PMC6651081.

[60] Moody, G.B., Mark, R.G. (2001). The impact of the MIT-BIH arrhythmia database. IEEE Engineering in Medicine and Biology Magazine, 20(3): 45–50. https://doi.org/10.1109/51.932724.

[61] Moody, G.B., Muldrow, W.E., Mark, R.G. (1984). A noise stress test for arrhythmia detectors. Computers in cardiology, 11:381–384. Doi: 10.13026/C2HS3T.

[62] Joonwan Kim; Poularikas, A.D. (2003). Comparison of two proposed methods in adaptive noise canceling. IEEE, Proceedings of the 35th Southeastern Symposiiim Sysfem Theory, pp. 400-403, 2003.

[63] S. Li and J. Lin. (2009).The optimal de-noising algorithm for ECG using stationary wavelet transform. IEEE, WRI World Congress on Computer Science and Information Engineering - Los Angeles, California USA. Vol: 6, pp. 469–473. DOI: 10.1109/CSIE.2009.999

[64] Awal MA, Mostafa SS, Ahmad M, Rashid MA. (2014). An adaptive level dependent wavelet thresholding for ECG denoising. Biocybernetics and Biomedical Engineering; 34:238–49. http://dx.doi.org/10.1016/j.bbe.2014.03.002.

[65] G.P. Nason; B. W. Silverman. (1995).The Stationary Wavelet Transform and some Statistical Applications .Lecture Notes in Statistics. Wavelets and Statistics, Volume 103, pp. 281-299. Springer-Verlag New York.

[66] Brani Vidakovic, Peter Müller. (1999). Bayesian Inference in Wavelet-Based Models. Lecture Notes in Statistics, volume 141. Springer-Verlag New York. DOI: 10.1007/978-1-4612-0567-8.

[67] Michel Misiti ; Yves Misiti ; Georges Oppenheim ; Jean-Michel Poggi. (2002).Wavelet Toolbox User's Guide, Mathematics and Wavelets and signal processing.
[68] Anestis Antoniadis. (2007). Wavelet methods in statistics: Some recent developments and their applications. Statistics Surveys. Vol. 1, pp: 16–55. DOI: 10.1214/07-SS014.
[69] ABID Tarek. (2008). Analyse du signal ECG par les ondelettes. Magister thesis. University of Badji Mokhtar Annaba.
[70] David, L, Donoho., Iain, M, Johnstone. (1994). Ideal spatial adaptation by wavelet shrinkage, Biometrika, 81(3):425-55. https://doi.org/10.1093/biomet/81.3.425
[71] A. Phinyomark, C. Limsakul, and P. Phukpattaranont. (2009).EMG denoising estimation based on adaptive wavelet thresholding for multifunction myoelectric control. Innovative Technologies in Intelligent Systems and Industrial Applications, pp. 171–176. DOI: 10.1109/CITISIA.2009.5224220
[72] Castillo E, Morales DP, Garcia A, Martinez-Marti F, Parrilla L, Palma AJ. (2013).Noise suppression in ECG signals through efficient one-step wavelet processing techniques Journal of Applied Mathematics. Vol (2013). doi:10.1155/2013/763903.
[73] Liu S. (2013). A novel thresholding method in removing noises of electrocardiogram based on wavelet transform. Journal of Information &Computational Science; 10:5031–41.
[74] Donoho DL. Denoising by soft-thresholding,IEEE Transuction. Inform.Theory 1995, 41(3):612-627.
[75] P. Rajmic. (2003). Exact risk analysis of wavelet spectrum thresholding rules" in Proc.10th IEEE International Conference of Electronics Circuits System, vol. 1–3, pp. 455–458.
[76] L. Breiman. (1995).Better Subset Regression Using the Nonnegative Garrote. Technometrics, Vol. 37, pp. 373-384. DOI: 10.2307/1269730.
[77] H-Y. Gao. (1998).Wavelet Shrinkage Denoising Using the Non-Negative Garrote. Journal of Computational and Graphical Statistics Vol. 7, No. 4, pp.469-488. DOI:10.1080/10618600.1998.10474789.
[78] Khiter, A., Mitiche, A.B.H.A., Mitiche, L. (2020). Muscle noise cancellation from ECG signal using self-correcting leaky normalized least mean square adaptive filter under varied step size and leakage coefficient. Traitement du Signal, Vol. 37, No. 2, pp. 263-269. https://doi.org/10.18280/ts.370212
[79] Mohamed lamine talbi. (2011). Analyse et traitement du signal électrocardiographique (ecg). Doctoral thesis in sciences. Mentouri university of Constantine faculty of engineering sciences.
[80] Sucharita Mitra (Sarkar); Priyanka Samanta. (2019). Evaluation of different parameters of noisy ECG signal generated by jointly using MIT-BIH Noise Stress Test Database and CSE multi-lead clear ECG database. Journal of Emerging Technologies and Innovative Research (JETIR), Volume 6, Issue 5.
[81] https://physionet.org/physiotools/wag/nst-1.htm.